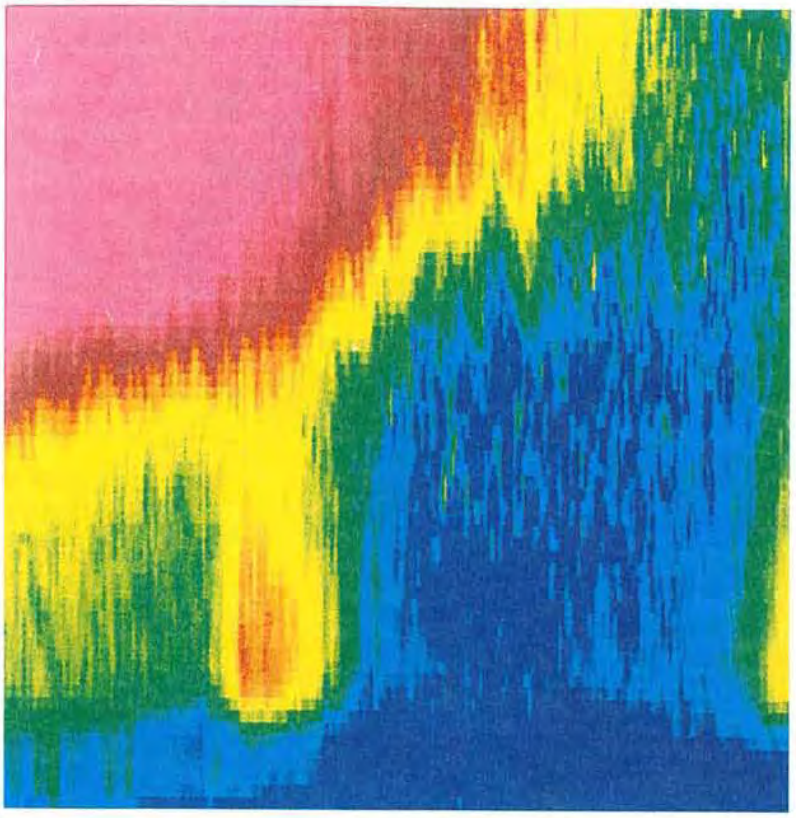

EISCAT

EUROPEAN INCOHERENT SCATTER SCIENTIFIC ASSOCIATION

ANNUAL REPORT 1993

S-981 28 KIRUNA, SWEDEN

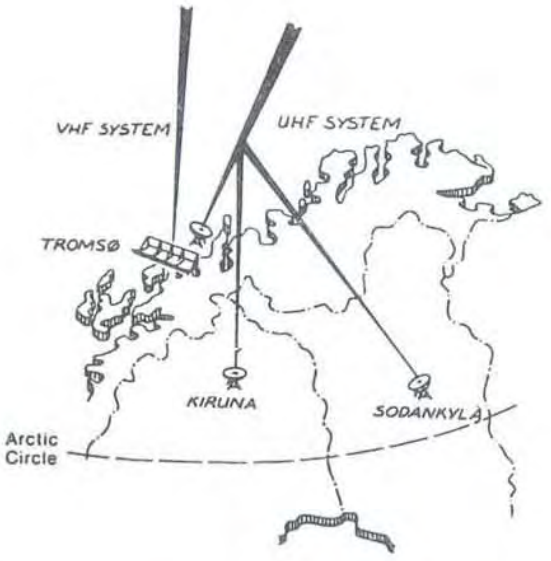

The EISCAT Radar Systems in Kiruna, Sodankylä and Tromsø
Operating Parameters 1993

	UHF Radar	**VHF Radar**
Centre operating frequency:	931.5 MHz	224.0 MHz
Tuneable bandwidth:	8 MHz	3 MHz
Pulse peak power:	1.5 MW	2 x 1.5 MW
Average power:	140 kW	2 x 140 kW
Pulse duration:	1 μs - 10 ms (phase/freq coded)	1 μs - 2 ms (phase/freq coded)
Minimum pulse interval:	1 ms	1 ms
Antennas:	Parabolic dishes 32 m diameter	Parabolic cylinder 40 m x 120 m
Feed systems:	Cassegrain	128 crossed dipole line
Gain:	48.1 dB	43.1 dB
Polarization:	Circular (Tromsø) Any (Receiving sites)	Circular
System Temperature:	90-110 K (Tromsø) 30-35 K (Receiving sites)	250-300 K

Geographic coordinates:	
Tromsø:	69.59° N, 19.23° E
Kiruna:	67.86° N, 20.44° E
Sodankylä:	67.36° N, 26.63° E
Invariant Latitude (Tromsø):	66.26° N
Geomagnetic Inclination:	77.50° N
L-shell (Tromsø):	6.17

The EISCAT Svalbard Radar (ESR) is being constructed near Longyearbyen on Spitsbergen, Svalbard (see system specifications on page 11). The **EISCAT Heating facility** in Tromsø is described on pages 24-26.

The cover illustration shows a colour-coded representation of electron concentration in the E- and F-regions for the period 11:00 to 20:00 UT (along the x-axis) over the altitude range 88-270 km (along the y-axis) measured by the EISCAT UHF radar on 16 February 1993. Red depicts regions of highest density and indicates an isolated region of E-region precipitation in the local afternoon sector beneath the slowly declining F-region as solar illumination diminished towards sunset. These results come from the first operation of experiment CP-1-K, which differs from the previous version of CP-1 in that the remote site antennas point continuously at the F-region, thereby providing continuous estimates of electric field. The results depicted are from the alternating code pulse modulation; this operation in February marked the first complete year of observations of common programmes using this pulse scheme. An overview of common programme operations is shown on page 23 of this report.

ANNUAL REPORT 1993

EISCAT, the European Incoherent Scatter Scientific Association, is established to conduct research on the lower, middle and upper atmosphere and ionosphere using the incoherent scatter radar technique. This technique is the most powerful ground-based tool for these research applications. EISCAT is also being used as a coherent scatter radar, for studying instabilities in the ionosphere, as well as for investigating the structure and dynamics of the middle atmosphere and as a diagnostic instrument in ionospheric modification experiments with the Heating facility.

There are seven facilities in the world applying the incoherent scatter radar technique, EISCAT operates the highest-standard incoherent scatter radars. The experimental sites of EISCAT are located in Scandinavia, north of the Arctic circle. They consist of two independent radar systems (see schematic and operating parameters on the inside of the front cover). The EISCAT Svalbard Radar (ESR) is being constructed and planned to be in initial operation end of year 1995 (see specifications on page 11).

The EISCAT UHF radar operates in the 931 MHz band with a peak transmitter power of 1.5 MW and 32 m, fully steerable parabolic dish antennas. The transmitter and one receiver are in Tromsø (Norway). Receiving sites are also located near Kiruna (Sweden) and Sodankylä (Finland), allowing continuous tristatic measurements to be made.

The monostatic VHF radar in Tromsø operates in the 224 MHz band with a peak transmitter power of 2 x 1.5 MW (to be raised to 4 MW) and a 120 m x 40 m parabolic cylinder antenna, which is subdivided into four sectors. It can be steered mechanically in the meridional plane from vertical to 60° north of the zenith; limited east-west steering is also possible using alternative phasing cables.

The basic data measured with the incoherent scatter radar technique are profiles of electron density, electron and ion temperature and ion velocity. Subsequent processing allows a wealth of further parameters, describing the ionosphere and neutral atmosphere, to be derived. A selection of well-designed radar pulse schemes are available to adapt the data-taking routines to many particular phenomena, occurring at altitudes between about 50 km and more than 2000 km. Depending on geophysical conditions, a best time resolution of less than one second and an altitude resolution of a few hundred meters can be achieved, whereas typical resolutions are of the order of minutes and kilometres. Tropospheric and stratospheric measurements are carried out with altitude resolution of some 100 m and 10-sec time resolution.

Operations of approximately 1500 hours each year are distributed equally between Common Programmes (CP) and Special Programmes (SP). At present, six well-defined Common Programmes are run regularly, for between one and six days, about 20 times each year to provide a data base for long term synoptic studies. Three Unusual Programmes (UP) can be started ad hoc during particular geophysical conditions. A large number of Special Programmes, defined individually by Associate scientists, are run to support national and international studies of both specific and global geophysical phenomena.

The Annual Reports present a summary of EISCAT's operations, developments, scientific results, publications and budget for each year. Further details of the EISCAT system and operation can be found in various EISCAT reports, including an illustrated brochure, which can be obtained from EISCAT Headquarters in Kiruna, Sweden.

The investments and operational costs of EISCAT are shared between:

Suomen Akatemia, Finland
Centre National de la Recherche Scientifique, France
Max-Planck-Gesellschaft, Federal Republic of Germany
Norges forskningsråd, Norway
Naturvetenskapliga forskningsrådet, Sweden
Science and Engineering Research Council, United Kingdom
(from April, 1994: Particle Physics and Astronomy Research Council, United Kingdom)

EISCAT ANNUAL REPORT 1993

CONTENTS

	Page
Council Chairman's Page	4
A Summary of the Year	5
Operations	
EISCAT Operations in 1993	19
Common Programme Operations During 1993	23
The Heating Facility	24
Scientific Research and Developments	
Aurora and Substorms	27
High Latitude Convection and Electrodynamics	33
Ionosphere-Thermosphere Coupling	36
Atmospheric Waves and Tides	38
Ionospheric Structure, Irregularities and Modelling	40
Mesosphere	48
Meteor Studies	49
Natural Ion-Acoustic Wave Enhancements	51
Gyro Lines	53
Natural Plasma Lines	53
Ionospheric Modification With Heating Experiments	55
Theory of Measurements	58
Interplanetary Scintillations	61
Appendices	
Publications 1993	
Journals and Books	62
Other Publications, Reports, Theses, etc.	65
EISCAT Reports and Meetings	66
Balance Sheet 1993	67
EISCAT Council, Committees and Senior Staff	68
The EISCAT Associates	Inside back cover
Addresses	Back cover

Annual Report 1993 of the EISCAT Scientific Association

EISCAT Headquarters, Kiruna, Sweden

Finishing and printing by
Institutet för Rymdfysik, Kiruna, Sweden

ISSN 0349-2710

Council Chairman's Page

The year 1993 stands in the history of EISCAT as the time when the EISCAT Scientific Association took the final step to develop a new radar facility on Svalbard. Already on January 1st, 1993, however, EISCAT assumed the responsibility of taking over the Heating facility at Ramfjordmoen from the Max-Planck-Gesellschaft. With this addition, the whole EISCAT community can now fully enjoy the scientific challenges in using the EISCAT radars as diagnostic tools to study the plasma-physical effects of active ionospheric experiments performed with the Heating facility.

On May 22nd a ceremony was held at the top of "Gruve 7 fjellet" close to Longyearbyen on Svalbard, the future site of the EISCAT Svalbard Radar, to celebrate the commencement of the construction phase of this radar. Thanks to exemplary planning and excellent team work, the main building was able to be closed in November to allow further work inside, and the antenna foundations had been made ready for the installation of the antenna in the summer of 1994.

In spite of this extra load on the EISCAT staff, the mainland EISCAT facility has been in regular operation without any great difficulties. This is also clearly apparent from the content of this Annual Report. It is principally by virtue of the staff that EISCAT could take on such a great challenge as to install a new radar in the rather hostile environment of the central Arctic.

The EISCAT decision to expand its activity to Svalbard is a remarkable one when considering the rather difficult economic situation that many of the Associate countries have been through. It is only by a strong belief in the future of EISCAT and convincing arguments for international co-operation in science, that the members of the EISCAT community could succeed in raising the funds needed to allow the Agreement on the Svalbard Radar to be signed on June 29th, 1993.

The work on adapting the original EISCAT agreement and financial rules to the new situation including the EISCAT Svalbard Radar has continued throughout 1993. When this work is completed, EISCAT will also be opened up for the participation of new member countries.

With their unique locations in the auroral zone and the polar cap, the EISCAT facilities with the new radar on Svalbard will represent one of the most advanced research facilities in the field of polar atmosphere research, and will hopefully be an attraction to scientists all around the world to join the scientific work in the EISCAT community.

We are indeed in a very exciting and stimulating period of EISCAT.

Asgeir Brekke

A Summary of the Year

Following several years of preparations and negotiations, the Heating facility at Ramfjordmoen, Tromsø was taken over by the EISCAT Scientific Association on 1 January 1993. The formal ceremony took place at the end of January in the presence of the first Director of EISCAT, Professor Tor Hagfors, who is now Director at the Max-Planck-Institut für Aeronomie. The Heating facility was constructed and operated by the Max-Planck-Institut prior to the take-over.

The Heating facility is used for ionospheric modification experiments applying high power HF transmissions to study plasma parameters. The co-located EISCAT UHF and VHF radars, as well as the digital ionosonde (Dynasonde) are very effective diagnostic instruments for these studies. A short description of the scientific achievements and expectations of these Heating experiments can be found later in this Report. The facility, now operated under EISCAT as the Tromsø Heating Division, consists of 12 transmitters of 100 kW CW power, which can be modulated, as well as 3 antenna arrays covering the frequency ranges 3.85 to 8 MHz. The Heating facility includes a transmitter hall and a building which houses operations, offices and accommodation. Fig. 1 shows the people who attended the take-over ceremony outside the Heating building on 28 January 1993.

Fig. 1 Take-over ceremony of the Heating facility at Ramfjordmoen, Tromsø on 28 January 1993.

In the main building of the Heating facility we have also located the offices of the personnel in charge of the preparations for the EISCAT Svalbard Radar (ESR).

During the year 1993 the Heating facility was used by all EISCAT Associates in a total of 104 accounted hours. Since most of these were together with the UHF and/or VHF radar, a total of 140 hours was charged to the Heating operations.

For the EISCAT radar operations, a grand total of 1653 hours were accounted, which were distributed as follows:

Common Programmes:		
CP-1	118 h	15 %
CP-2	142 h	18 %
CP-3	98 h	12 %
CP-4	110 h	14 %
CP-6	157 h	20 %
CP-7	178 h	22 %
UP	0	0 %
Total:	**803 h**	

Special Programmes:		
Finland	34 h	4 %
France	218 h	26 %
Germany	177 h	21 %
Norway	100 h	12 %
Sweden	96 h	11 %
UK	177 h	21 %
EISCAT	48 h	6 %
Total:	**850 h**	

The accumulated total of Special Programme operations of the Associates over the lifetime of EISCAT is, up to the end of 1993:

Finland	524 h	4.90 %
France	2723 h	25.46 %
Germany	2419 h	22.61 %
Norway	1067 h	9.97 %
Sweden	1097 h	10.26 %
UK	2867 h	26.80 %

Usually, the Common Programmes were run in the dual radar mode: CP-1 (UHF) and CP-2 (UHF) mainly with CP-6 (VHF), and CP-3 (UHF) with CP-7 (VHF). CP-6 and CP-7 operations were usually in the two-klystron mode. CP-4 is a VHF program applying two beam directions pointing North at azimuth angles of 344.7° and 359.5°, and 30° elevation angle. Dual radar operations amounted to 743 hours, the single UHF system to 337 hours, and the single VHF system to 393 hours, respectively. 80 hours of passive operations were performed with the UHF system. All these numbers comprise real operating hours, as against accounted hours used in the tables above. A further break-up of the EISCAT operating time and a summary of the scientific campaigns can be found on pages 19-22.

The Common Programme analysis was performed regularly and all results dispatched as usual to the Associates and the World Day results also to the CEDAR data base. Some problems occurred in the CP-1 alternating code, and in the CP-7 high altitude program. These problems were related to hardware faults, which could be fixed in the meantime. The calibration of Common Programme analysis was regularly done by using the Dynasonde at the Heating facility. The Common Programme summary is shown on page 23.

The technical site affairs were of course governed by the extensive experiment operations, but also maintenance and repair needed substantial attention. Also regular EISCAT staff became more involved in work for the EISCAT Svalbard Radar preparations.

The operation of the Kiruna site was stable. Most of the staff were more or less involved in ESR preparations, besides their work for site system maintenance. The site leader was mostly committed to ESR antenna preparations. Timing, exciter, receiver and SUN workstation hardware and software developments were performed. Tests of GPS time/frequency standards showed acceptable results and proved that we can use such devices to replace the conventional Cesium standards.

The site operations in Sodankylä were fulfilled reliably. Several staff members, in particular the site leader and site scientist, were occupied by preparations of digital hard- and software for the ESR. The antenna hub-room air-conditioning machine in Sodankylä had to be replaced. The Kitinen river water level has reached its final state, but no effects on the antenna have been noticed so far. The new telephone exchange, as part of the Sodankylä Geophysical Observatory system, is in use. The site buildings were transferred from the Observatory to the Finnish National Building Board (Rakennushallitus), and the renovation of site offices has begun.

Some peculiar interference was observed on 929.25 MHz in Kiruna and Sodankylä. It seems likely that this could be due to harmonics of satellite-borne transmissions. There is also increased interference resulting from snow scooters and cars close to the Kiruna site, which we are trying to minimise. The complications caused by the mobile telephone systems in northern Scandinavia have not increased during this year.

At Tromsø site the interference is mainly to the VHF system, partially due to television channel 11 transmissions and partially due to local communication on 224.725 MHz. This results in the restriction of the EISCAT VHF radar operation to a few channels only. The matter on the disturbance of a neighbour at Ramfjordmoen caused by the EISCAT radar transmissions has been settled during the year. There are continuous endeavours necessary to keep track of minor interference reports and to modify equipment of other neighbours, which is affected by the transmissions. We also reached a proper mutual arrangement with the users of the horse-race track, which was constructed close to the Heating antenna field.

The VHF transmitter was operating reliably. In the two-klystron mode it is tedious to keep both transmitter sides at the same output power level. Both klystrons have been run successfully for a total of more than 3000 hours each. It is now also possible to run VHF experiments with two milliseconds pulse length, which improves the long-range observations, for instance those with Common Programme Seven.

The second UHF klystron, which was rebuilt by the Varian company and run at 2 MW in the factory, was not accepted because of higher order mode oscillations and localised heating. It was to be shipped to Tromsø after modifications at the end of 1993. The UHF klystron in the transmitter performed reliably and had accumulated more than 8500 beam hours. During the time when the second klystron was not available, this klystron was safe-guarded by running it at slightly reduced power.

The UHF antenna sub-reflector in Tromsø had lost small parts of its surface and was provisionally repaired in December using conductive paint. Since similar problems were not observed in Kiruna and Sodankylä, it must be assumed that the sub-reflector surface was destroyed by the high power density during transmission. It is planned that a total repair or replacement of the sub-reflector should be done as soon as possible.

During a major wind storm in early January some reflector panels of the VHF antenna were torn off and blew away. The reflector surface could be replaced quickly. At the beginning of summer a high-power coaxial cable connecting the VHF antenna to the transmitter burnt and affected also a rotary joint. This resulted in the availability of only one VHF transmitter side over an almost two months period. The cable and rotary joint were soon repaired after the replacement parts were received at the site. The VHF antenna servo system and almost all of the dipoles of the antenna feed have now been serviced. Manual phasing of the VHF antenna to steer one half of the antenna in azimuth was done for certain experiments, such as Common Programme Four and some Special Programmes.

The computing systems were adapted and improved at all sites and Headquarters. At Kiruna site a local Ethernet was implemented and the network at Headquarters was expanded. At Tromsø the computer network had been extended by an optical fibre link to the Heating/ESR office and the Tromsø University building. A direct connection to the Internet became possible. A local area network was introduced at the Heating/ESR office building. Several new SUN workstations were acquired, which are essential development tools for the ESR software design. All sites and Headquarters are now equipped with networked workstations, PCs as well as the aging ND computers. A UNIX course was held in October for all EISCAT personnel involved in computing. The data archiving of the EISCAT radar systems as well as the Dynasonde on Exabyte and DAT tape was further advanced. However, data copies are still available on the standard 6250 bpi tapes.

Updated procedures for EISCAT Special Programme experiments were issued in March, introducing the new experiment accounting system, which handles the use of the Heating facility and dual-radar operation. Many campaigns and Special Programme operations were successfully performed, such as observations of polar F-layer patches, quiet auroral arcs and pulsating aurora, plasma line tracking and gyro-line studies, passive observations for studies of interplanetary scintillations, investigations of polar mesosphere summer echoes in the NLC-93 campaign, meteor echo studies, topside-ionosphere observations, as well as coordinated observations with the UARS and Freja satellites. Also the first experiments with the multi-channel finite impulse response filter and integrator device (MUFFIN), designed at the Sodankylä site, were successfully carried out with the VHF system in the beginning of August.

Due to the involvement of many EISCAT staff members in the preparation and design of the EISCAT Svalbard Radar, the further evolution of the EISCAT systems in Kiruna, Sodankylä and Tromsø was decided to be paused, but repair work still should be done with priority. As summarised in this report, the EISCAT Radar and Heating systems had suffered several breakdowns, which usually could be restored in due time and a sufficiently large number of operating hours could be achieved.

The major events of the year 1993 were of course governed by the EISCAT Svalbard Radar project. Following the years of preparations on the technical, organizational and funding procedures, the Agreement on the Svalbard Radar was signed in 1993.

AGREEMENT ON A SVALBARD RADAR

The Associates of the EISCAT Scientific Association

Suomen Akatemia, Finland
Centre National de la Recherche Scientifique, France
Max-Planck-Gesellschaft, Federal Republic of Germany
Norges forskningsråd, Norway
Naturvetenskapliga forskningsrådet, Sweden
Science and Engineering Research Council, United Kingdom

- agree to develop and operate a radar facility on Svalbard, called the EISCAT Svalbard Radar (ESR) in accordance with the plans summarized in the enclosed Proposal (Enclosure 1), where the contributions of the Associates during the years 1992 to 1996 are given in Table 6;

- agree to operate the existing EISCAT radar facilities with the reduced resources summarized in Enclosure 1, Section 5;

- agree to modify the EISCAT Agreement, Statutes and related documents in order to allow additional Associates into the Association, and so that the basis for calculating the observing time available to each Associate will continue to reflect the total contribution of each Associate to the construction and operation budget of the present EISCAT and the EISCAT Svalbard Radar (as described in Enclosure 1);

- agree that this Agreement shall come into force as soon as all Associates have signed it.

The Agreement on a Svalbard Radar, signed by the EISCAT Associates in the year 1993. (The referenced enclosures and tables are part of the Agreement and not included in this report).

On 29 June 1993 this Agreement had been signed by all six EISCAT Associates and was filed at EISCAT Headquarters. This resulted also in a careful adjustment and revision procedure of the EISCAT Agreement and Statutes. One of the main revisions is for instance the adjustment of the time share, which is based on the total contributions to the EISCAT operations in Kiruna-Sodankylä-Tromsø and the EISCAT Svalbard Radar. According to a special formula, these should in future be, when the EISCAT Svalbard Radar is operational: Finland 6%, France 22%, Germany 21%, Norway 14%, Sweden 12%, and United Kingdom 25%.

Fig. 2. The EISCAT sites and Svalbard. Circles around the poles (GP, MP) indicate boundaries of daytime auroral observations in winter and the footprint of the magnetospheric cusp at noon.

Magnetospheric cusp observations are some of the most essential reasons for initiating the EISCAT Svalbard Radar (ESR). On this map (Fig. 2) of the Arctic the bold circles indicate the geographic pole (GP) and the magnetic pole (MP). The circles around these poles represent the boundary accessible to daytime auroral observations in winter and the ionospheric footprint of the magnetospheric cusp. It is noted that the location of the EISCAT Svalbard Radar is ideal for combined radar and optical observations of the polar ionosphere and cusp region.

The preparations of the EISCAT Svalbard Radar project have been ongoing for the past five years and the history can be found in descriptions published in earlier EISCAT Annual Reports. The scientific needs and the corresponding technical specifications (see table opposite) had been very carefully designed to suit the scientific user requirements in an optimum way, taking into account the limited funds available for this project.

The completion of the signature of the Agreement on a Svalbard Radar by the EISCAT Associates in June 1993 was immediately followed by the signature of the major contract of this project: the design, construction and erection of the antenna by Kamfab, Karlstad, Sweden. The contract is a result of several thorough meetings and it incorporates an optimised strategy. An Antenna Design Presentation Meeting was held at the end of July in Risø, Denmark, where the main subcontractor of Kamfab, the Nordic Telescope Group (NTG) has its offices. The Final Design Review Meeting was held in the middle of October in Karlstad, when details of the antenna design were presented to EISCAT and in principle accepted. The antenna should be erected on Svalbard in summer 1994. The project manager for the ESR antenna design, Dr. Torben Andersen (NTG), was invited to give a presentation on the antenna project at the EISCAT Council meeting in November 1993 in Hamburg.

Baseline work for design and construction of the ESR receiver, digital signal processing, time keeping, control and monitoring was in appropriate progress. As an example, the basic lay-out of the receiver is shown in Fig. 3. EISCAT personnel at Sodankylä, Kiruna and Tromsø sites are involved in this work. The design specifications and construction of the ESR instrumentation are performed under the direction and supervision of the Deputy Director Technical. The ESR Baseline Description Document, updated and compiled by the Deputy Director Science, was issued in March 1993. The first transmitter module (250 kW), which was ordered from Harris TVT, Cambridge, UK in November 1992, was successfully tested in-plant at the end of July 1993, then shipped to Tromsø for temporary installation and careful tests. These were performed during the following winter under the supervision of the ESR radar engineer. The second module and klystrons were ordered at the end of September 1993 for delivery to Svalbard in spring 1994 (see Fig. 4 for installation plan). This set-up will provide a peak output power of 500 kW.

The EISCAT Svalbard Radar
System Specifications 1993

	Location: 78°09'N, 16°03'E	near Longyearbyen on Spitsbergen, Svalbard
Operating Frequency:		500 MHz
Bandwidth:	Transmitting: Receiving:	± 2 MHz ± 10 MHz
Antenna:	Parabolic dish: Beamwidth: Gain: Aperture: Polarization: Steerability:	one (upgradable to >1) 1.6° (one-way) 42 dBi ≈ 500 m² circular all azimuths, 5-175 degrees elevation
Transmitter:	Peak Power: Average Power: Tubes: Pulse Length: Modulation: Interpulse: Radar controller: Program memory:	0.5 MW, modular system (upgradable to 1MW) 0.125 MW TV-klystrons 1 µs - 2 ms amplitude and phase coding min. 0.1 ms address space 20 bits 1 MW memory 32 bit control word with 100 ns resolution
Receiver:	Dual superheterodyne Noise temp.: System Temp.: IF: Output channels: ADC: Complex digital mixer and filter: Digital multiplier: FIR filter:	≤ 20 K ≤ 100 K 70 MHz ± 5 MHz up to 4 10 MHz min. 12 bit min. 10 MHz bandwidth 10 MHz data rate 16 bit coeff. accur.
Digital Signal Processing:	Bus environment: Host processor: Lag profile proc.: Input data format: Output data format: Processing rate:	Narrow- and wide-band VME Sparc or 68040 TMS 'C40 16+16 bit complex 32+32 bit complex 30 MOPS/channel
Total System Figure of Merit:		Peak Power x Aperture per System Temp.: 2.5 MW m²/K

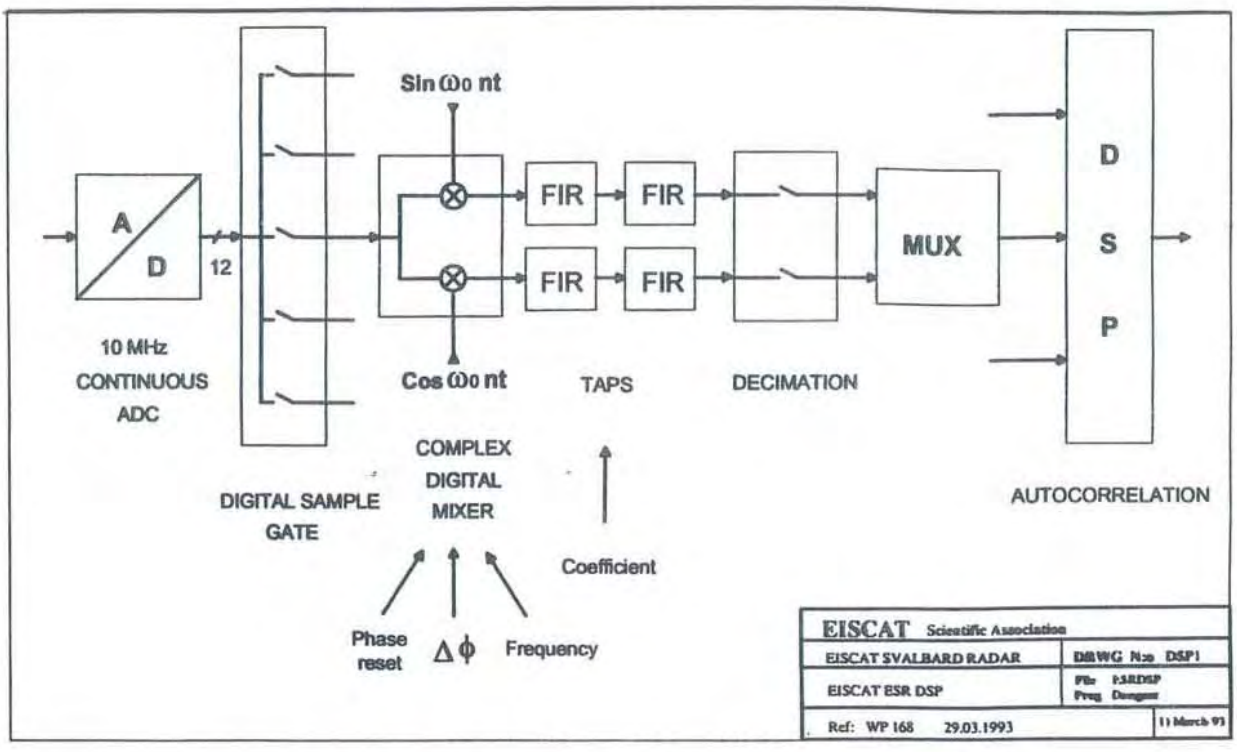

Fig. 3. Block diagram of the digital part of the EISCAT Svalbard Radar Receiver.

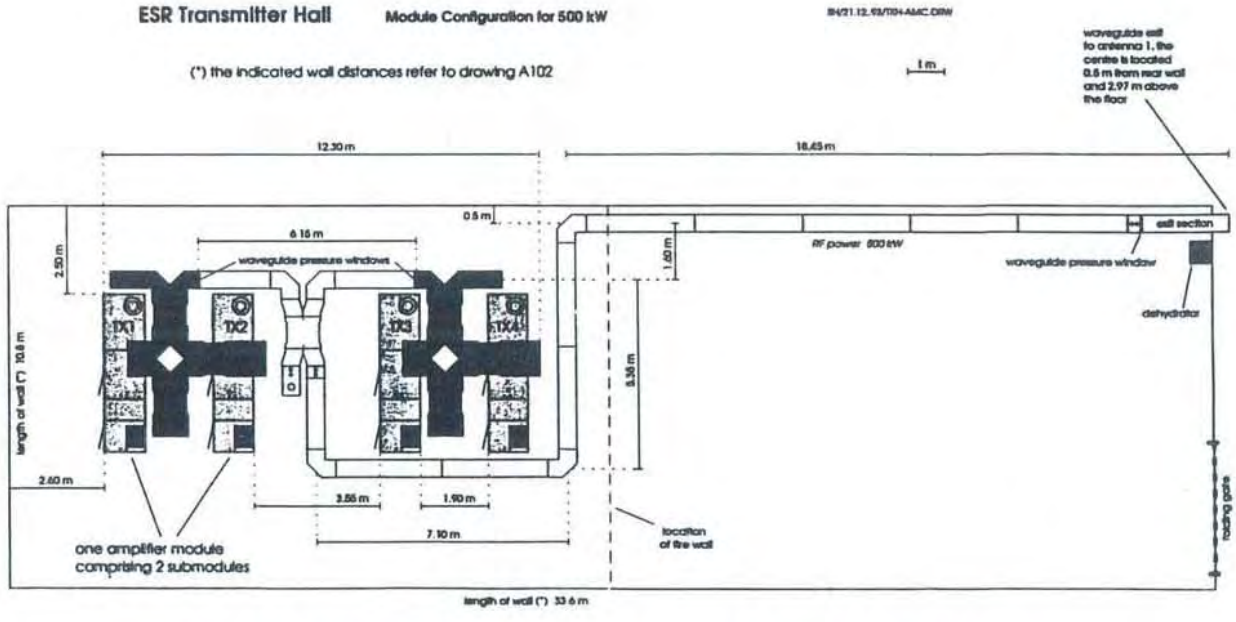

Fig. 4. Lay-out of the two transmitter modules, yielding 500 kW peak output power, to be installed in 1994/1995 in the hall at the EISCAT Svalbard Radar site.

A new pattern for the ESR hardware software-user interfacing, introducing two basic levels numbered 1 and 2, was proposed and adopted as a working basis. This layout was recommended to precede the advanced definitions of the system software, applications software and the user software. The system software and the specialised applications software allowing the provision of basic data at the Level 1 operation are to be provided by EISCAT. Level 2 will include the analysis, experiment preparation and performance part, interfacing the system with the users at the final stage and was planned as in-kind contribution from Associates. A substantial part of the Level 2 software development, in particular related to the experiment preparation and data analysis, will be done as in-kind contribution by Finland. Particular agreements for this purpose had correspondingly been arranged with the Suomen Akatemia. Another proposal for user software development was received by EISCAT from the UK at the end of October 1993.

The Scientific Advisory Committee (SAC) had adopted the modified GUISDAP scheme as well as an adapted MIDAS system for the purpose of Level 2. In order to streamline these developments and the interface to the system, the ESR Software Project Group (ESPG) had been formed by the SAC. The Director had taken the responsibility to coordinate the activities of this ESPG, which held a first meeting on 18-19 November 1993 in Hamburg.

The ESR site near Longyearbyen on Svalbard was opened on 22 May 1993 by the Norwegian minister for Research, Education and Church, Gudmund Hernes, who unveiled a plaque showing the new EISCAT logo (Fig. 5) in the presence of the Svalbard governor, distinguished Norwegian representatives and members of the EISCAT Council and executive. This logo is not vastly different from the original one, and just indicates the combination of the three EISCAT sites and the new ESR on Svalbard. The road and building construction at the site began in May 1993 (Fig. 6), as soon as the permissions from the Norwegian administrations had been received and the construction contracts with the main companies Barlindhaug Utbygging in Tromsø and Veidekke Rothing in Haugesund, Norway, had been signed. The infra-structure preparations and on-site work on Svalbard were progressing quickly. The road from the mine to the site had been completed in the summer by the Store Norske Spitsbergen Kulkompani (SNSK). The antenna and building foundation (Fig. 7) had been cast in July. All building material had been shipped to Longyearbyen soon after the first ship was able to reach Longyearbyen after the winter. The main building construction was basically finished in November 1993 (Fig. 8), when the internal work started. Several further contracts had been prepared and signed, or letters of intent been forwarded for this purpose. Work on electric power connections, frequency clearance, etc. on Svalbard as well as preparation of installing the air warning radar on the antenna made significant progress. The agreement with SNSK on provision of land for the ESR had been negotiated and was prepared for signature.

The ESR project work breakdown structure was regularly adjusted according to demands and developments. A notable number of regular EISCAT staff members is involved in the project. We note a lot of enthusiasm on the ESR project, although we have to regard the potential overload of certain staff members working on too many diversified tasks. This holds in particular for those who are responsible for continuing EISCAT operation as well as certain work packages or tasks of the ESR project. The coordination of the project was not an easy undertaking for management and staff. The reason is at least two-fold: the twin-responsibilities of several staff members working on the ESR and the regular EISCAT, and the fact that the work for ESR has to take place at separated locations, namely Kiruna, Tromsø, Sodankylä and Longyearbyen, notwithstanding the contacts to companies.

To control and coordinate the ESR project, regular management meetings (MM) were held:

MM-05	19 January	1993	EISCAT HQ
MM-06	4 March	1993	EISCAT HQ
MM-07a	22 June	1993	EISCAT HQ
MM-07b	15 July	1993	Tromsø site
MM-08	16-17 September	1993	EISCAT HQ
MM-09	9-10 November	1993	EISCAT HQ
MM-10	8- 9 December	1993	EISCAT HQ

The management meetings in March and September were combined with short executive and budget meetings regarding the common site operations. In addition many trips between the sites, Headquarters as well as Longyearbyen were performed by staff and the directorate. A most complete ESR filing system is being installed at Tromsø and Headquarters, which, however, will take a while to be fully congruous. During the auditor's visit to Headquarters in September a general overview was given and agreement was found on the way to record investment and recurrent expenditures for the EISCAT Svalbard Radar. A particular call-up from the Associates for the new ESR funds had been established and the total status is recorded regularly. In order to prepare the staff for the necessary installation and operation missions of the ESR, which will commence in the coming year, the Annual Review Meeting of 1993 was combined with the 1994 meeting to be held in the beginning of March 1994 in Longyearbyen. We started also considering possibilities how to accommodate staff during these installation, test and operation periods on Svalbard.

In July the initial version of the EISCAT Svalbard Radar Brochure was published. An updated version was edited in September, and a final version was issued at the end of the year. Fig. 5 shows the photograph, which became the basis for the cover of the ESR brochure.

Fig. 5. On 22 May 1993 the site of the EISCAT Svalbard Radar was opened close to mine 7 near Longyearbyen.

Fig. 6. A view of the ESR site on the opening day with a mock-up of the antenna inserted.

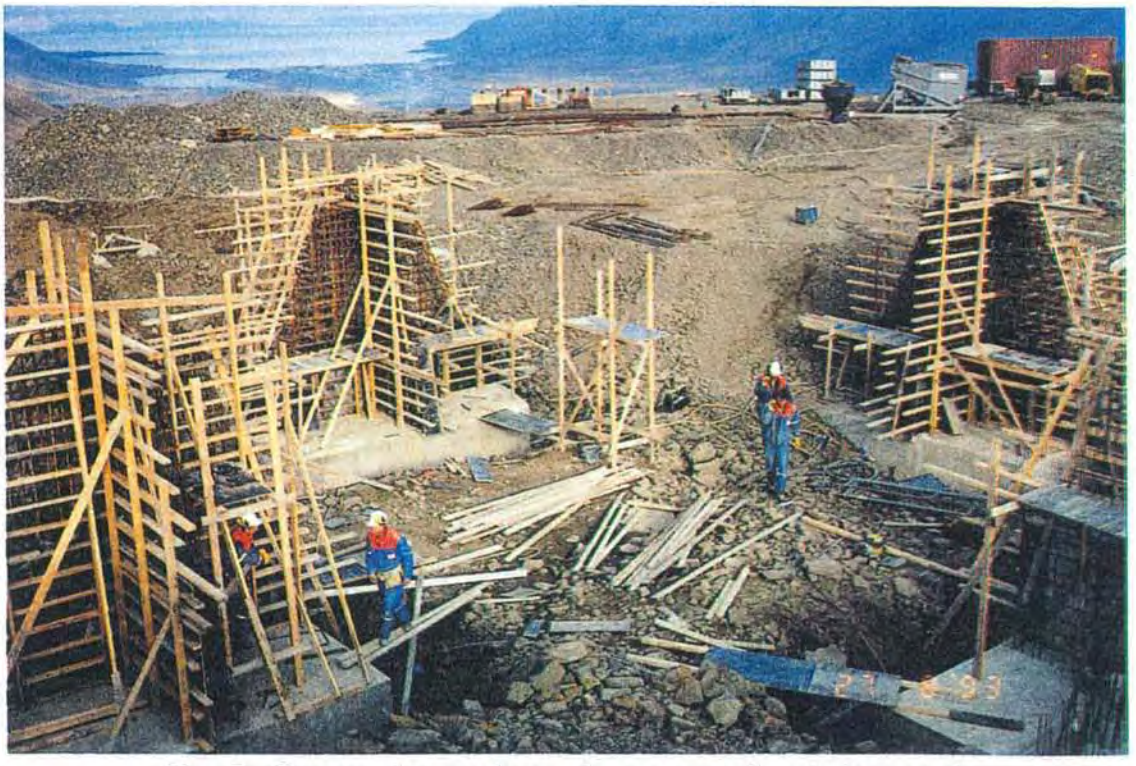

Fig. 7. Construction work on the antenna foundations at the EISCAT Svalbard Radar site on 27 August 1993.

Fig. 8. The EISCAT Svalbard Radar operations building on 5 November 1993. On the left-hand side the four cornerstones of the antenna foundations can be seen.

The EISCAT Svalbard Radar project has found a wide international interest. For several years contacts between EISCAT and the Solar Terrestrial Environment Laboratory (STEL) of Nagoya University have grown to prepare a joint venture between EISCAT and Japan to obtain funds for a second antenna for the EISCAT Svalbard Radar.

During the General Assembly of the International Union of Radio Science (URSI), which was held at the end of August 1993 in Kyoto, Japan, an exhibition stand "ESR - International Collaboration" was prepared by the STEL of Nagoya University and EISCAT. This permitted a proper advertisement of the ESR project to the scientific community and displayed the intentions of Japan to join EISCAT and participate in the experiments with the EISCAT Svalbard Radar. During this conference Prof. Tudor B. Jones, EISCAT Council member and one of the strongest supporters of the EISCAT Svalbard Radar, was honoured by URSI in receiving the Appleton Prize for significant contributions to the field of ionospheric physics.

After the URSI General Assembly the EISCAT Council Chairman, the Director and the Council member Prof. Kangas were received by the President of Nagoya University. The President and the Administrative Director of the University expressed great interest in the ESR project. Following this meeting, the Director and the Council Chairman, together with the Director of STEL and the project leader Prof. Matuura, met the Director for International Affairs at the Japanese Ministry for Education (Monbusho). They introduced the ESR project together with expressing EISCAT's view to see Japan as a welcome partner in the Association. Both meetings were regarded as very useful and more detailed reports will be given at the Council meeting. The proposal by the Solar Terrestrial Environment Laboratory at Nagoya University for the second ESR antenna and additional operations costs was approved by Nagoya University.

Personnel Dec.1993	Kiruna Headq.	Kiruna Site	Sodankylä Site	Tromsø Radar	Tromsø Heating	Tromsø ESR
Directing:	2	-	-	1	-	-
Scientific:	1	-	1	2	1	-
Engineer.:	-	4	3	7	2	2
Computing:	2	1	1	1	-	1
Admin.etc.:	5	-	-	3	-	1
Total:	10	5	5	14	3	4
Budget expenses in 1993						
Recurrent chapter in MSEK	6.41	2.40	2.32	8.30	1.72	3.39

Total spent in 1993:

Recurrent chapt. (total): 25.06 MSEK (incl. Council and Committee meetings and ESR)

Capital investm. (KST): 4.99 MSEK (+ 4.64 MSEK total transfer for evolution)

Invest. + recur. (ESR): 31.37 MSEK

This table summarises the staff complement and the annual expenses for the operation of the KST sites, as well as the investments for these operations and the EISCAT Svalbard Radar.

The staff development of EISCAT was in general stable. On the average one third of the staff was working for the ESR project. The positions of the Heating technician, the Tromsø staff scientist and the administrative assistant in Tromsø were filled. Also personnel for the ESR design work were installed: the software engineer, the system integration engineer and the systems programmer. The ESR project administrator position was converted into a project consultant. In December 1993 the head of computer operations, Dr. Stephan Buchert, left EISCAT. Dr Buchert had over the years of his work at EISCAT HQ contributed substantially to the growth of EISCAT and the initial design of the ESR digital system.

The funding contributions of 20.27 MSEK were received from the Associates for the normal Kiruna-Sodankylä-Tromsø operations. In addition 38.14 MSEK were received in 1993 from the Associates for the construction of the EISCAT Svalbard Radar.

My thanks are again directed to the dedicated staff of EISCAT, who took great care to keep the whole system in a reliable shape for continuing scientific experiments together with performing an excellent job for the preparations and construction of the EISCAT Svalbard Radar - the evolution of the EISCAT Scientific Association.

Jürgen Röttger

Sixth EISCAT Scientific Workshop

Sept. 27th. – Oct. 1st., 1993, Andenes, Norway

INTRODUCTION

The number six has a special significance for EISCAT. It is no mere coincidence that the Sixth EISCAT Scientific Workshop in some ways closes a chapter—and consequently opens a new one—in the history of EISCAT. We have now gone full circle with all associates having hosted one workshop. A review of the attendace to the six workshops (see the last page of this book)—not to mention the published Proceedings—shows a community full of vitality. It is significant that the closing of this EISCAT cycle is coincident with the opening of new research horizons in the development of EISCAT, namely the construction of the EISCAT Svalbard Radar. All the right conditions seem at present to be converging to make the next EISCAT workshop cycle even more fruitful and exciting, and, we all hope, of a longer period than the cycle we just completed. After all there is nothing magic about the number six.

The final count for this Workshop is 96 participants and 88 papers of which 71 are oral and 17 posters. The number of oral papers has been constrained entirely by the available time and the duration of each talk of 20 minutes. We are convinced that this quantitative success will be surpassed by the science achieved.

As you know, the Workshop Proceedings will be published in a special issue of the Journal of Atmospheric and Terrestrial Physics. It is our intention to encourage the publication of all the scientific papers presented at this Workshop. We need the cooperation of every one of you, authors and otherwise (as reviewers), so that the review and publication processes can be done in an efficient and timely manner. We suggest Jan. 15th 1994 the deadline for submission of manuscripts. However, we wish to have your input on this and other related matters, so please take the time to fill out the form provided with the registration material and turn it in before the end of the Workshop.

This Workshop would not have been possible without your enthusiastic attendance and without the help from the Andøya Rocket Range, Andrikken Hotel, the Andøya Municipality, the EISCAT Tromsø site and the Norwegian Research Council.

The Sixth EISCAT Scientific Workshop was held in October 1993 in Andenes, Norway. The meeting was convened by the University of Tromsø in collaboration with the Andøya Rocket Range and the EISCAT Tromsø site. The introduction above appears in the program booklet prepared by the organising committee.

EISCAT OPERATIONS IN 1993

For 1993, 200 hours were added to the pool of Special Programme hours to be used primarily for Heating campaigns. These hours, however, are interchangeable with UHF/VHF radar hours and add up to a total reservoir of 1700 hours for Common and Special Programmes in 1993. Out of these, 1653 were used; 803 hours on Common Programmes and 850 hours on Special Programmes as shown in the spreadsheet on page 20. The dual radar operation amounted to 1008 accountable hours, the UHF radar 280 hours and the VHF 352 hours. Heating alone accounted for 13, but embedded in the radar hours are 134 hours associated with the Heating facility. Passive experiments represented 20 hours of UHF use.

The upper panel on page 20 shows the distribution of Common Programmes in 1993. Highlights and changes from 1992 include the following features.

The CP-1 experiment changed from version J to K in that the Sodankylä and Kiruna antennas do not scan, but take measurements continuously from the F-region at 279 km altitude. The post-integration time for standard analysis was changed from 5 minutes to 2 minutes in order to take advantage of the better performance of the recently-introduced alternating-code modulation scheme. A new version of the CP-3 experiment, CP-3-G, was implemented, where the scan was reversed from the original north-south motion in order to make the scans more closely follow constant local time. Two-klystron CP-6 and CP-7 versions continued, including a test of a 2 msec version of the CP-7.

In January, a 5-day run of CP-2 and CP-6 was scheduled to cover the MLTCS campaign, which continued for another 5 days with Special Programmes. The 6 hours of CP-1 in January are the result of a failure in one of the antenna elevation drive motors which caused a change in experiments from the scanning CP-2 to the stationary CP-1. Calibration measurements using the Heating facility were performed both in May and November.

As shown in Fig. 9, April, May, and June were relatively quiet months for operations, whereas peak activity occurred in the winter months, between September and March. Dual radar operations now represent a large fraction of the total operation. However, single radar operations are often also co-ordinated with optical instruments, satellites and rockets.

The lifetime total of operations of the EISCAT Associates is shown in Fig. 10. The deviation from their allocated percentage (FR, GE and UK 25%, NO and SW 10% and FI 5%) is only a few percent.

The Special Programmes in 1993 were run on the basis of a huge variety of scientific objectives. Many of the results are described later in this report, but some of the objectives can be mentioned here. These included plasma convection south of Svalbard, auroral arc formation, pulsating auroras and H^+ and O^+ outflows, ion acoustic wave instabilities, plasma line studies for the detection of field-aligned currents, use of the chirp to obtain the necessary time and frequency resolution, gyro lines (particularly to distinguish them from meteor showers), polar mesospheric summer echoes with a special focus on the role of charged particles, including fine structure by spatial interferometry, and morphology and drifts in conjunction with rocket determination of in situ parameters.

Passive observations were used for investigation of the solar wind close to the Sun using the interplanetary scintillation technique.

The Heating facility was involved in the comparison of chirp and standard techniques to determine the altitude of the excited region, comparison of natural and heater-induced plasma lines with the chirp technique, large scale heating of the ionosphere (together with Dynasonde operation) for aeronomy purposes using the artificial periodic irregularity technique, excitation of ULF/VLF signals (Alfven maser), the modulation of D- and E-region conductivity, simultaneous observations of HF enhanced radar spectra and stimulated electro-magnetic emissions, and determinations of the levels of electron temperature and density modulation during modulated RF heating for a variety of geophysical conditions in the E-region.

COMMON PROGRAMMES 1993

	Jan	Feb	Mar	Apr	May	Jun	Jul	Aug	Sep	Oct	Nov	Dec	Tot	%
CP1	6	28		36			18			30			118	15
CP2	107					35							142	18
CP3			28		34						36		98	12
CP4									50			60	110	14
CP6	56					18	8		60	15			157	20
CP7		14	13	18	17						76	40	178	22
UPs														
Total	169	42	41	54	51	53	26		110	45	112	100	**803**	100 %
%	21	5	5	7	6	7	3		14	6	14	12	100 %	

Achieved						Target					
CP1	CP2	CP3	CP4&CP5	CP6&CP7	UPs	CP1	CP2	CP3	CP4&CP5	CP6&CP7	UPs
15	18	12	14	42		16	16	12	10	38	8 %

SPECIAL PROGRAMMES 1993

	Jan	Feb	Mar	Apr	May	Jun	Jul	Aug	Sep	Oct	Nov	Dec	Tot	%
EI				1		2	6	7	1		31		48	6
FI	15							4	5		10		34	4
FR	30		86				5	1	2	34		60	218	26
GE	20		63		7			20	18	35	14		177	21
NO	42	11					21	16		10			100	12
SW		35					22	21	1		17		96	11
UK	37	40					9	1	2	67	21		177	21
Total	144	86	149	1	7	2	63	70	29	146	93	60	**850**	100 %
%	17	10	18	0	1	0	7	8	3	17	11	7	100 %	

EI	FI	FR	GE	NO	SW	UK		
6	4	26	21	12	11	21	100 %	(of 850 hrs)
5	4	23	19	11	10	19	89 %	(of 950 hrs)

The upper box shows the distribution of EISCAT Common Programme operations for 1993 by month and programme type. The lower box shows the distribution of EISCAT Special Programme operations for 1993 by month and Associate. Also shown is the proportion of the total Special Programme time used by each Associate.

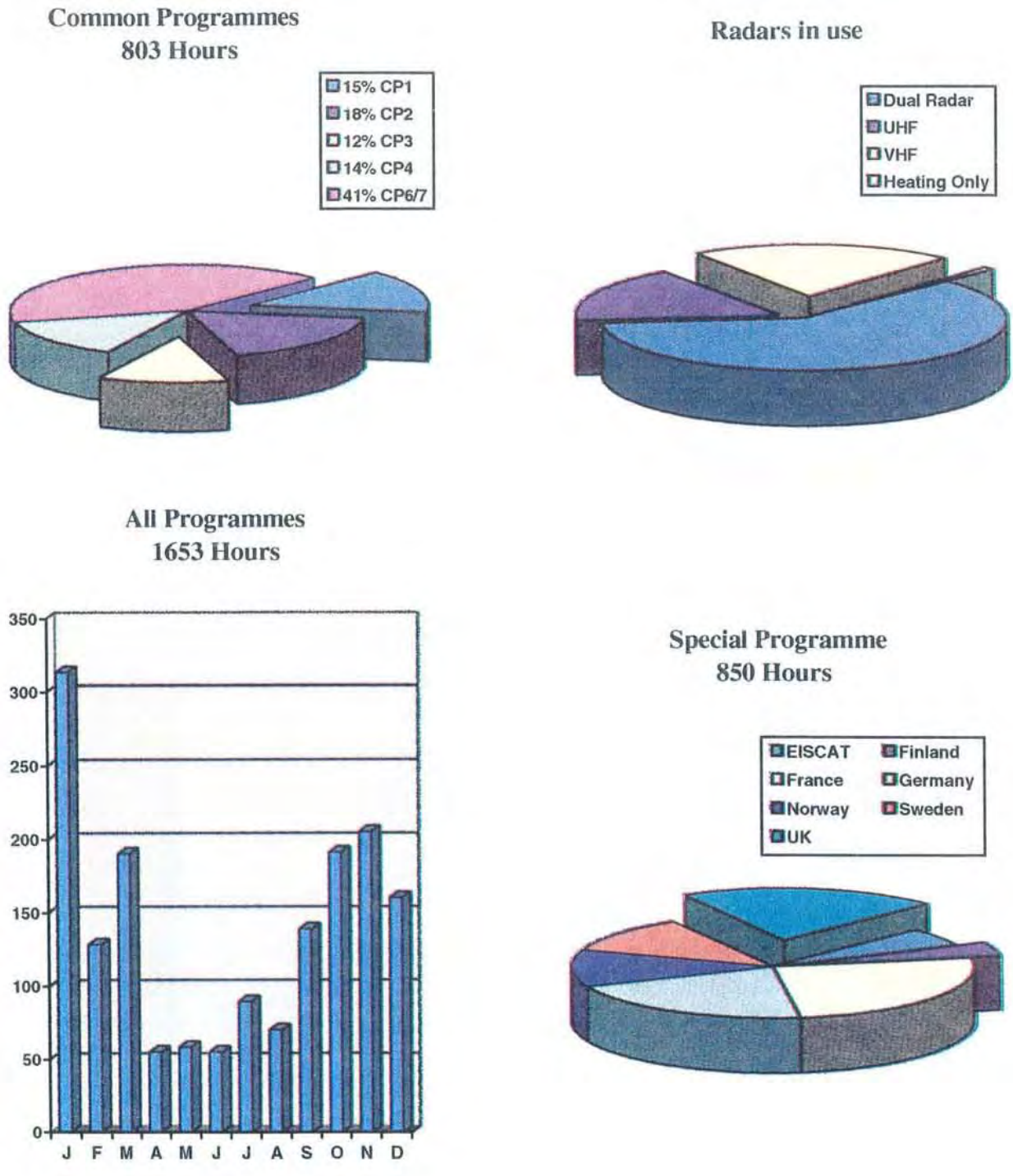

Fig. 9. Total EISCAT Common and Special Programme operations in 1993 distributed by programme (upper left) and Associate (lower right). The other panels show the monthly distribution of total operating hours (lower left) and the dual and single radar hours (upper right).

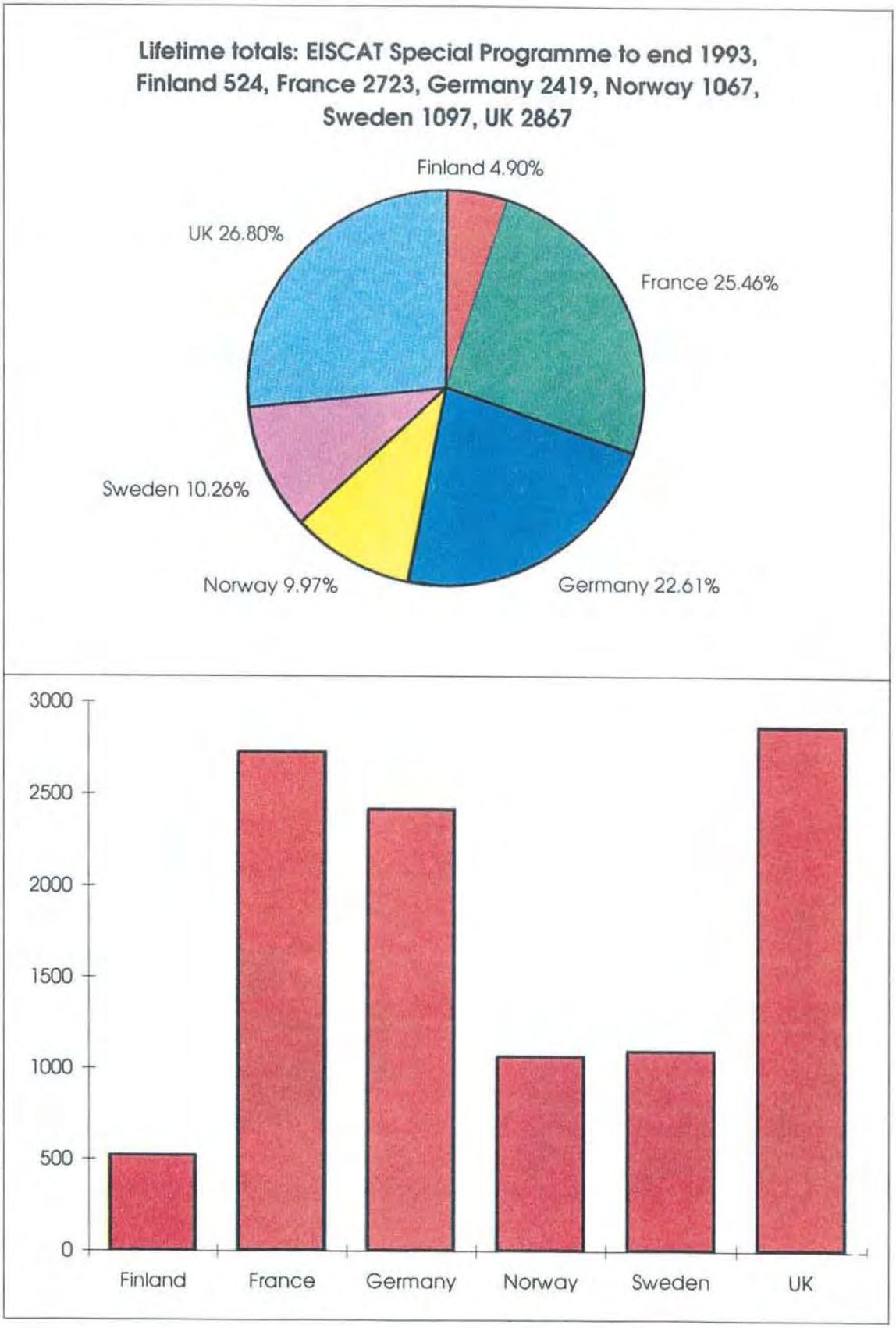

Fig. 10. Lifetime total (in hours) of Special Programme operations up to the end of 1993.

COMMON PROGRAMME OPERATIONS DURING 1993

UHF Common Programmes

START		END			
date	time	date	time	expt	
93-01-20	16UT	01-25	10UT	CP-2-E	WD
93-01-25	16UT	01-25	22UT	CP-1-J	WD
93-02-16	10UT	02-17	22UT	CP-1-K	
93-03-17	16UT	03-18	22UT	CP-3-G	WD
93-04-20	10UT	04-21	22UT	CP-1-K	
93-05-18	12UT	05-19	22UT	CP-3-G	WD
93-06-15	09UT	06-16	22UT	CP-2-E	WD
93-07-20	22UT	07-21	22UT	CP-1-K	WD
93-10-18	14UT	10-19	23UT	CP-1-K	WD
93-11-09	11UT	11-10	23UT	CP-3-G	WD

VHF Common Programmes

START		END			
date	time	date	time	expt	
93-01-20	16UT	01-25	22UT	CP-6-B	WD
93-02-16	10UT	02-17	22UT	CP-7-E	
93-03-17	18UT	03-18	22UT	CP-7-E	WD
93-05-18	12UT	05-19	22UT	CP-7-E	WD
93-06-15	08UT	06-16	22UT	CP-6-B	WD
93-07-20	22UT	07-21	22UT	CP-6-B	WD
93-09-14	09UT	09-16	22UT	CP-6-B	
93-09-28	09UT	09-30	11UT	CP-4-B	
93-10-18	14UT	10-19	23UT	CP-6-B	WD
93-11-09	11UT	11-10	23UT	CP-7-E	WD
93-12-04	15UT	12-06	05UT	CP-7-F	
93-12-07	06UT	12-09	18UT	CP-4-B	WD

Overview of EISCAT Common Programme experiments during 1993. WD indicates a World Day operation, the results from which are sent to the CEDAR data base at NCAR in Boulder, USA.

Operating Modes Employed in 1993

Common Programme One, CP-1, uses a fixed transmitting antenna, pointing along the geomagnetic field direction. The three-dimensional velocity and anisotropy in other parameters are measured by means of the receiving stations at Kiruna and Sodankylä (see map, inside front cover). CP-1 is capable of providing results with very good time resolution and is suitable for the study of substorm phenomena, particularly auroral processes where conditions might change rapidly. On longer time scales, CP-1 measurements support studies of diurnal changes, such as atmospheric tides, as well as seasonal and solar-cycle variations. The present scheme uses alternating codes and long pulses for ACF measurements, as well as short pulses for power profiles.

Common Programme Two, CP-2, is designed to make measurements from a small, rapid transmitter antenna scan. One aim is to identify wave-like phenomena with length and time scales comparable with, or larger than, the scan (a few tens of km and about ten minutes). The present version consists of a four position scan which is completed in six minutes. The first three positions form a triangle with vertical, south and south-east positions, while the fourth is aligned with the geomagnetic field. The remote site antennas provide three-dimensional velocity measurements in the F-region. The pulse scheme is identical with that of CP-1.

Common Programme Three, CP-3, covers a 10° latitudinal range (in the F-region) with a 17 position scan up to 74°N in a 30 minute cycle. The observations are made in a plane defined by the magnetic meridian through Tromsø, with the remote site antennas making continuous measurements at 275 km altitude. A power profile and long pulse ACFs are measured.

Common Programmes One to Three are run on the UHF radar. Three further programmes are designed for use with the VHF system. When applicable, it is increasingly common practice to have operations with one UHF and one VHF experiment running simultaneously.

Common Programme Four, CP-4, covers latitudes up to almost 80°N (77°N invariant latitude) using a low elevation, split-beam configuration. CP-4 is particularly suitable for studies of high latitude plasma convection and polar cap phenomena.

Common Programme Six, CP-6, is designed for low altitude studies, providing spectral measurements at mesospheric heights. Vertical antenna pointing is normally used.

Common Programme Seven, CP-7, probes high altitudes and is particularly aimed at polar wind studies. The present version uses both of the VHF klystrons and is designed to cover altitudes up to 2500 km vertically above Ramfjordmoen.

THE HEATING FACILITY

The Heating facility, originally built by the Max-Planck-Institut für Aeronomie in co-operation with the University of Tromsø, started operation in 1981. The facility generates up to 1.2 MW of CW power in the frequency range from 3.85-8 MHz with twelve linear class-AB tetrode amplifiers each of 100 kW driven by a solid state wideband exciter. The low level RF signals are generated by twelve frequency synthesisers under computer control. The output from the transmitters is switched to one of three antenna arrays using remotely-controlled co-axial switches in the feedlines. Fig. 11(a) (taken from Rietveld et al., 1993) shows a schematic diagram of the layout of the three antenna arrays.

Two of the antenna arrays are used to cover the frequency ranges 4 - 5.5 and 5.5 - 8 MHz respectively. They consist of 6 x 6 crossed full-wave dipoles giving a total gain of 24 dBi, a beam width of 14.5° and an effective radiated power of 300 MW. One pair of transmitters feeds one east-west aligned row of antennas as outlined in Fig. 11(b). The modular nature of the transmitters and their synthesisers allows the radiation pattern to be tilted in the north-south plane by up to about 30° from the zenith using electronic steering.

A third antenna was rebuilt in 1990 to cover the frequency range 5.5 - 8 MHz using 12 x 12 dipoles to give a gain of 30 dBi, a beam width of 7° and an effective radiated power of 1.2 GW. To date this represents the most powerful heating facility in the world.

Transmissions can be circularly or linearly polarised with modulation from continuous wave to pulses as short as 30 μs. Timing and frequency stability are locked to that of the EISCAT radars.

The Heating facility also consists of an advanced digital ionospheric sounder covering the frequency range 1 to 30 MHz. This is a NOAA-built dynasonde which was upgraded to be controlled by a PC. This provides important diagnostic information during heating experiments as well as during other radar operations. Interfaced to the heater transmitters, it can also be used for special HF radar experiments requiring high transmitter power.

A major area of investigation is that of Langmuir wave turbulence in the F-region. In recent years the simultaneous use of UHF and VHF radars to diagnose the modified region has provided crucial new data to test the theories which are improving rapidly. The dual radar use, the ongoing implementation of advanced modulation techniques to provide high-spatial as well as high-temporal and high-spectral resolution, and the use of the chirp technique are just beginning to provide the quality of data needed to resolve the scientific questions.

Other areas, such as modification of the D- and E-regions are being investigated with new vigour. To observe the modifications with incoherent scatter radars is not as easy as might at first be thought, which has meant that in the past this area has been somewhat neglected. Fresh attempts are being made to provide experimental input to recent theoretical models of the effects of heating on the D- and E-regions.

Using the heater to produce artificial irregularities that act as tracers of the natural ionosphere is a technique newly applied at EISCAT to the high latitude ionosphere and promises to provide better understanding of the ionosphere.

Some of the results of these investigations can be found towards the end of the following section describing scientific research and developments. The list of publications now includes heating, as well as radar, work.

Fig. 12 shows a small part of the co-axial feed-system of the Heating facility. As a result of the takeover 200 extra hours were added to the operating hours and extra staff were employed.

The Dynasonde is used regularly in support of most EISCAT radar operations, as well as providing invaluable information in the choice of operating parameters for the Heating facility during special experiments.

The facility is used also to check the calibration of Common Programme electron densities, as illustrated in Fig. 13. This figure shows the effect of high power HF waves on the backscattered power from the F-region measured with the VHF radar during the

operation of CP-7-E on 19 May 1993. The dark red areas show strongly enhanced backscatter just below the F-region peak measured on one of the power profile channels, while the other colours show the electron density from 75 to 450 km for an interval of one hour starting at 11 UT. The heater was on for only two short periods of a few minutes, and the strong signal appears at the height where the 5.4 MHz HF waves from the Heating facility are reflected from the F-region, allowing an accurate calibration of the radar-derived densities during Common as well as Special Programmes.

Understanding the physical mechanism behind such heater-enhanced signals is an active area of research as described further starting on page 55 together with other results from the Heating facility.

(a)

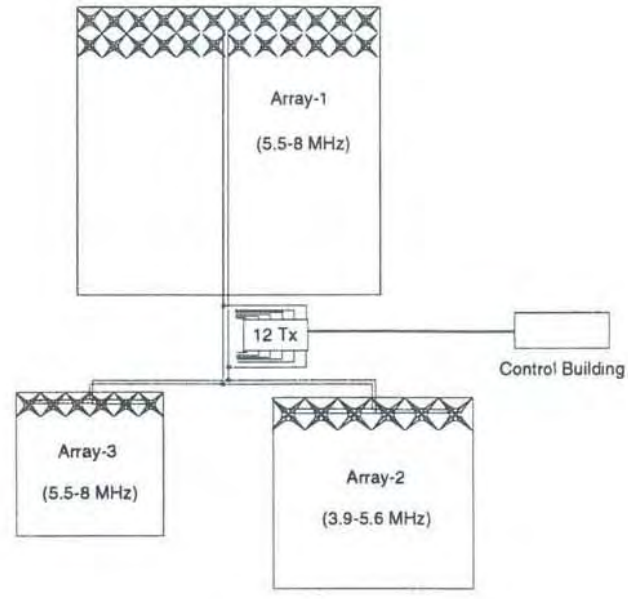

(b)

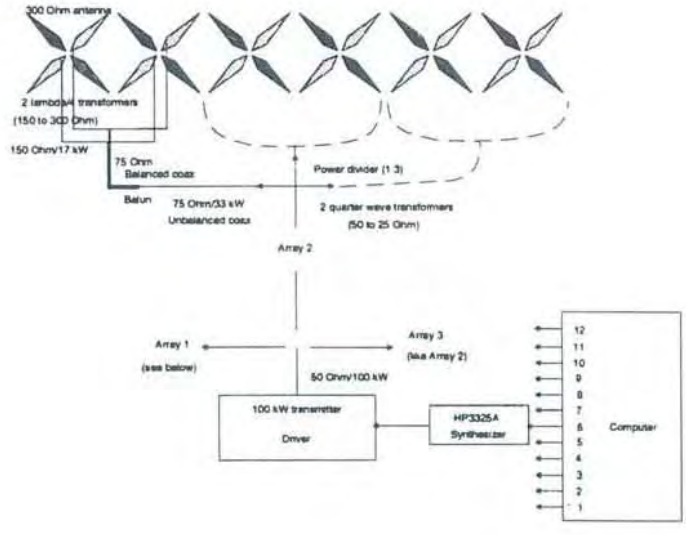

Fig. 11. (a) Schematic of the antenna arrays showing how a row of crossed dipoles antennas in any of the arrays is driven by two transmitters. (b) Schematic of the transmission line system from one transmitter to half the antennas in a given row, for arrays 2 and 3.

Fig. 12. The Heating Senior Scientist Dr. Michael Rietveld and Knut Helvig inspecting the antenna feed system of the Heating Facility at Ramfjordmoen.

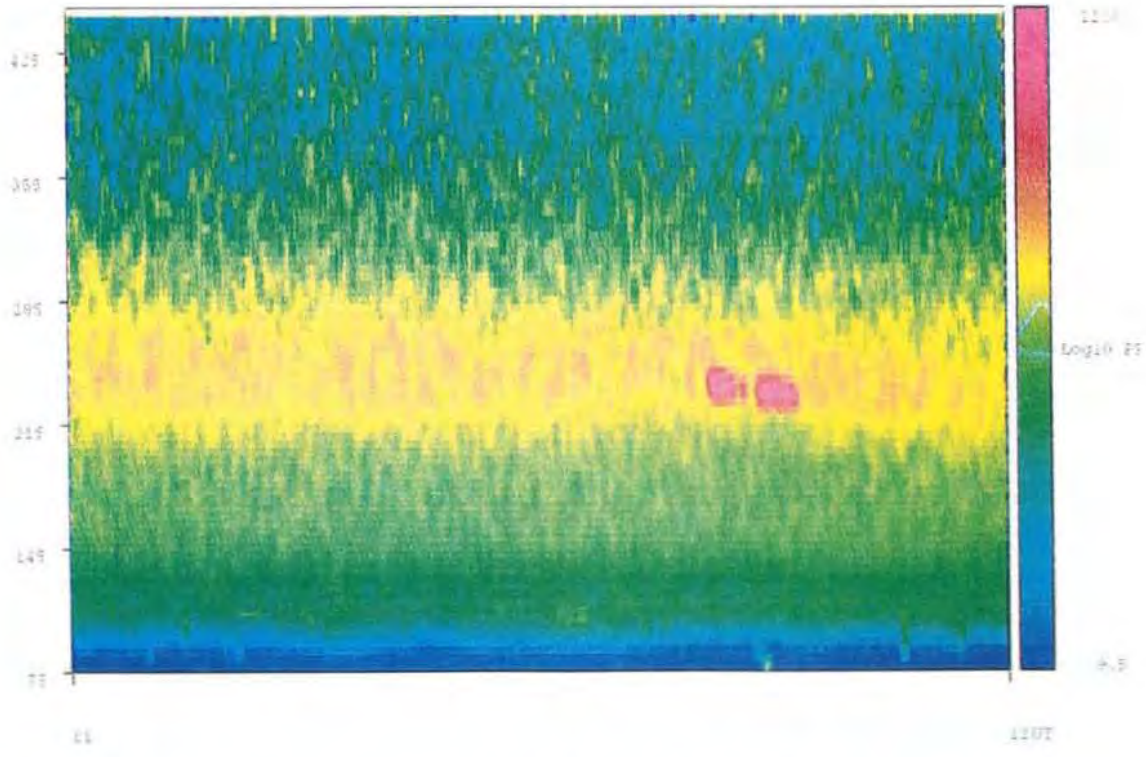

Fig. 13. Heater-induced backscatter (dark red) observed in CP-7 power profile measurements.

SCIENTIFIC RESEARCH AND DEVELOPMENTS

In this section we present a review of recent results related to the EISCAT facility. The system is used for a wide range of studies of the neutral atmosphere and ionosphere using the incoherent scatter technique. In other applications, the radars detect signals from coherent scatter processes. Geophysical and plasma-physical phenomena are investigated with the aid of the Heating facility, and passive measurements of astronomical radio sources are used to determine characteristics of the solar wind.

AURORA AND SUBSTORMS

A central theme of the broad scope of topics explored with the EISCAT system, and one of the principle reasons for the high-latitude location of the facility, is the study of auroral disturbances and substorm phenomena. The capabilities of the system in providing measurements with good spatial and temporal resolution are often pushed to the limits in the investigation of the associated small-scale, rapidly-varying phenomena. Such observations are often combined with other ground-based or satellite-borne measurements in order to obtain as full a picture as possible of the underlying processes.

Auroral arcs are sometimes observed to fade briefly before the onset of a substorm. This phenomenon was seen just before the break-up of a substorm on 5 October, 1986, during a period of EISCAT observations coordinated with the Viking spacecraft. The fading of the onset arc was associated with a clear local decrease of the preexisting westward electrojet, and the E-region ionization seen by EISCAT (Fig. 14). The onset itself was characterized by very energetic particle precipitation (> 30 keV), producing ionisation at altitudes below 90 km. The observations of both the fading and extreme particle energization are in agreement with a near-Earth disruption of the magnetospheric cross-tail current, where a strong induced electric field initially inhibits the growth phase mechanism of particle precipitation, leading to a momentary fading of the growth phase arc. The same electric field leads shortly afterwards to a very much energized and enhanced particle precipitation, as can clearly be seen in Fig. 14 (Pellinen, Pulkkinen, Huuskonen, Kauristie, Heikkila, Opgenoorth, Pudovkin)*.

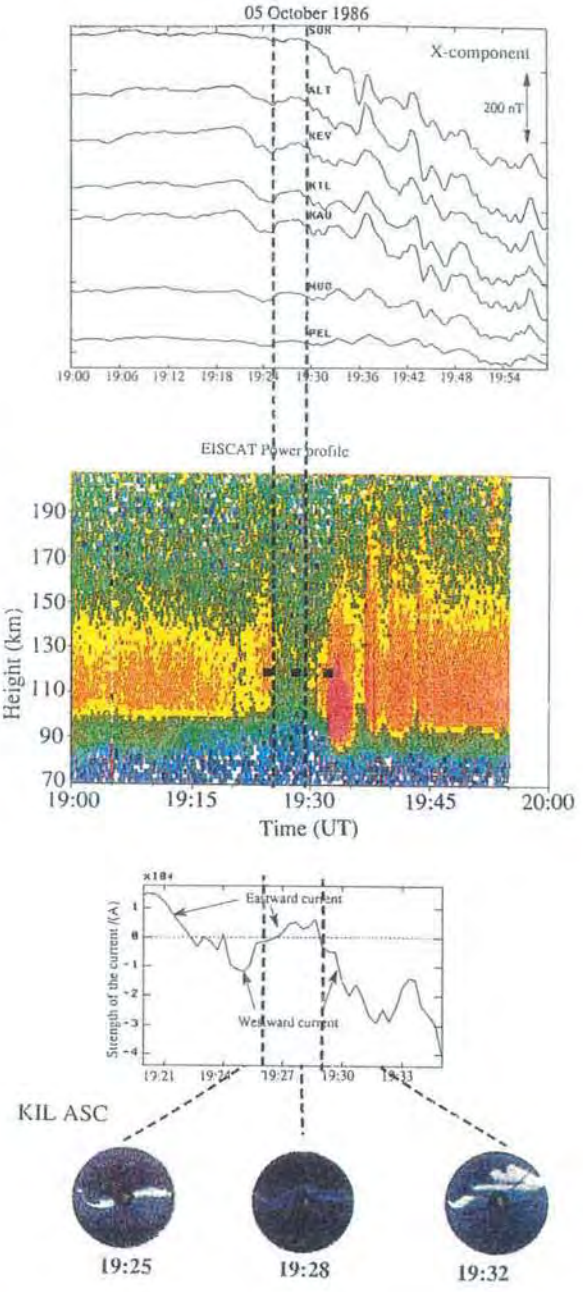

Fig. 14. Ground-based observations on 5 October, 1986. Panels from top to bottom: EISCAT magnetometer cross data (X-component), EISCAT raw electron density (green $10^{10.8}$ m^{-3}; yellow $10^{11.4}$ m^{-3}; red 10^{12} m^{-3}, respectively), model calculation of the electrojet current strength, and all-sky camera pictures from Kilpisjärvi, Finland.

* References in the text which include the year can be found in the list of publications towards the end of this Report; those without a date indicate work not published before the end of 1993.

EISCAT continues to play a role in the study of ionospheric flow bursts. It has been suggested that there are three possible patterns of behaviour that EISCAT might record as a flow burst. A long-lived but narrow band of intense plasma flow, probably associated with an auroral arc, might drift through the EISCAT beam. The plasma flow in the electrojet might be relatively smooth, but the boundaries of the electrojet might oscillate in latitude, possibly in response to a wave-like phenomenon, so that the electrojet moves in and out of the EISCAT beam. A flow burst might also occur simultaneously over several degrees of latitude and longitude (Lewis et al., 1993).

A combined study using EISCAT and the Kilpisjärvi all-sky camera has shown that an enhanced electric field on one side of an auroral arc can indeed be responsible for the signature of a plasma flow burst. The auroral arc and the band of enhanced electric field were observed to drift slowly equatorward at the same speed (i.e. as an entire structure), and this was the same speed as the meridional component of the average F-region plasma velocity at the time, suggesting that the whole structure was drifting with the background convection velocity. EISCAT data for the vertical position in the CP-2 cycle is displayed in Fig. 15. The top panel shows height profiles of electron concentration. The sharp increase at 2030 UT corresponds to the passage of the arc through the EISCAT beam. The middle panel shows an enhanced electric field preceding the density enhancement. This electric field is directed perpendicular to the east-west aligned arc and northward (i.e. in the same direction as the background convection field). This is consistent with previous observations in the evening sector. The validity of the electric field measurements are confirmed by the associated ion frictional heating, displayed in the bottom panel. Comparison of the first two panels also shows that in the region of enhanced electric field, the electron density is significantly reduced below the background level. This has important implications for the electrodynamics associated with the auroral arc. The observations are in excellent agreement with a model of arc-associated three-dimensional current flow which consists of a pair of field-aligned currents either side of the step-like change in ionospheric conductivity. To close the circuit between the downward and upward field-aligned currents, an enhanced electric field is required in order to drive an enhanced Pedersen current over the sharp conductivity gradient (Lewis, Williams, Jones, Opgenoorth, Persson).

Observational campaigns in conjunction with the Freja spacecraft continued through 1993. In a coordinated study utilizing EISCAT, magnetometers, auroral cameras and data from Freja it was found that the initial substorm onset can occur on very low magnetospheric L-shells, near the poleward edge of the region of stably trapped particles as seen by Freja. As shown in Fig. 16, southward drifting quiet arcs, which are a typical phenomenon of the substorm growth phase, continued to drift southward on the poleward side of the expanding substorm aurora, throughout the initial substorm expansion phase. This indicates two basically different and independent systems of particle acceleration in the distant and near-Earth magnetospheric tail, and favours a substorm model based on a current disruption at the inner edge of the plasma sheet. The formation of a near-Earth neutral-line at substorm onset would noticeably have affected the plasma-sheet boundary layer, and thereby disturbed the southward drift of the growth-phase arcs. At the moment of substorm onset, Freja detected clear signatures of an Alfven wave in a region of upward field-aligned current flow (Persson, Opgenoorth, Pulkkinen, Ericsson, Dovner, Reeves, Belian, Andre, Blomberg, Erlandson, Boehm, Aikio, Häggström).

A total of 266 hours of special experiment time was pooled from contributions by various EISCAT Associate countries for the radar observations which were coordinated with Freja, and the data are freely available in the EISCAT community. Quick-look plots of the EISCAT data from these campaigns were made available on the World Wide Web network.The dataset contains combinations of simultaneous experiments on both the UHF and VHF facility. After an initial campaign in 1992 (November 17 - 29) the campaigns in 1993 were February 24 - March 16, and September 20 - 24. A further campaign was also scheduled for January 3 - 7, 1994.

Since the end of 1992, significant effort has been expended on the coordination of ground-based observations with ESA's upcoming multi-satellite mission, Cluster, including the planning of the Cluster science data system CSDS. Opgenoorth (1993b) has summarized the plans for a global coordination of ground-based observations during the Cluster mission. It

is planned to establish a common ground-based data base for such observations, and the (by then) newly operating EISCAT Svalbard radar will be one of the key instruments in the network of Scandinavian ground-based facilities.

The substorm recovery phase has been studied by comparing the dynamics of visible auroral forms determined with a low-light level TV system with simultaneous EISCAT observations. Fig. 17 shows results from the recovery phase

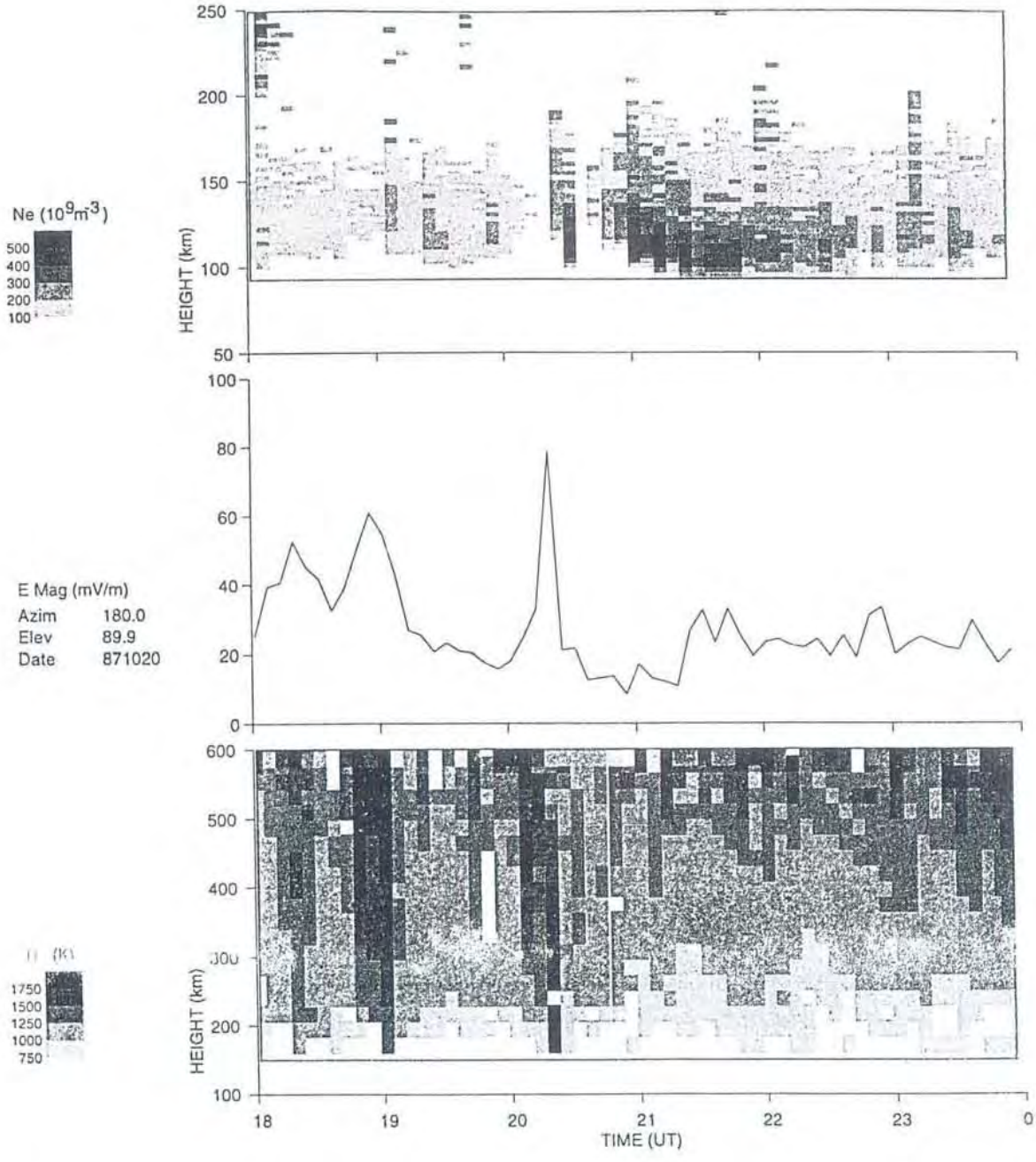

Fig. 15. Height profiles of electron concentration from 90 to 250 km measured with the multipulse scheme (top panel), magnitudes of electric field at a height of approximately 279 km (middle panel) and height profiles of ion temperature from 150 to 600 km from the long pulse modulation (bottom panel) measured by the EISCAT common programme CP-2-D on 20 October 1987. These results are from the vertical antenna position in the four-position scan, providing ~1-min averages every 6 minutes.

of a substorm as the main auroral arc drifted southwards through the radar beam. The top panel compares the 557.7 nm luminosity observed at locations 10 km poleward, along, and 10 km to the south of the radar beam (at 110 km altitude), showing a pair of east-west aligned arcs moving southwards at 500 ms^{-1}. The third feature is a swirl in the arc which moved longitudinally along the arc. The motion of the arc was found to be the same as the southward plasma flow seen by EISCAT (second panel). Ahead of each arc, a burst of westward flow was observed (panel 3) and the multipulse data appear to show that the precipitation was hardest on the leading edge of each arc and softer near its poleward edge. This behaviour contrasts with some southward-moving arcs observed in the late expansion phase and growth phase of the optical substorm. East-west aligned southward-moving arcs were then seen to move

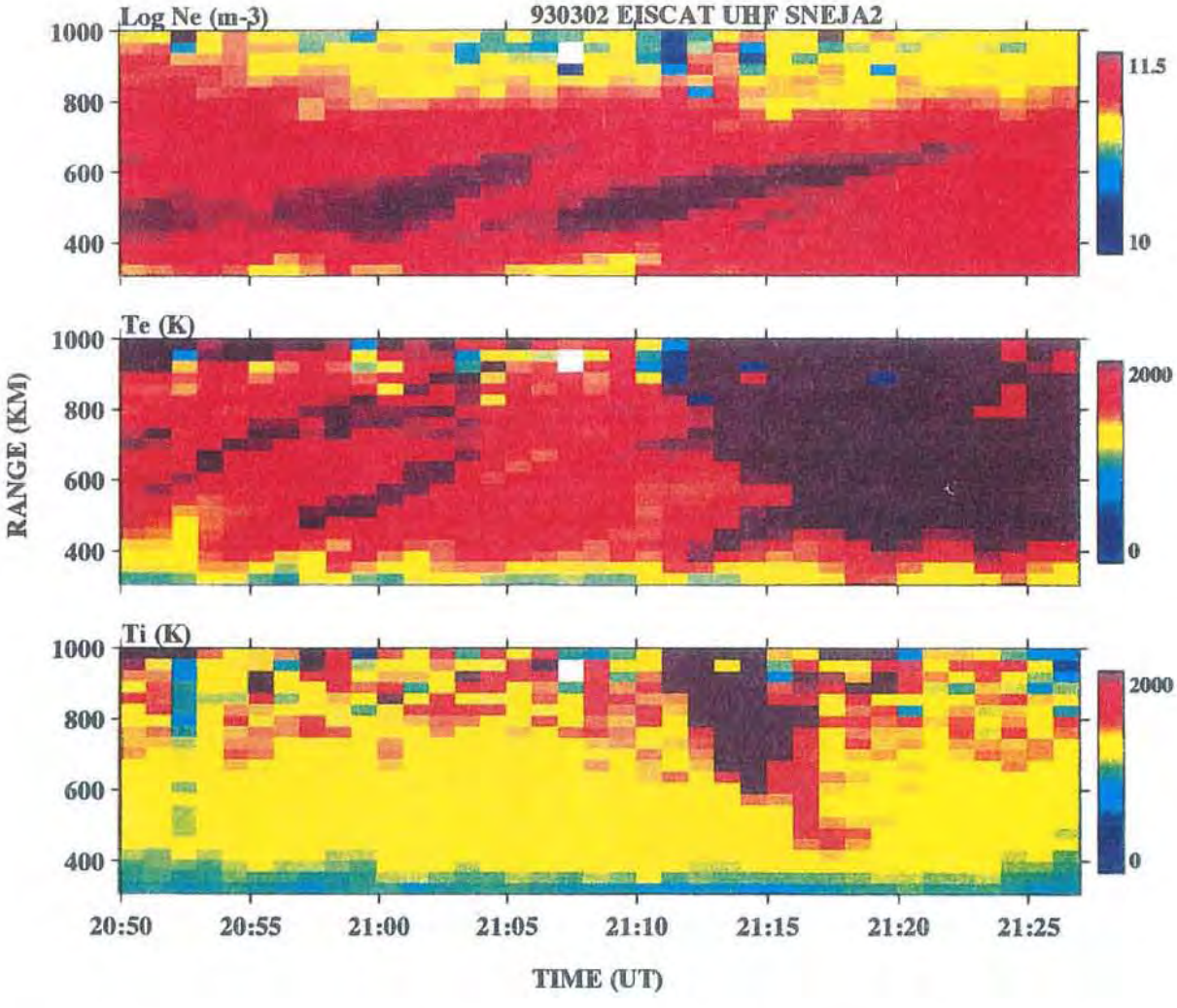

Fig. 16. EISCAT measurements of electron density, electron temperature and ion temperature versus range and time, pointing southward at an elevation of 40°. Due to the low elevation of the radar beam, altitudinally extended structures in the electron density and temperature (which are associated with auroral particle precipitation) appear as oblique structures in the chosen data presentation. Motion from near to far ranges corresponds to southward drift and motion from far to near ranges to northward drift of precipitation zones. After 2110 UT the panel for the electron temperature shows the coexistence of southward drifting arcs to the north of a northward expanding substorm aurora. The EISCAT data is in agreement with auroral all sky camera data.

at 1.0 ± 0.5 kms^{-1}, which appeared to exceed the southward plasma flow speed, indicating an equatorward phase motion of the source. These arcs merged with the main electrojet which was seen to expand rapidly polewards over the EISCAT beam. Interpretation of these data shows that the earliest that a plasmoid could be pinched off at the observed MLT near 21 hours is 11 min after the first onset signatures and that the westward travelling surge and the current wedge do not expand over this location until 14 minutes after onset. The EISCAT data show that flows are initially low in the main electrojet region and that flow streamlines avoid the high conductivity region, giving enhanced flows poleward of the main substorm region (Gazey, Lockwood, Smith, Coles, Bunting Lester, Aylward).

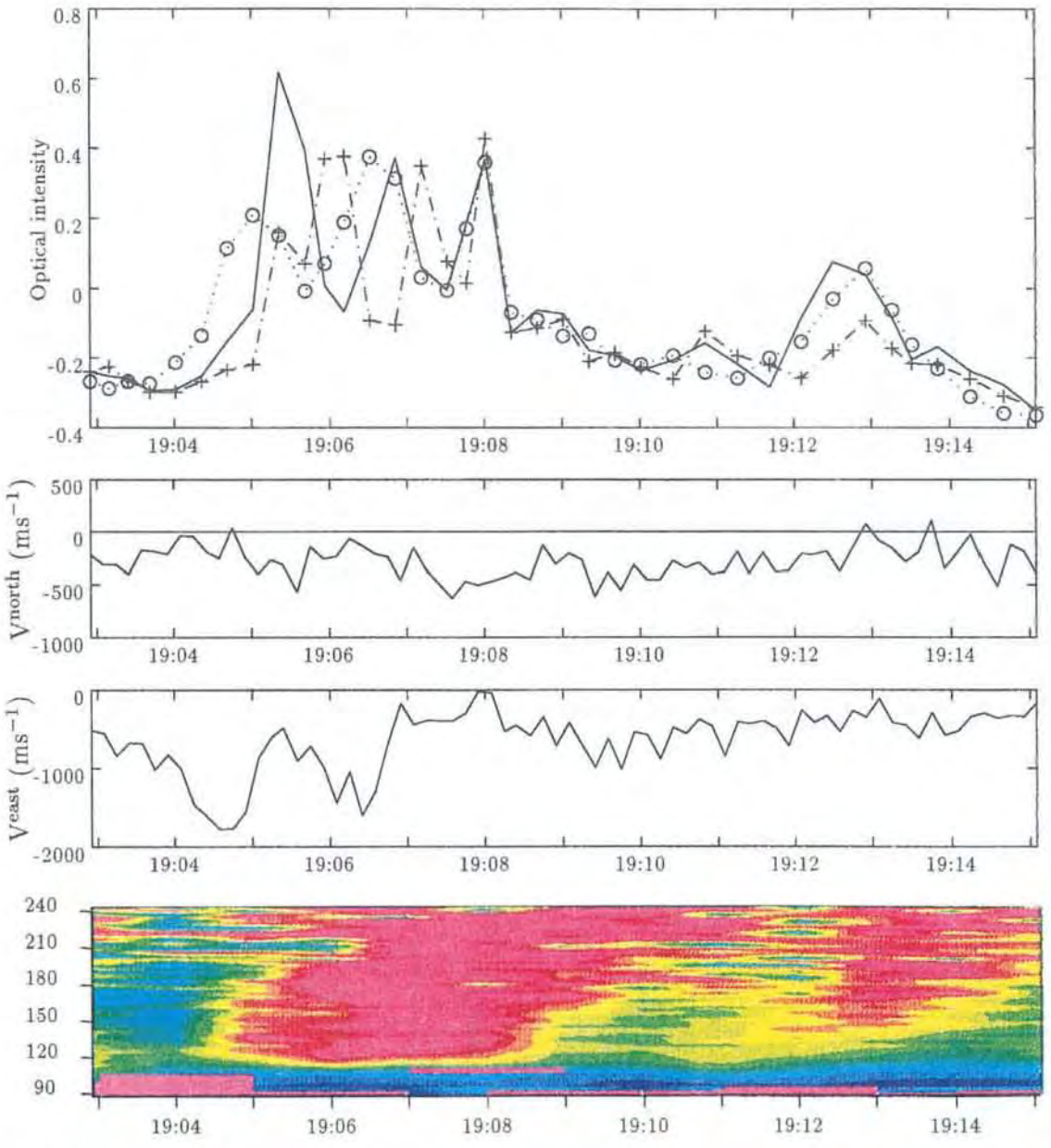

Fig. 17. Measurements of optical intensity (top) near the EISCAT beam, field-perpendicular ion velocity (centre two panels) and E-region electron density (bottom). In the top panel, the solid line shows the intensity in the EISCAT beam itself, the dotted line (circles) shows the intensity 10 km to the (geographic) north, and the dashed line (crosses) shows the intensity 10 km to the (geographic) south of the EISCAT beam.

Rapidly varying events have been investigated with power profile measurements in the E-region at a time resolution of 0.2 seconds. The electric field was determined at time resolutions from 2 minutes down to 3 seconds. A filter photometer and narrow angle TV were pointed along the magnetic field, as was the radar. One event that has been studied is shown in Fig. 18, where the electron density profiles are plotted in colour for an interval of 90 seconds, in which a band of narrow arc filaments crossed the radar beam. Just after 2000 UT there was an intensification in the arc as it was in the radar beam, and at this instant the height of the peak electron density decreased. TV images were crucial for the interpretation of these changes; the temporal brightening was part of a large-scale curl structure that moved through the arc from west to east. Electron density profiles were modelled by solving the transport, continuity and energy equations. One of the inputs is an electron energy spectrum, which is varied in the model until a good fit is made with the radar measurements. The profiles of Fig. 18 could not be reproduced by assuming a Maxwellian spectrum. Instead, a monoenergetic electron flux gave an excellent fit to the measurements. Model results of the electron density from monochromatic and Maxwellian input energy spectra are shown in Fig. 19 together with a profile measured during the bright event. The model was run with time steps of 3 seconds and 0.2 seconds, and it was found that the profiles could not be matched nearly as well with the longer time resolution, which gave much lower values of the energy flux required to produce the luminosity in the arc. The flux estimated (with 0.2s time steps) was 0.4 Wm^{-2},carried by an 8 keV monochromatic electron flux, equivalent to a current density of 50 μAm^{-2} (Lanchester, Palmer, Rees, Lummerzheim, Kaila, Turunen).

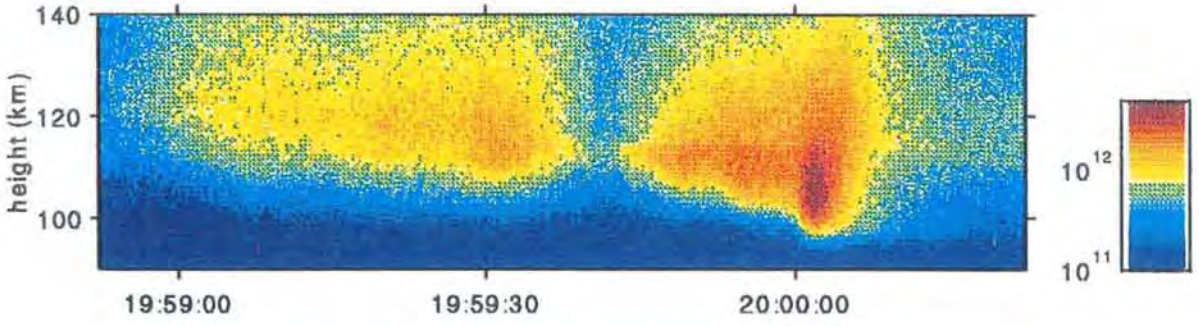

Fig. 18. Electron density (m^{-3}) measured with EISCAT at 0.2s resolution.

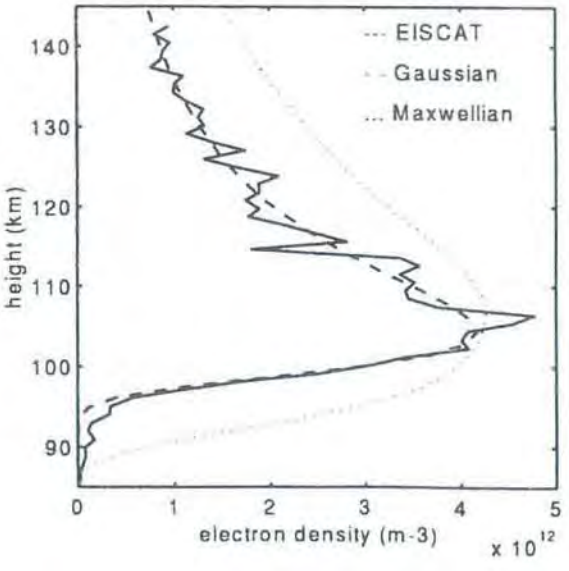

Fig. 19. Measured electron density profile (solid) and results of Maxwellian and Gaussian input electron spectra, at 20:00:02 UT.

HIGH LATITUDE CONVECTION AND ELECTRODYNAMICS

A combined study of convection, ionisation and conductivity has been made using latitude-scanning CP-3 data for an event of steady magnetospheric convection (SMC) on 27 April, 1988. Such SMC events (long active intervals without substorms) are rare and the large-scale patterns of the electrodynamic parameters have not been explored earlier. The conditions were characterised by a large width of the nightside auroral oval (~10° in latitude), a high cross-polar-cap potential difference (estimated to be >80 kV) and a distinct convection throat pattern near midnight (~15 kV per hour of MLT, Fig. 20) without Harang discontinuity signatures. Otherwise, the event would correspond to only modest magnetic activity (Kp ~2, AE ~250 nT). The stationarity of the large scale pattern allowed the estimation of field-aligned current (FAC) densities. Due to the equatorward gradient of conductivity in the convection throat region (Fig. 20), there exists an upward FAC in the central part of the near-midnight auroral zone (Fig. 21) which may be an important, or indeed constituent, component of magnetosphere-ionosphere coupling. In particular, this upward FAC generated at the conductivity gradient may provide the current closure for the upward FAC generated inside the mid-tail plasma sheet due to the dawn-dusk asymmetry of the plasma sheet parameters. If so, the current continuity may occur without the charge accumulation and resulting modification of the electric field pattern which should otherwise lead to the formation of the Harang discontinuity pattern (Sergeev, Aikio, Bösinger, Brekke, Häkkinen, Kangas, Pellinen, Pollari).

Ionospheric and magnetospheric phenomena at latitudes well to the north of EISCAT have been studied with both special programmes and CP-4. These modes employ two radar beams, aligned with the geographic and magnetic meridians, operating at 10-second resolution and at low elevations to the north of Tromso. Two configurations have been used: in one the VHF and UHF radars are operated simultaneously, in the other a second VHF beam is phased to point along the magnetic meridian. The elevation angles employed are 20° for the UHF and 30° for the VHF. Both radars then cover similar latitude ranges, roughly between Bjørnøya and Ny Ålesund, but at different altitudes. Flow vectors can be produced every 10 seconds by combining the line-of-sight velocities observed along the two beam directions with the assumptions that the effects of field-parallel flows are negligible and the convection is uniform along the L-shells between the two beams. The validity of the first assumption means that the northward component is directly measured, but the second assumption is frequently violated, such that under many conditions only the polarity (and not the magnitude) of the eastward component can be believed. In these cases, the estimates of the scalar quantities are used to evaluate the magnitude of the flow from the frictional heating equation.

An example of a dayside transient flow event is presented in Fig. 22. This shows the ion temperatures observed by the UHF radar as a function of time and invariant latitude. Superposed are the 10-second vectors derived from the line-of-sight velocities in both azimuths. A clear event onset is seen near 72° at 0940 UT and subsequently there is a general, but not precise, correspondence of high flow velocities and high ion temperature. The same feature was also seen by the VHF radar, showing that it extended longitudinally for more than the 200 km between the two radar beams. The similarity of the event, despite the difference in the elevation angles, reveals that the structure is a latitudinal, and not an altitudinal, feature and that the second assumption used to derive the vectors is generally valid. The flows within the event were westward (revealing a positive B_y component of the magnetosheath field), but the event onset is 86 seconds earlier at the UHF than the VHF, implying an eastward expansion (away from noon around the afternoon sector) of the event at about 2.5 km s^{-1}. This expansion away from noon has also been observed in EISCAT observations of flow transients in association with optical transients observed from Svalbard (Lockwood).

The enhanced zonal flow defines such events as being newly-opened flux tubes, produced by magnetic reconnection at the dayside magnetopause, on which the magnetic curvature force acts. In addition, this is consistent with the zonal-then-poleward direction of both the flow and the phase motion of the event as a whole. However, there has been debate as to whether the appearance of such events results from a burst of magnetopause reconnection or from an enhancement of the magnetosheath B_y component, possibly caused by a compression of the sheath by a solar wind dynamic pressure pulse. This debate is resolved

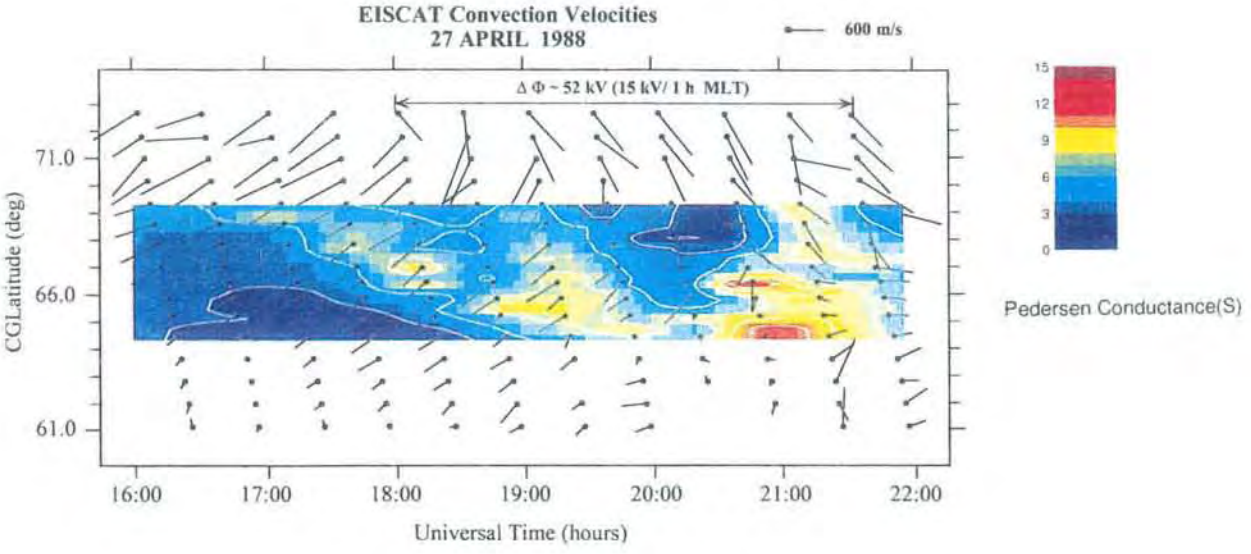

Fig. 20. The ionospheric plasma flow patterns as measured by EISCAT and given in CGL-UT coordinates. The Pedersen conductance contour line plot has been superimposed for comparison. The difference in latitude coverage between the plasma flow vectors and the conductance results represents the intersection of the obliquely-directed radar beam with the F-region, and the E-region, respectively. The tristatic velocity measurements were made at 275 km altitude in each of the 17 positions in the 30-min scan.

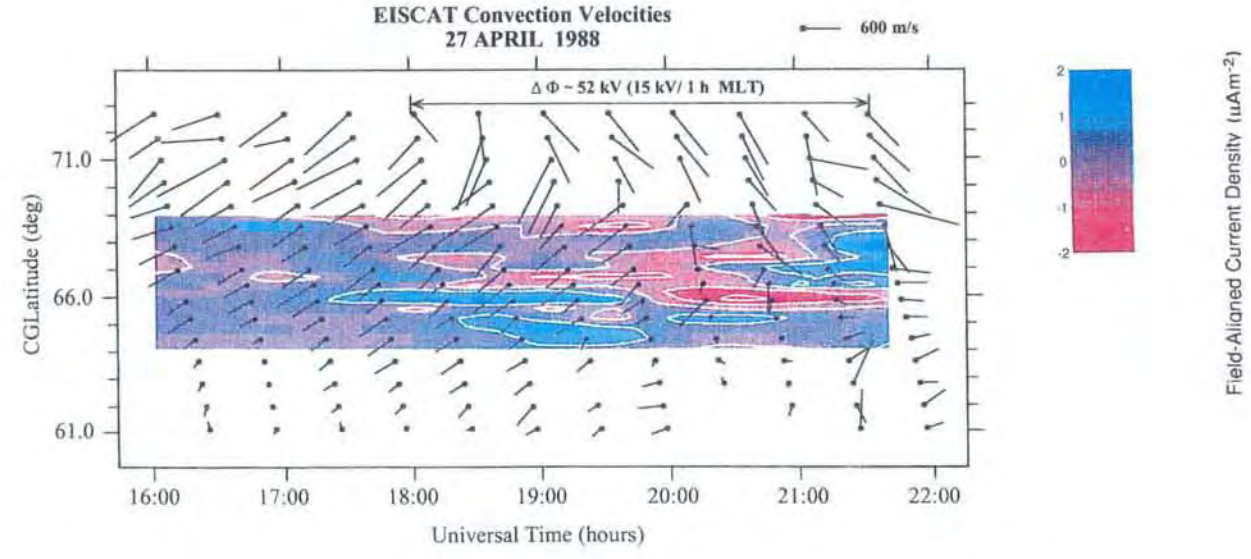

Fig. 21. The field-aligned currents derived from EISCAT data in a contour line presentation (positive downwards, negative upwards) in μAm^{-2}, in the same frame and for the same interval as Fig. 20.

by studying such events in association with optical observations of the dayside red-line aurora from the Svalbard islands (Lockwood, Cowley, Sandholt, Løvhaug). These combined studies show that the transient flow events are accompanied by 630 nm transients which repetitively move across the radar in the same direction as the plasma flow. This is as predicted by the pulsed reconnection model, but is inconsistent with the model of transient sheath B_y enhancements, for which the 630 nm aurora would move back and forth in the east-west direction.

The EISCAT observations of dayside transients have also provoked much debate about how pulsed magnetopause reconnection can be, with estimates of contributions of ~30 kV to the transpolar voltage in some cases. The radar data are of particular value here as they give the latitudinal width of the events and are not complicated by the effects of integrating the luminosity along a slant path, as in the optical observations. In one set of observations of transient flow events a persistent flow channel was observed between the events, revealing ongoing reconnection at a lower rate between the pulses which give the events. The reconnection rate within the pulses must be bigger than that between the pulses by the ratio of the latitudinal widths of the events to the background flow channel (>150 km and <30 km, respectively). From these measurements, it can be shown that the events contribute at least 17 kV to convection, which is half the average dayside reconnection rate at this time (Lockwood).

From the EISCAT-optical observations of dayside transients, it has been possible to construct a model of the dayside aurora for general variations in the magnetopause reconnection rate. The model predictions will be able to be tested using the ESR-EISCAT radars with the CLUSTER spacecraft (Davis, Lockwood, Palmer).

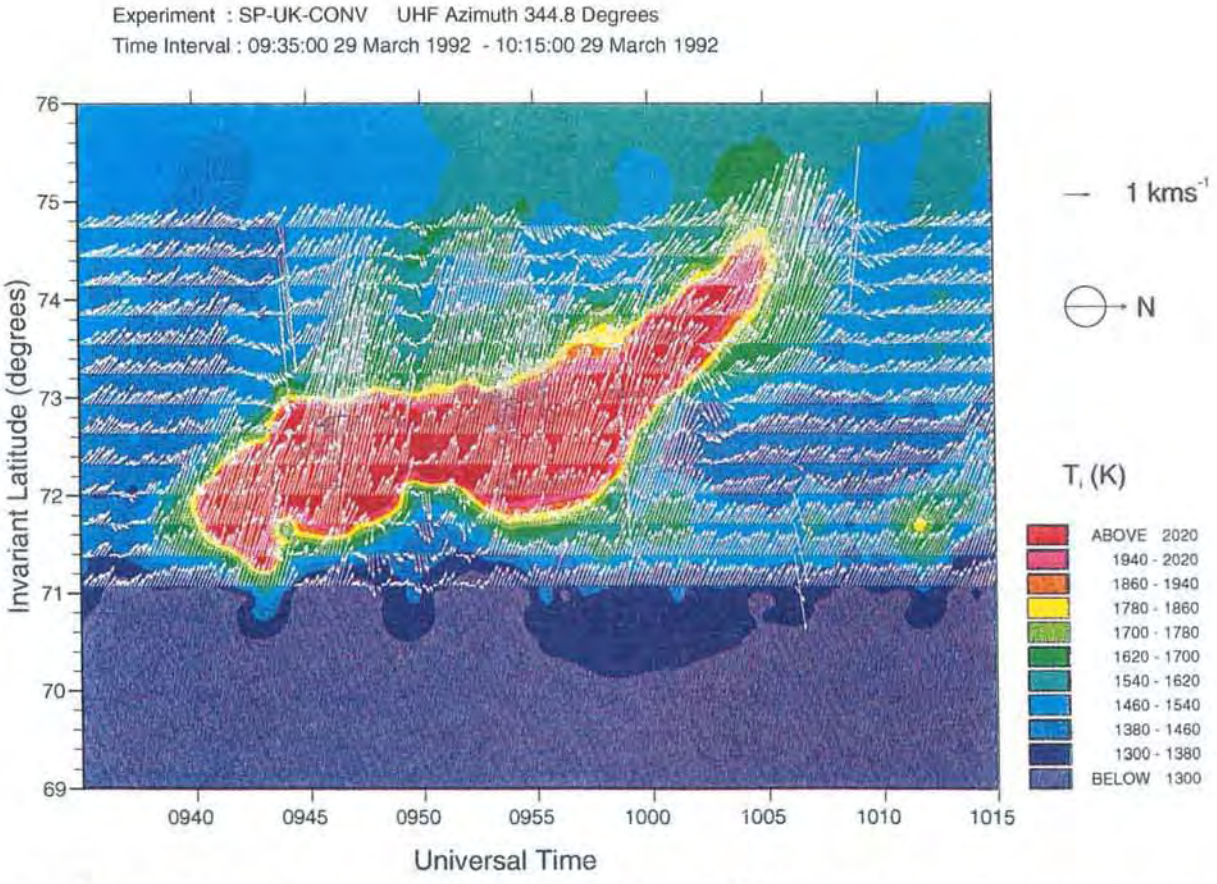

Fig. 22. Dayside transient flow event seen on 29 March 1992. The plot shows the ion temperature measured by the UHF radar between 0935-1015 UT. Superposed are the 10-second velocity vectors derived from the line-of-sight observations in the two azimuthal directions.

In the absence of ion loss during the sunward steady-state convection of the magnetospheric plasma, the effects of region 2 field-aligned currents, generated by magnetospheric pressure gradients, can be modelled in terms of an equivalent magnetospheric Hall conductance. In the framework of the linearized fluid theory, Peymirat and Richmond (1993) took into account the effects due to magnetospheric ion losses, resulting in an additional equivalent magnetospheric conductance. This new term contributes to reduce the initial Hall conductance, and to add a new Pedersen component. Its influence on the convection potential pattern is evaluated as a reduction of the eastward rotation and a non-negligible contribution to the shielding effect. This linear formalism reproduces up to the first order the non-linear self-consistent convection model of Peymirat and Fontaine. It provides a simple way to introduce the effects of region 2 field-aligned currents into models coupling the ionosphere with the magnetosphere or the thermosphere.

IONOSPHERE-THERMOSPHERE COUPLING

The altitude variation of field-parallel ion temperature and ion vector velocity through the lower F- and E-regions during intervals of enhanced magnetospheric electric field has been investigated using more than 320 hours of EISCAT CP-1-J and CP-1-K observations. Statistical analysis of the field-parallel ion temperature, at altitudes between 108 and 150 km during intervals of ion frictional heating, which are identified by an enhancement in the F-region field-parallel ion temperature exceeding 100K, revealed a steady reduction in the field-parallel ion temperature enhancement below 125 km altitude, which is a result of enhanced collisional coupling with decreasing altitude. Above this altitude, the enhancement in the field-parallel ion temperature is comparable to that at 312 km.

CP-1-J observations of field-parallel ion temperature enhancement through the E- and lower F-regions, during an extended interval of intense ion frictional heating after local geomagnetic noon on 3 April 1992, were compared with those predicted by a simplified ion energy balance equation containing solely a frictional heating term. The measurements and model results exhibit good qualitative agreement through the altitude range under consideration, although the model tends to overestimate the observed field-parallel ion temperature enhancement by more than 50% at some altitudes. By employing tristatic observations from the EISCAT CP-1-J experiment, the behaviour of the ion vector velocity, in both magnitude and direction, was also examined, principally in the E-region. Rotation of the ion vector velocity in the field-orthogonal plane from zonal eastwards to meridional northwards with decreasing altitude was noted during the aforementioned ion frictional heating event, a rotation from the **E x B** direction to that of the electric field due to the increasing frequency of ion-neutral collisions. A rapid reduction in the ion velocity magnitude was observed, predominantly at altitudes below 125 km, which is consistent with the results of the statistical analysis of the field-parallel ion temperatures (Davies and Lester).

The same extended period of intense dayside frictional heating has been modelled with the aid of the Sheffield University plasmasphere-ionosphere (SUPIM) model. The maximum enhancement in the field-parallel ion temperature measured at 300 km altitude exceeded 700 K at this time (see Fig. 23). The electron concentration in the F-region was substantially depleted during the interval of heating, resulting in an increase in the F-region electron temperature as, at the local time of the event, the ionosphere was solar illuminated. Input of the zonal ion drift to the model leads to ion heating and ion temperature anisotropy. The model field-parallel ion temperature can be brought into agreement with the EISCAT measurements by allowing for a neutral air wind with a velocity of the order of 700 ms^{-1}. This wind is caused by ion-drag by the relatively dense dayside ionosphere (Davies, Lester, Jenkins, Moffett).

Neutral winds in the E region (north-south, east-west and vertical components) have been calculated for the two long CP-2 campaigns of October 1992 and January 1993. The winds were derived using simultaneously-measured ion-neutral collision frequency derived from the alternating code pulse scheme. The tidal parameters of the horizontal winds were compared with models and the vertical component determined in two independent ways. Very large vertical winds were obtained from the analysis of the disturbed day of the October campaign. Such large values are not reproduced in any presently-available model (Kofman, Lathuillere, Pibaret).

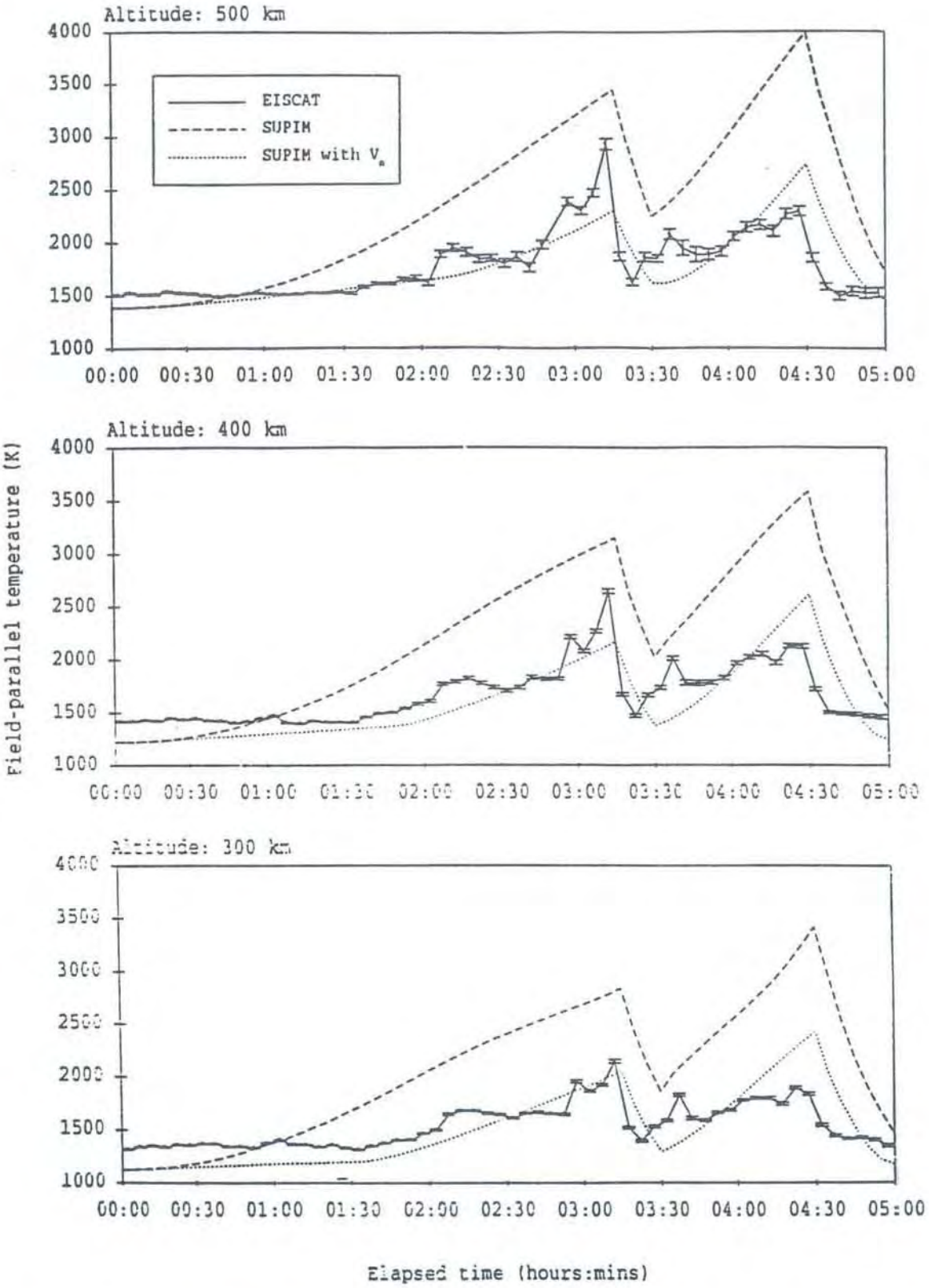

Fig. 23. EISCAT CP-1-J long pulse measurements of field-parallel ion temperature with associated error (solid line), as observed on 3 April 1992; field-parallel O^+ temperature from SUPIM calculation, with neutral wind velocity set to zero (dashed line), and with non-zero neutral wind velocity (dotted line), see text.

ATMOSPHERIC WAVES AND TIDES

Atmospheric gravity waves produce quasi-periodic fluctuations of the ionospheric plasma parameters which are called Travelling Ionospheric Disturbances (TIDs). The average amplitude behaviour of the TID parameters electron density Ne, ion velocity along the geomagnetic field line Vi, ion temperature Ti and electron temperature Te was derived using 45 TIDs of EISCAT CP-1 and CP-2 data from 1987-1991. The amplitude profiles in Fig. 24 show the different response of the ionospheric plasma parameters to gravity waves. The average amplitudes are well defined for the ensemble of the 45 TIDs since the boxes (denoting the middle half of the measured amplitude value range) are relatively small compared to the difference between the minimal and maximal value.

The amplitude relationships between the various TID parameters and their height dependence allow, together with the average phase differences between the TID parameters (see EISCAT Annual Report 1992, Figure 17) a reliable and certain detection of gravity waves in incoherent scatter data. Furthermore the derived amplitude and phase behaviour can be used for realistic TID simulations in ionospheric models (Hocke and Schlegel).

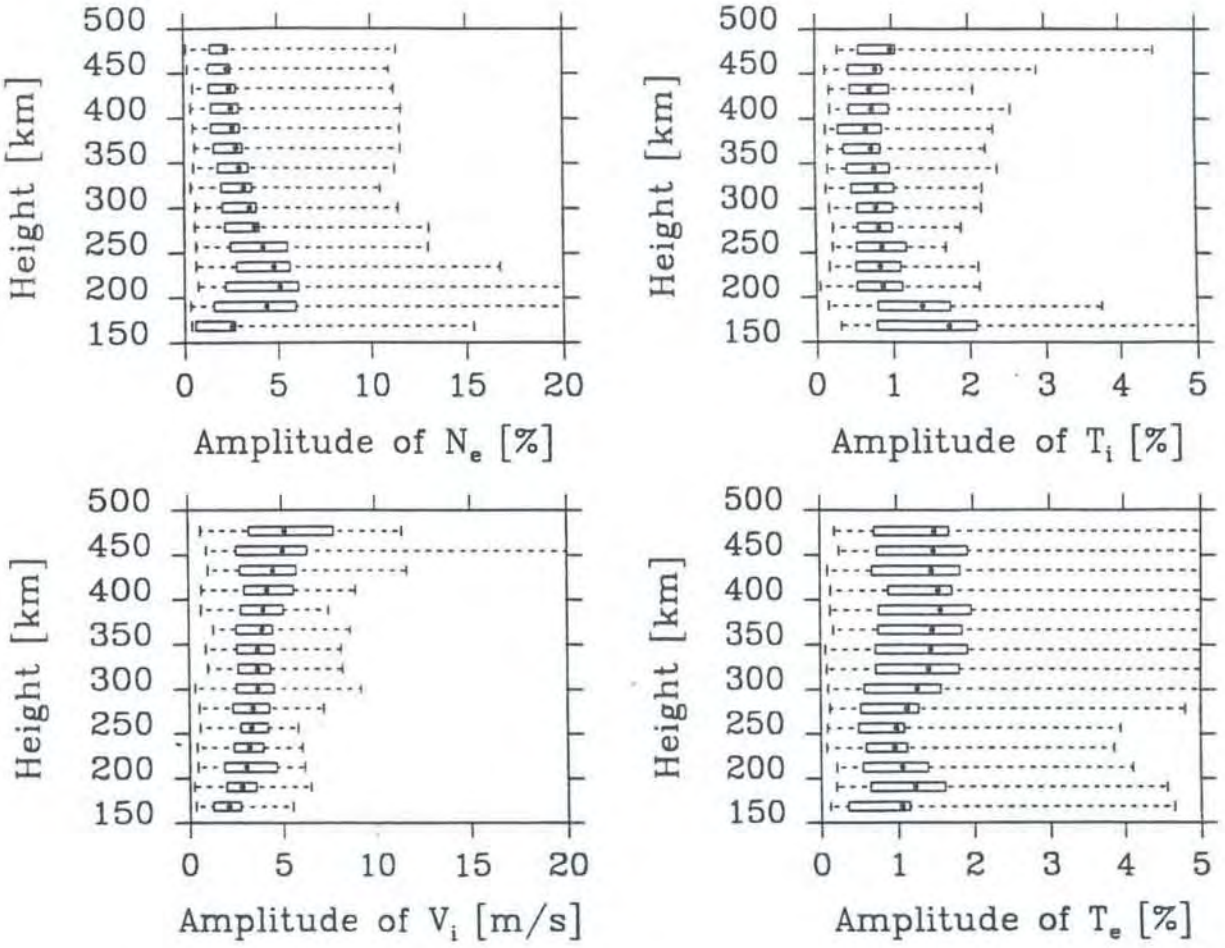

Fig. 24. Amplitude profiles of Ne, Vi, Ti and Te fluctuations. The box contains the middle half of the measured amplitude values while the point inside the box indicates the arithmetic average of all amplitude values. The dotted line reaches from the minimal to the maximal value.

Lanchester et al. (1993) suggested that a harmonic relationship exists between the spectral components of TIDs. Ma and Schlegel (1993) interpreted this to be due to wave-wave interactions between components of the Atmospheric Gravity Wave (AGW) spectrum. Alternatively, modelling studies suggest that in the presence of large amplitude gravity waves, significant electron density flux divergence occurs as a direct consequence of the advective term of the transport equations, which can result in the generation of higher-order waves in the electron density from monochromatic neutral waves with significant amplitudes. A Fourier band-pass filter was applied to twelve hours of EISCAT CP-1-J electron density data which admitted waves with periods between 17 minutes and 3 hours. The field parallel ion velocity was used to approximate the speed of the neutral gravity waves. There is a reasonable agreement between the wave and the electron density field in accordance with perturbation theory. This agreement breaks down for larger waves where higher frequency components are important in the electron density. The model also suggests that the harmonics generated by non-linear advection are forced rather than free modes and as such do not always exhibit conventional wave-like characteristics including constant phase speed. This might help to account for the absence of residual higher order components when the velocity is reduced (Arnold and Robinson).

EISCAT measurements of the electric field, electric currents, Lorentz forcing and Joule heating in the auroral electrojet have been compared with the signature of TIDs propagating equatorward as observed by an HF-doppler network in the UK. At night-time the onset of auroral activity was usually followed by the arrival of a TID at lower latitude. Cross-correlation of the time-variation of the electric-field measured by EISCAT with the frequency-offset recorded by the HF-doppler system confirmed the relationship between the auroral activity and the gravity wave, indicating both the travel time and the periodicity of the wave. An example is shown in Fig. 25, which shows for 13-14 April 1988 the coefficient of cross-correlation between the two sets of data as a function of the time lag between the EISCAT data and the HF-doppler data, and also the level at which the correlation is significant. The maximum correlation is 45% at a lag of 60 minutes, and the result is significant at 0.04%.

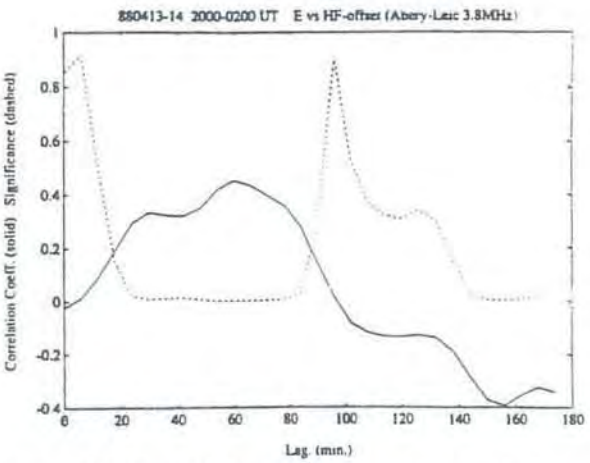

Fig. 25. The solid line indicates the correlation coefficient between the time variation of the electric field measured by EISCAT between 2000 and 0200 UT on the night of 13-14 April 1988 and the frequency shift of the HF-doppler radar over a 6-hr window delayed by a time lag, τ. The significance level of the correlation is indicated by the dotted line.

However, it is not surprising that the maximum correlation is less than 50%. From observations alone there is no easy way of distinguishing whether Joule heating or Lorentz forcing is the most important generating mechanism for AGWs as the time signature of both depends on the time variation of the electric field. No single function can represent both. The position of the electrojet varies with time so in all probability EISCAT does not lie in the centre of the electrojet throughout the window used in the correlation analysis. The neutral wind, ion drag and the sensitivity of the HF-doppler will also all have an effect to degrade any underlying correlation. The only satisfactory way to incorporate the overall effect of these factors in any comparison is to use a thermosphere-ionosphere coupled, global model to calculate the disturbance caused by a surge in the electrojet electric field. When the observed electric field was used as input to the Sheffield/UCL/SEL coupled model, it predicted the time signature of the observed HF-doppler variation reasonably well but seriously underestimated the amplitude of the disturbance. Examination of this discrepancy may lead to a better understanding of the mechanisms involved in the generation and propagation of atmospheric gravity waves (Lewis, Williams, Millward, Quegan).

Quiet-time E-region wind data from EISCAT have been analysed in order to establish the background mean neutral velocities as well

as tidal influences on the wind. There is a rather strong and persistent mean eastward wind present in all seasons in the E-region below 120 km. It is strongest in summer (~60 ms^{-1}) weak in the autumn and spring, and weaker in winter (~20 ms^{-1}). The zonal wind is westward above 120 km, in general stronger in winter (~70 ms^{-1}) and weaker in the other seasons (~30 ms^{-1}). The northward mean wind is rather small (~10 ms^{-1}) and changes gradually from being mainly southward in winter to northward in summer. The mean vertical velocity is of the order of 5 ms^{-1}. The amplitude of the diurnal tides of the vertical component have broad minima in the height region between 90 and 120 km (Fig. 26). The horizontal diurnal tide is dominant in the upper E-region while the semidiurnal tide has a maximum at 110 km, in particular in the eastward component. The 8- and 6-hour tides are rather constant in amplitude with height. These results are in agreement with findings from other incoherent scatter radar measurements. The comparison with theoretical models underlines the need for more modelling of the auroral E-region neutral tides including the ionised plasma as well as electric fields and mean background winds. Theoretical studies of the vertical motion with respect to the influence of tides are especially lacking in this important region (Brekke, Nozawa, Sparr).

IONOSPHERIC STRUCTURE, IRREGULARITIES AND MODELLING

Experimental ionospheric tomography has made rapid progress with the EISCAT radar playing an important role in providing independent verification of the electron density images Simultaneous tomographic and CP-3 measurements demonstrated the potential of tomography for the imaging of large-scale ionospheric structures and led to the development of an EISCAT Special Programme. This programme has proved to be invaluable for comparison with the tomographic reconstructions, and has been used in the development of improved imaging algorithms (Fig. 27) Of particular significance has been the incorporation of ionosonde information into the reconstruction process to improve the quality of the image close to the layer peak (Kersley, Pryse, Heaton, Raymund).

Studies of structuring of the auroral ionosphere on scales of tens of kilometres have continued. Three different types of structuring mechanisms occurring within a time interval of about two hours have been studied. These are a long-lived blob of cold plasma convecting with the background drift, an ionisation enhancement produced *in situ* by precipitation into the E-region, and a density depletion associated with ion heating. Results from the most recent campaign show a steep ionisation gradient with densities increasing by about five-fold over some 0.25° latitude. This long-lived feature, which is extended in altitude, has been shown to be closely aligned with the geomagnetic field (Pryse, Kersley, Walker).

A re-examination of all of the runs of the UK EP-103 special programme has given a statistical summary of the occurrence, magnitude and height of irregular structures in the F-region. It also gives information on their motion and temperatures, which bear on the question of their origins. Blobs are classified according to type. Types 1 and 2 correspond with the most intense fluctuations in electron content and occur between 250km and 400km altitude. At the edge of a blob, the change in electron content can be as much as $1.10^{17} m^{-2}$ in 30 seconds. The intensity of these blobs is higher during years of high solar activity and their temperatures indicate that they are not produced locally. Type 3 blobs occur below 250 km altitude and are found to be hotter than the surrounding plasma, which suggests that they are more likely to have been created just previously by local particle precipitation. A method of measuring the drift speed indicates that the irregularities drift with the plasma (Burns and Hargreaves).

These observations indicate that there are two significant production mechanisms - local soft particle precipitation, and transport of solar induced plasma from the dayside. Some features may also have been produced at an earlier time by some other mechanism. Regardless of the source of the irregularities, there is clear evidence that the structures drift with the convection. Their drift speeds compare well with those of polar cap patches which have been observed to drift anti-sunwards at speeds between 250 and 700 ms^{-1}. Other authors have shown that convection could distort a patch into a form resembling a blob that would be located at the equatorward boundary of the auroral zone, and this may be further enhanced by local soft particle precipitation. Although the EP-103 observations do not extend to the equatorward boundary, this type of process may be happening in the case where type 2

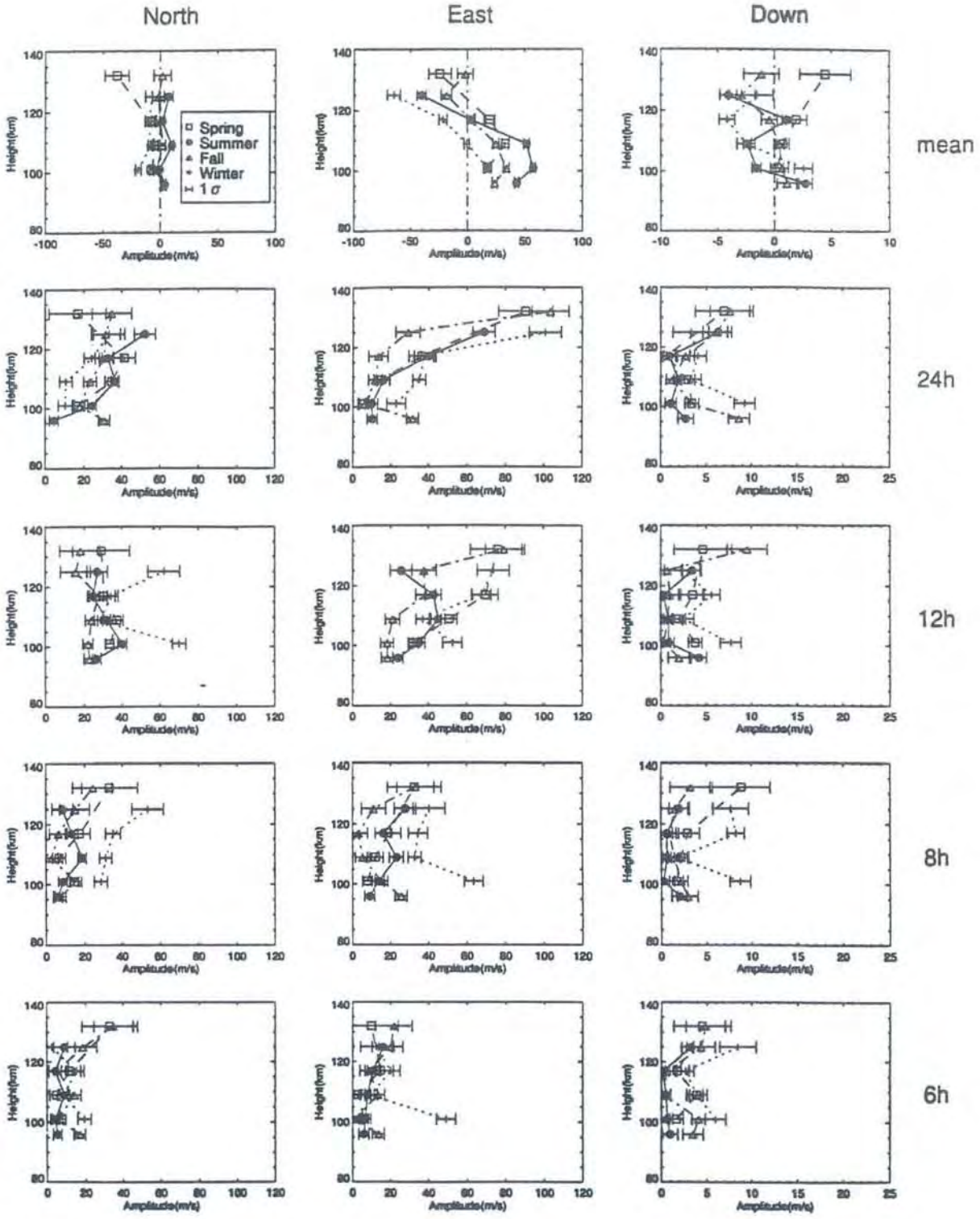

Fig. 26. Seasonally-averaged neutral wind components derived from EISCAT CP-1 data. The upper row of panels shows the mean north, east and downward components as a function of height of the averaged neutral wind for the four seasons. The following four rows show the corresponding amplitudes as a function of height for the diurnal, semidiurnal, 8-h and 6-h tidal components. The bars indicate the standard deviations.

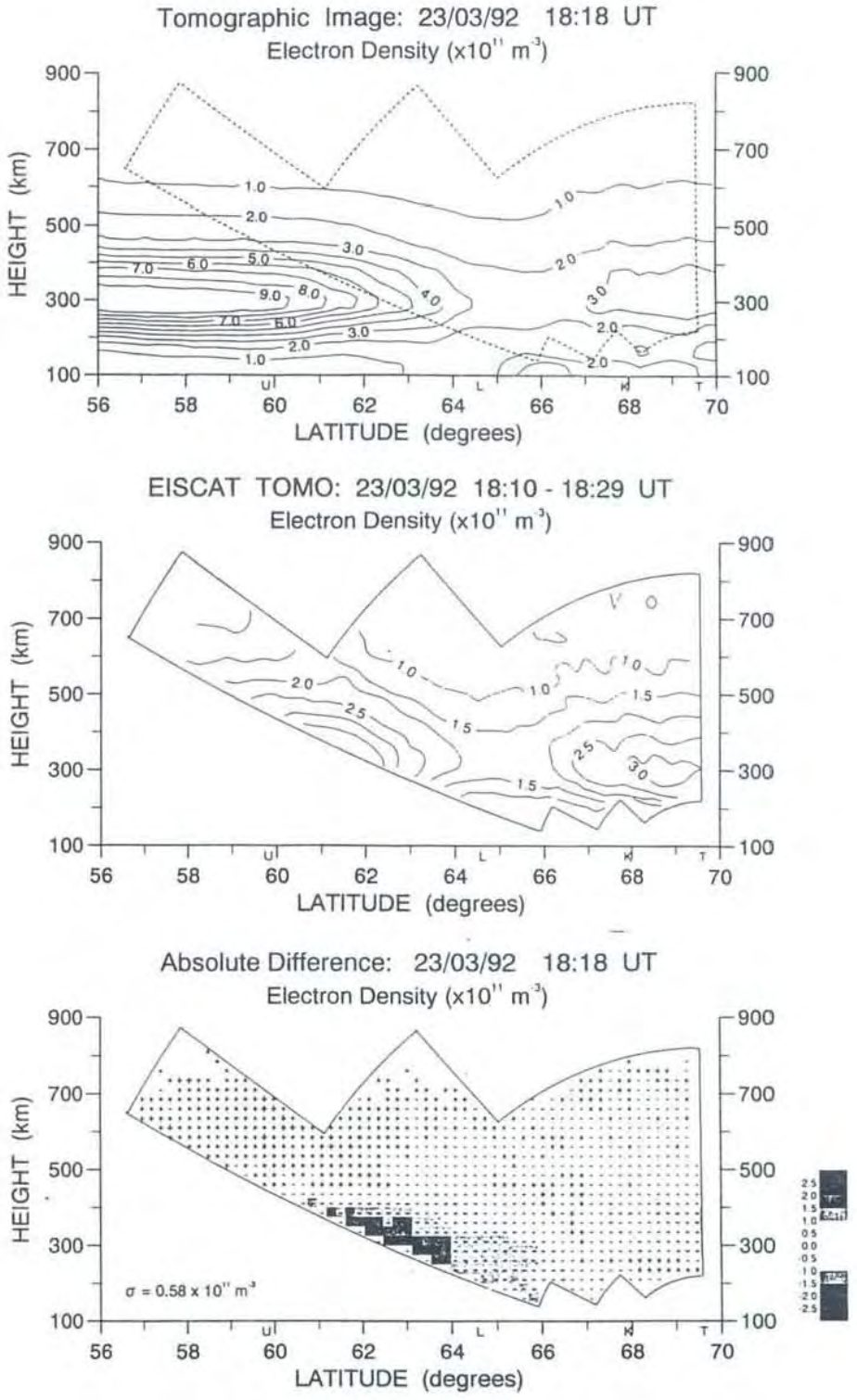

Fig. 27. (Top) Tomographic image of electron density derived from the NNSS satellite pass at 1818 UT on 23 March 1992 with background ionosphere based on the Utah State University model. The letters U, K, L and T denote the latitudes of the four receiving stations at Uppsala, Lycksele, Kiruna and Tromsø. The area enclosed by the dashed line shows the viewing region of the EISCAT experiment scan. (Centre) Electron densities obtained from the EISCAT scan between 1810 and 1829 UT on 23 March 1992. (Bottom) Absolute differences between each EISCAT measurement of electron density and the corresponding density value in the tomographic image. A + sign denotes a region where the EISCAT density is in excess of the reconstructed density, and a - sign vice versa. The root mean square value, σ, of the differences is indicated at the bottom of the figure.

blobs are observed. Clearly further work is needed to relate polar cap patches and blobs in the auroral zone. Simultaneous observations in the polar cap and auroral zone, as will be possible with EISCAT and the ESR, will be invaluable in this regard.

The results obtained from the COherent SCATter (COSCAT) experiment now constitute one of the most complete data sets of short wavelength (16cm) irregularities. The moments of the coherent scatter spectra have been derived, and the simultaneous F-region ion velocity has been determined by using the line-of-sight velocities from two EISCAT sites and assuming that the field-parallel velocity is negligible. The comparison of the velocities with the spectral moments has shown that both the phase speed and spectral width are functions of the line-of-sight component of the F-region plasma flow.

These 16 cm irregularities are of particular interest since kinetic theory is required to interpret their characteristics, as opposed to fluid theory. Nonlinear theory predicts differences between properties of irregularities in the fluid and kinetic regimes. Furthermore, it has been possible to make comparisons between the COSCAT observations and those at longer wavelengths, such as SABRE (1 m) and PACE (7-18 m). An important result of the study of irregularities at different wavelengths is the establishment of the wave number (k) dependence of the spectral width. A linear fit to the data indicates that the spectral width is proportional to $k^{1.2}$. This suggests that the scattering irregularities are relatively stable waves and the broadening arises due to turbulence in the background plasma flow, which gives rise to a k^1 dependence. in contrast, a k^2 dependence is predicted if the broadening arises due to the rapid decay of short-lived irregularities (Eglitis, Robinson, McCrea, Schlegel, Nygrén, Rodger).

Active COSCAT experiments have allowed the relationship between the irregularity phase speed and the magnitude of the plasma drift to be investigated. The phase speed exhibits a steady increase with increasing flow speed, the form of which is believed to be characteristic of backscatter from low altitudes (just below 100 km). In Fig. 28 the average irregularity phase speed measured by EISCAT has been plotted for 200 ms^{-1} bins of the plasma drift speed. The bottom panel presents data from a similar comparison between SABRE (1 m wavelength irregularities) and EISCAT. Theoretical curves are included for both non-linear fluid theory and non-linear kinetic theory. At the 1 m irregularity wavelength both fluid and kinetic theory compares well with the data. At the 16 cm wavelength, the data are best fitted by kinetic theory. This confirms the kinetic behaviour of the irregularity properties at short wavelengths (Robinson and Eglitis).

A number of other relationships between 16 cm irregularity characteristics and the plasma flow have been established. There is evidence of marginal excitation of the scattering irregularities for line-of-sight flow components of the order 400 ms^{-1}, although this is very variable from backscatter event to event. The coherent spectra become initially narrower with increasing flow speed, but there is evidence of increased broadening above 700 to 800 ms^{-1}. There is no clear relationship between the flow speed and the coherent scatter power (Eglitis, McCrea, Robinson, Jones, Schlegel, Nygrén).

EISCAT CP-1 data in the period 1985-1992 have been analysed to calculate the integrated electron content along the field-aligned beam from the power profile (~90-150 km) and processed ACFs (~150-730 km). A Chapman layer is fitted to the F-region data with a variable peak height and peak electron density, and a chi-squared test used to reject uncharacteristic profiles (<90% confidence). From this fitted profile the electron density is extrapolated to calculate a value for the Total Electron Content (TEC). The International Reference Ionosphere (IRI) is used to provide model values for TEC, peak height and peak electron density for each of the EISCAT profiles. From these values, the mean difference and standard deviation from the model are calculated for every day during which CP-1 data are available (Fig. 29). The results for the peak density and TEC show a consistent correlation with the IRI model, with the errors increasing at solar minimum due to a low signal-to-noise ratio associated with the EISCAT data. The comparison for peak altitude shows large variations with respect to the solar cycle and exhibits significant differences between the IRI model values for this quantity and the measured values.

The development of the University College, Wales model relating F-region electron concentration and electron temperature to changes in the ratio of molecular nitrogen to

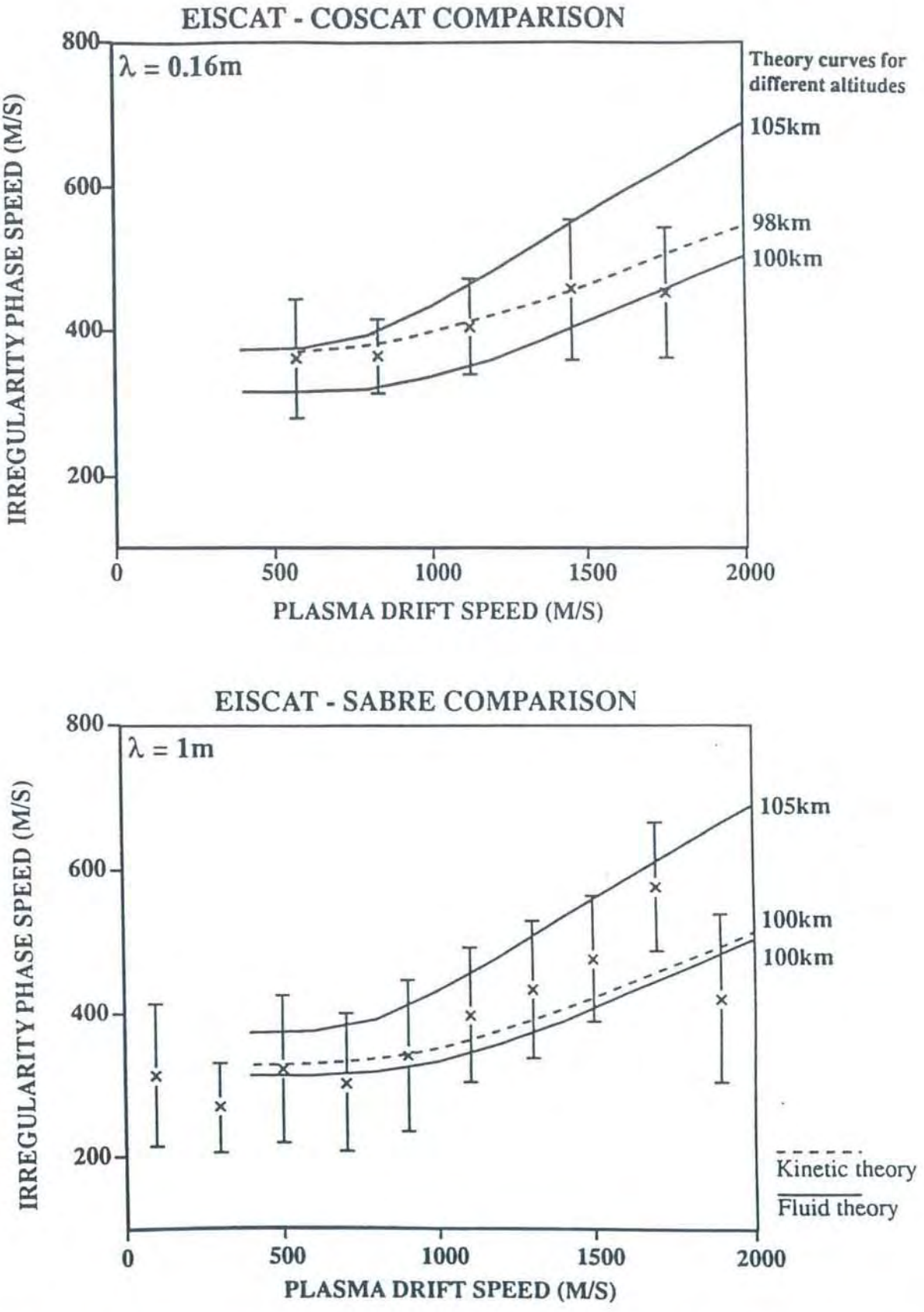

Fig. 28. The average irregularity phase speed calculated for 200 ms^{-1} bins of plasma drift speed for COSCAT and Wick (SABRE). The data are compared to theoretical predictions from both fluid theory and kinetic theory.

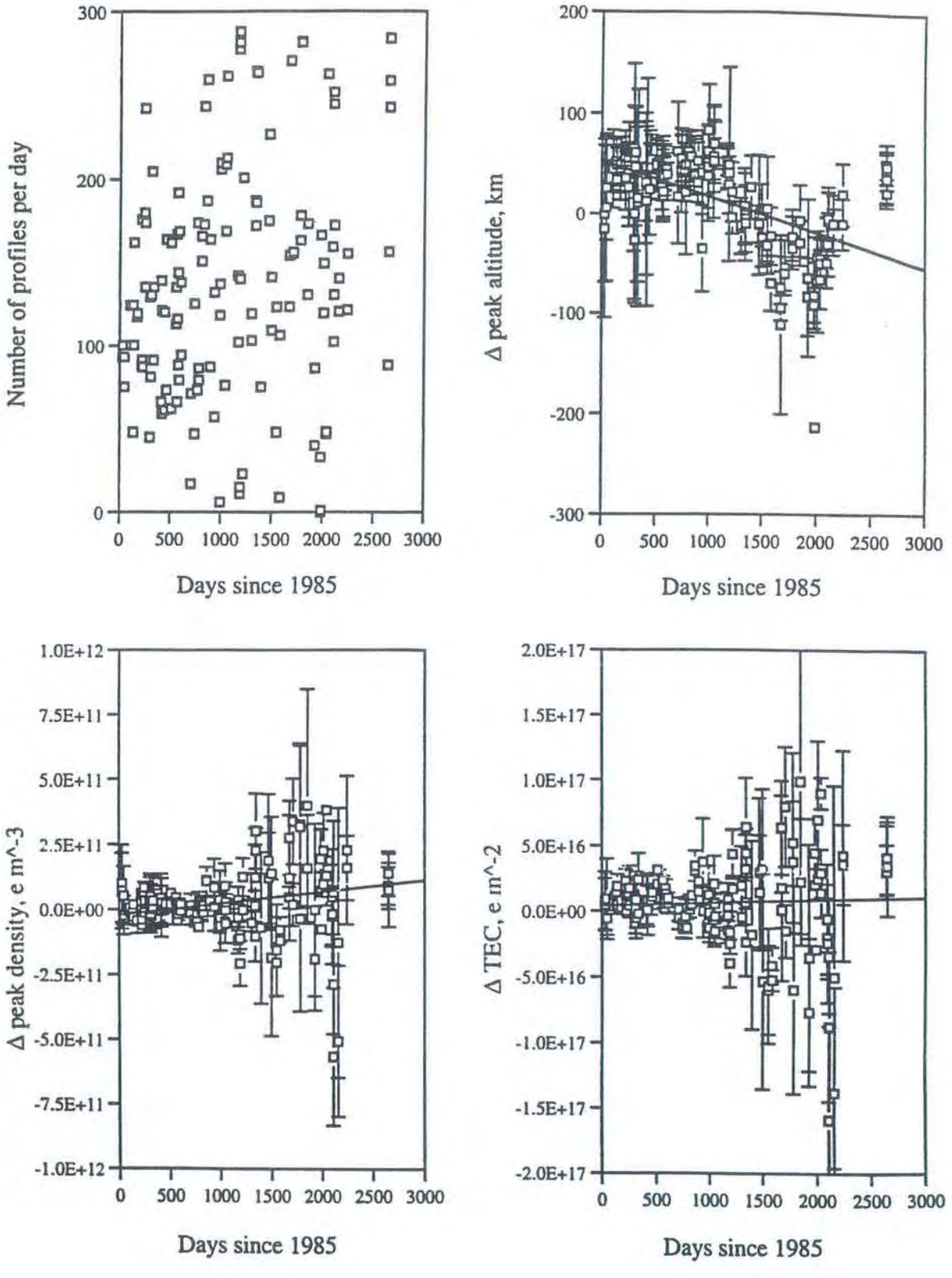

Fig. 29. Daily mean differences between EISCAT CP-1 data and the International Reference Ionosphere in the period 1985-1992.

atomic oxygen has continued. The current version of the model (UW-93) includes the effects of metastable excited states of oxygen ions and nitrogen molecules on the ionisation loss rate and gives extremely good agreement with EISCAT observations made under quiet conditions. The values of $[N_2]$ derived from this model are now consistent with the predictions of the MSIS-86 model. UW-93 estimates of electron temperature have also been compared with the predictions of the IRI-86 ionospheric model: the UW-93 electron temperatures agreed much more closely with EISCAT temperature measurements (Breen and Williams).

The inclusion of metastable excited states in UW-93 has reduced both the direct electron heating and cooling rates relative to earlier versions of the model. As a result, the model is more sensitive to the effects of heat conduction along the field line. The rate at which the electron gas is cooled by conduction is proportional to the rate of change with height of the gradient in electron temperature raised to the power of 7/2. This parameter can be estimated from IS measurements of electron temperature but such estimates are very sensitive to the errors in the temperature measurements and to the method used to derive the gradients. EISCAT Common and Special Programme data have been used to derive a general formula for the uncertainty in temperature measurements. An important result of this study is that $\Delta T_i/T_i > \Delta T_e/T_e$, which was not predicted by the simple theory of errors in IS temperature measurements. A statistically rigorous method of determining the optimum order of function to fit to a profile of $T_e^{7/2}$ measurements has been developed which can be used to determine the heat flux and resultant cooling of the electron gas (Breen, Williams, Etemadi, Davda).

In a further study, of an ion heating event at night-time, ion composition and the required adjustment of the EISCAT field-parallel ion temperature were shown to be the dominant factors needed to get agreement with the Sheffield University plasmasphere-ionosphere model (SUPIM). The event was observed on 5 September 1989 from 2115 UT to 2230 UT. The eastward component of the ion drift velocity increased to a maximum of 2.2 kms^{-1} and then decreased to typical background values. SUPIM (with distinct O^+ and NO^+) predicts that during the event the abundance of NO^+ at 300 km altitude rises from less than 5% to 70%, with the NO^+ temperature anisotropy less than that of the O^+ temperature.

VHF operations (including CP-7) allow observations up to 1600 km and above on a routine basis. Two numerical 1-D and time-dependent models of the topside ionosphere have been developed for the altitude range from 200 to 1000 km. It was shown that both near-winter and near-summer quiet time and diurnal VHF observations can be reproduced by the models with extremely good agreement, Fig. 30.

To obtain such agreement, the only external inputs for the models are the mean downward electron heat flow inferred from the data, and indexed models of solar EUV fluxes and of the neutral atmosphere (Robineau, Blelly and Fontanari). The comparison of the models with disturbances such as Joule heating and O^+ ion outflows exhibits similar good agreement when downward heat flow (or upward field-aligned currents) inferred from the data are used as the sole driving mechanisms (Blelly, Robineau, Alcaydé).

Using a similar approach, a 16-moment ionospheric model was developed in order to be able to study anisotropic ionospheric behaviour: the resulting quiet-time ionosphere model results are very close to the 8-moment approximations, and initial results on anisotropy developments due to downwards electron heat flow and to perpendicular convective E-field (frictional) events have been presented (Blelly, Robineau, Alcaydé).

The topside ionosphere models are being extended to lower altitudes in order to adequately model the chemistry in the regions between 100 and 300 km altitude: complete molecular and atomic chemistry of N^+, N_2^+, NO^+, O_2^+ and O^+ and derivatives is simulated, while simultaneously solving for the continuity equation for each ion, and velocity equations for molecular and atomic ions. The model is time dependent, so that effects such as chemical changes in the ionospheric composition due to intense Joule (frictional) heating can be modeled allowing comparisons with empirical EISCAT-UHF composition models. This model has also been used for simulating the predicted ionosphere above Tromsø and Svalbard at the time of the initial Svalbard operations in 1996 (Alcaydé, Robineau, Blelly, Fontanari).

A steady-state solution of the heat flux equation in the 13-moment approximation has been derived for a multispecies gas, by taking into account the effects of gradient temperature and of drift velocities between species. This general solution is applied to the case of the topside ionosphere where the gradients of field-aligned velocities play a minor role relative to the collisions. The O^+ and H^+ heat fluxes are then computed from EISCAT data and compared to the predictions of Fourier's law, which is found to significantly underestimate them. The computation of the heat conduction from the general solution also demonstrates that Fourier's law would lead to an opposite height variation, which would produce an opposite contribution to the H^+ energy balance and to the H^+ temperature. Finally the H^+ heat flux is found to be upward not only in the supersonic regime, as observed by DE-1, but also in the subsonic regime at lower altitudes, as inferred from EISCAT data (Wu and Taieb, 1993).

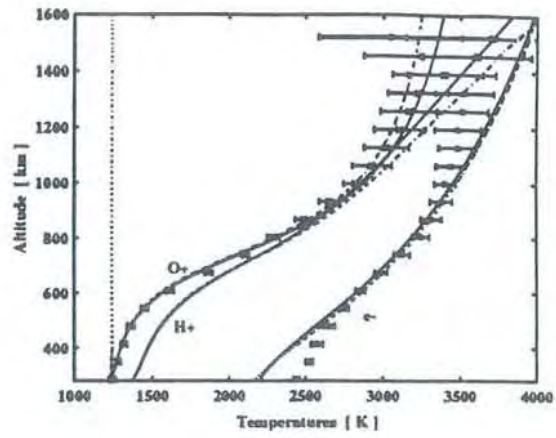

a

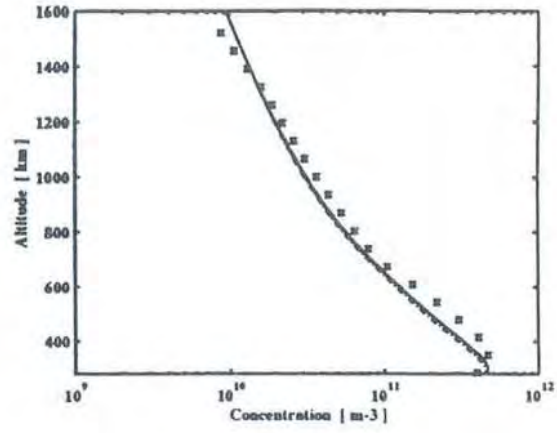

b

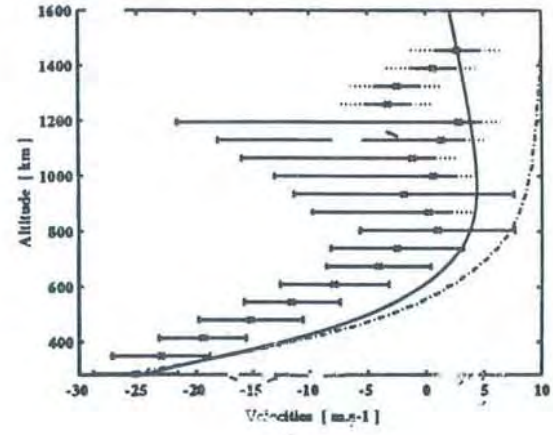

c

Fig. 30. A comparison of model results and measurements from EISCAT's VHF experiment on 12 May 1991: vertical profiles of raw data (cross) with error bars and noon steady state profiles for O^+ and H^+ ions, and for electrons, from two models based on different numerical schemes:
(a) ion and electron temperatures
(b) O^+ ion concentration
(c) O^+ ion velocity

MESOSPHERE

The EISCAT radars have been used intensively during recent years to study the polar mesosphere summer echoes, PMSE, as summarised by Röttger (1993). Dynamical features in the PMSE can show quasi-sinusoidal gravity wave modulations as well as steepening, previously seen only in the vertical velocity measured with the VHF radar. In order to detect wind corners in the horizontal wind, the spatial interferometer technique has been applied. Fig. 31 shows height-time-intensity diagrams of signal-to-noise ratio, Doppler velocity and spectrum width for a 45-minute interval on 11 August 1992. The sheet at about 83 km, which shows a short uplift a few minutes before 0900 UT has been analysed with the spatial interferometer technique in the frequency domain to yield cross-spectra, phases and coherency. Fig. 32 shows the essentials of the observations. The horizontal trace velocity of the scatterers can be deduced from the slope of the phase ϕ. A shallow phase slope is consistent with large velocity, and a steep slope with small velocity. The lower panel in Fig. 32 displays the velocity vector in the east-west-vertical plane. Between 0852 and 0854 UT there was a strong upward and horizontal velocity with considerable eastward component. Both these velocities decreased to almost zero at 0856 UT, ie. within 1-2 minutes. During the following 1-2 minutes, both grew again to about the same magnitude as earlier, but with opposite sign. This behaviour is very similar to features observed in wind corners and assumed to be a sign of a solitary wave (Röttger and Alcala).

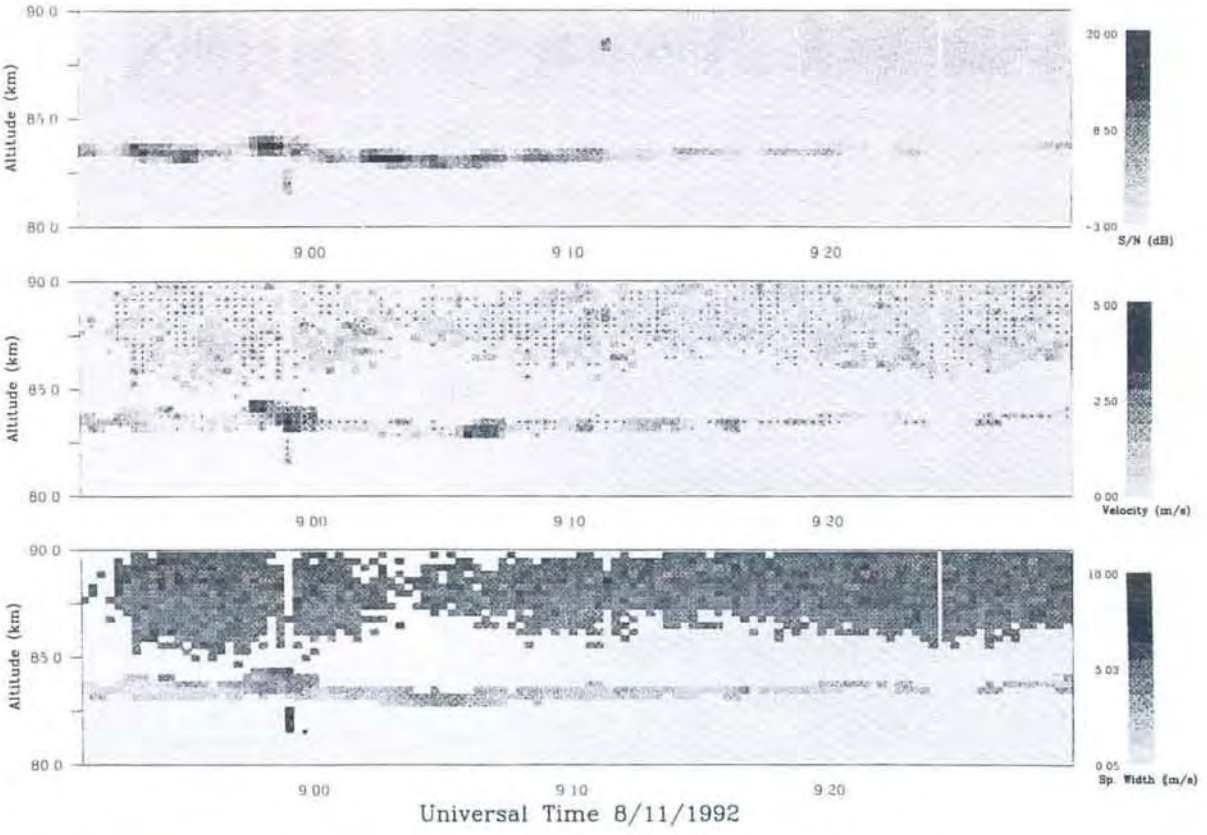

Fig. 31. Height-time-intensity plots of signal-to-noise ratio, Doppler velocity and spectrum width of PMSE observed with the EISCAT VHF radar. They display the typical characteristics of PMSE, ie. fairly narrow and persistent sheets of scatterers with small spectral width (ie. negligible turbulence) below about 85 km, and wide layers with broad spectral width, which are not as persistent but are fairly turbulent, above 85 km.

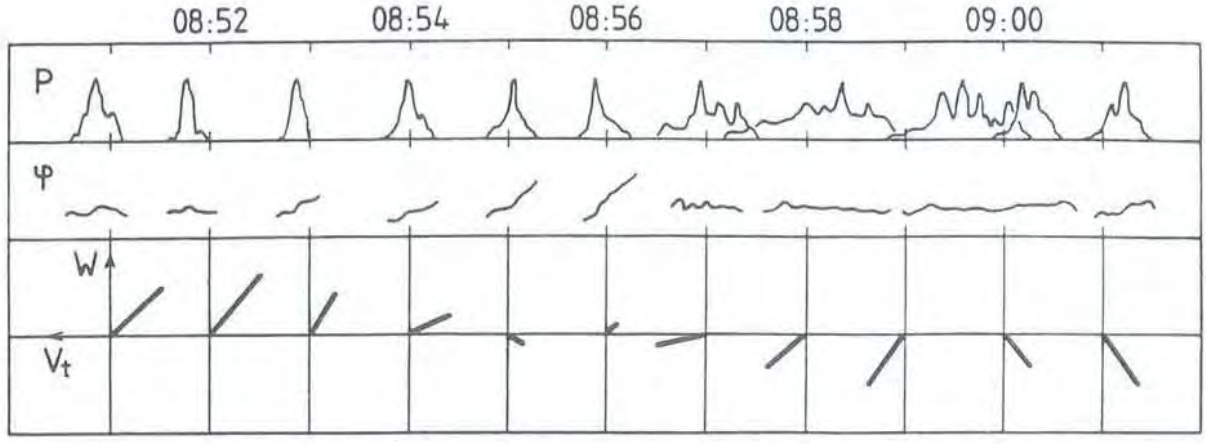

Fig. 32. Schematic Doppler power spectra P, phase ϕ of cross spectra, and the corresponding vector composed of vertical velocity W (deduced from the mean of the power spectra) and west-east trace velocity V_t (deduced from the phase ϕ as a function of Doppler frequency).

Analysis of PMSE data taken with the EISCAT VHF radar in the campaigns during the summer of 1991 has shown that the mean height of PMSE was ~85 km during daytime and ~87 km at night, with a markedly enhanced probability of occurrence during daytime. In addition, the probability of occurrence is higher during geomagnetically quiet periods than when conditions are disturbed. There were indications of PMSE modulations by atmospheric gravity waves as well as by 2-day waves, suggesting the importance of temperature changes on backscattered power levels. Comparison with simultaneous PMSE observations at 46.9 MHz demonstrates common features as well as clear differences. The differences are probably due to different scattering mechanisms at the two frequencies (Bremer, Singer, Keuer, Hoffmann, Röttger).

METEOR STUDIES

Observations with EISCAT show both direct signatures from meteor trails and from fast moving scattering centres with speeds comparable to meteor velocities. Fig. 33 shows an example of trail echoes from Geminid data. The first and the last dumps show only the background ionosphere with a weak E layer. In the two middle dumps there is a strong peak in the power profile at about 150 km altitude, while the autocorrelation functions and spectra in gates 2 to 5 (from 135 to 161 km altitude) show gradually varying forms. The appearance and disappearance of the echo from the trail are probably caused by a transverse drift velocity component across the beam. The power profiles show that the whole trail is drifting with a downward velocity component of about 750 ms^{-1}. This trail is estimated to have a 25° angle to the radar beam, to have been produced by an 8 mm meteor, and to have been expanding for about 9 seconds before it was observed. The spectral line shapes to the right in the affected range gates are strongly asymmetric and exhibit one-sided enhancements close to the ion acoustic frequency. The right ion-acoustic peak is enhanced by a factor of three. In the case of a homogeneous plasma containing a destabilized ion-acoustic wave population, the asymmetries would have been indicative of net downward electron flow. In this case of a spatially very inhomogeneous range gate containing a meteor trail, there is another explanation. The trail contains a significant portion of iron. Iron has an atomic mass number 56, which is almost twice as heavy as the background NO^+ ion mass of 30. The width of the incoherent scatter spectrum is inversely proportional to the square root of the mass, thus for equal ion temperatures the spectrum width for Fe^+ ions is about 70% of the NO^+ spectrum width. As the trail is drifting down within the beam, its velocity of about 750 ms^{-1} corresponds to a frequency shift of about 5 kHz for the whole spectrum. This means that the narrow trail spectrum which is superimposed on the ordinary ionospheric spectrum is

upshifted by 5 kHz for this trail. As the background spectra are about 20 kHz wide, the Doppler shifted meteor ion spectrum ends up on the right shoulder of the broader background ionospheric spectrum. The results are spectra that look like destabilized strongly asymmetric ion-acoustic spectra (Pellinen-Wannberg and Wannberg).

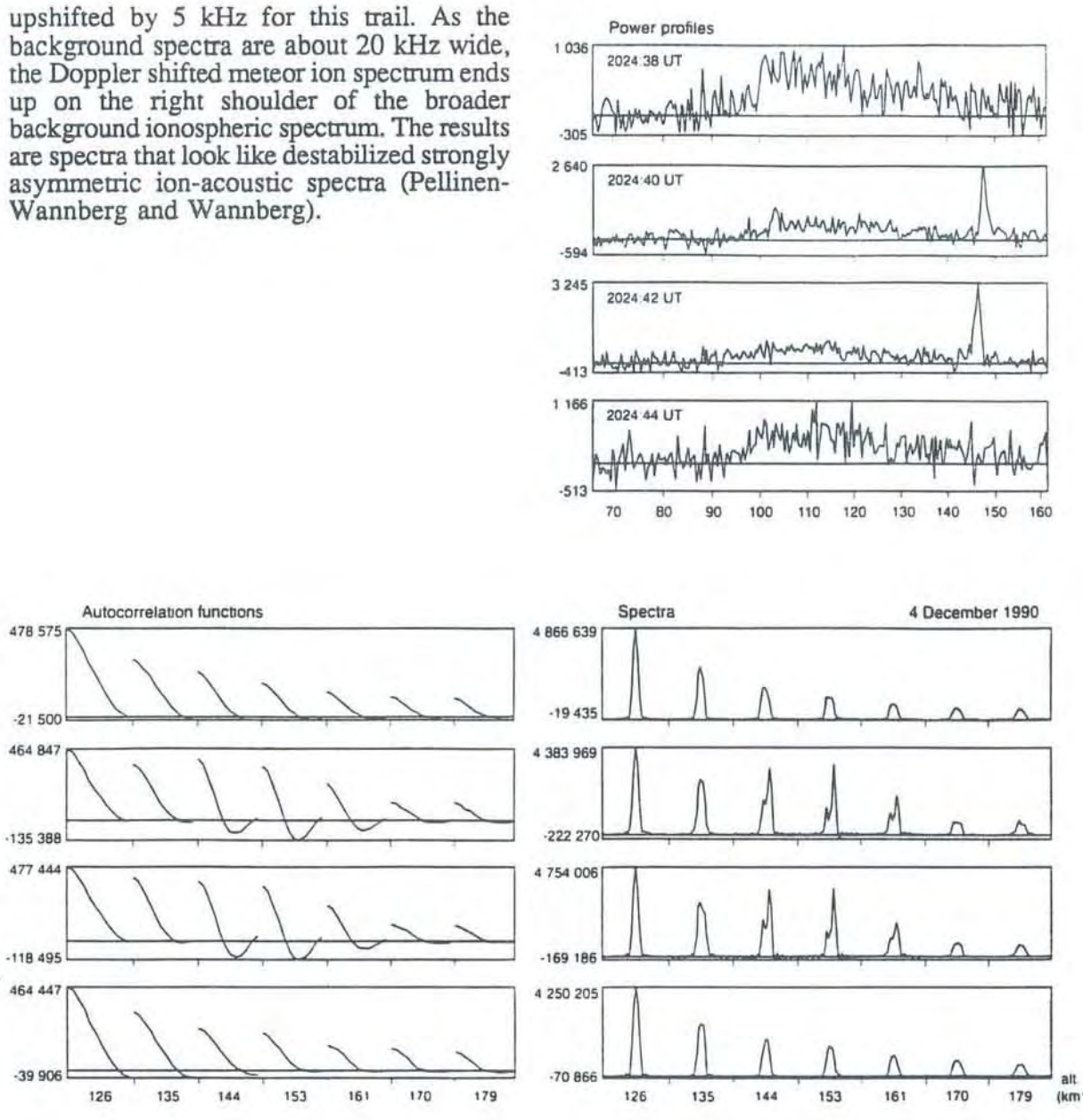

Fig. 33. A meteor trail appearing in two out of four consecutive 2-sec data dumps. Power profiles are in the top right panel, ACFs at lower left and the corresponding spectra at lower right (all background subtracted). The meteor trail echo is seen in the two middle dumps in the power profile at about 150 km altitude, and in the gates 2 to 5 in the ACFs and spectra.

NATURAL ION-ACOUSTIC WAVE ENHANCEMENTS

Enhanced ion-acoustic fluctuations are detected in the topside ionosphere in connection with increases of the electron temperature of up to 8000 K. This electron heating correlates with electron density enhancements in the altitude range 150-250 km, indicating soft electron precipitation in the energy range 100-500 eV. The direct collisional heating due to this precipitation probably contributes to the observed electron heating, but the major heat source for the topside ionospheric electrons has been suggested to come from low-frequency turbulence (Wahlund et al., 1993). An evaluation of the turbulent heating rate was computed from a 1-D time-dependent model for different current-driven instabilities. The effect of these instabilities was taken into account by using effective plasma collision frequencies enhanced above usual values. The resulting computed heating rate was found to be consistent with observations (Forme et al., 1993). Previously-suggested processes able to trigger ion-acoustic waves are based on a large relative drift between two populations; either electrons and ions (current driven instability) or two ion populations (ion-ion two stream instability). These may operate in the ionosphere, but the implied extreme conditions make it difficult to apply these explanations to explain the whole set of observations. Forme (1993) has suggested that Langmuir waves, generated by the beam of soft electron precipitation, could decay into other backscattered Langmuir waves and ion-acoustic waves. Estimations inferred from EISCAT data of the characteristic parameters of the beam and the waves are of the same order of magnitude as in-situ observations onboard satellites.

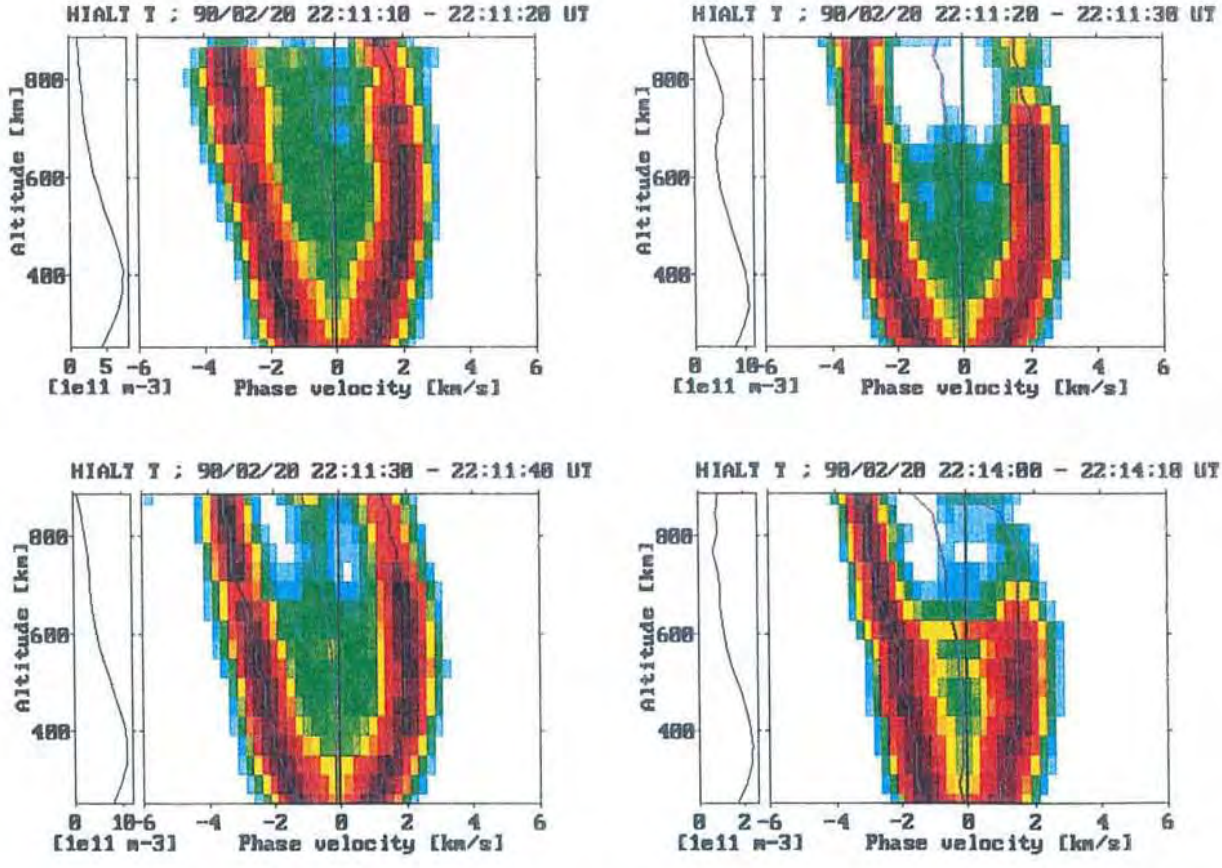

Fig. 34. Colour coded ion line spectra versus altitude for three consecutive and one isolated case of anomalous F-region spectra. In the first three panels it can be seen how the asymmetry of the spectra increases and decreases within a 30 sec time interval. The bulk upward ion outflow can clearly be recognized from the negative Doppler shift of the spectral centre (centre line). As the colour code is normalized for each image the left panel is included to show the absolute backscatter power. The maximum scatter enhancement occurred in the upper right panel at about 750 km altitude.

One problem of investigating such spectra in detail, for example with high time resolution, is to determine reliable plasma parameters in the vicinity of such events. Fig. 34 is an example of anomalous spectra during several 10 s intervals. Even though the determination of plasma parameters from the spectral shape is impossible when the spectra are asymmetric and anomalously enhanced, the upward bulk plasma velocity can still be estimated from the Doppler shift of the centre of the ion line spectra. In the example in Fig. 34 it is mainly the upward directed ion acoustic line which is enhanced, though other examples have also been found, and at lower altitudes the downward directed ion line is more likely to be enhanced (Cabrit).

The enhancement of one, or both, of the ion acoustic shoulders of scattered spectra, is also observed in UHF data, though on far fewer occasions. Although these observations do not usually extend as far into the topside as the VHF measurements, they do reveal additional characteristics which need to be explained, including tristatic measurements. The finer time resolution of the gathered UHF data (5-sec vs 10-sec) reveals that the features can appear and disappear abruptly, that the affected altitude may change considerably, and that the affected spectral shoulder may switch to the opposite one, within 5 seconds. These measurements also reveal the same features localised in height in the E-region, Fig. 35 (Rietveld, Collis, van Eyken, Løvhaug).

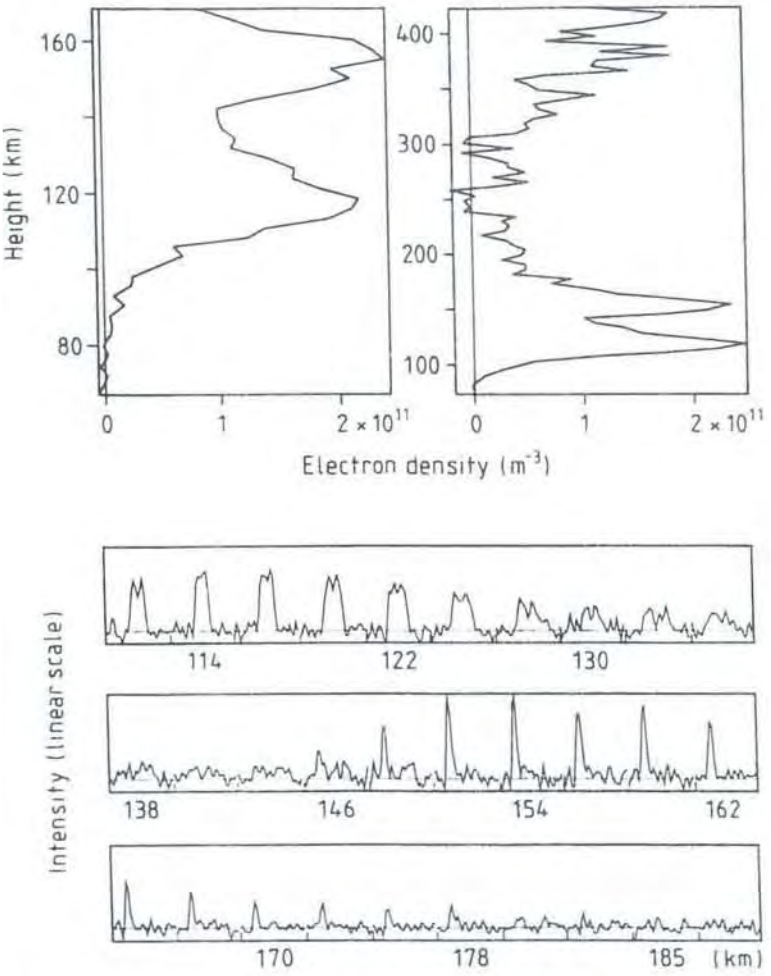

Fig. 35. High spatial resolution data of an approximately 20 km wide region of downshifted enhanced ion acoustic echoes above an auroral E-layer. The two power profiles, obtained with 2.7 and 4.5 km resolution respectively, show the region of enhanced backscatter in terms of equivalent electron density. The multipulse spectra below show that the two regions are caused by quite different backscatter mechanisms; the lower one containing normal incoherent scatter spectra and the upper one with an enhanced downshifted line. The results are from a single 5-sec measurement.

GYRO LINES

Gyro lines are a pair of resonance lines in the incoherent scatter spectrum which are offset from the transmitter frequency by $\omega_g \approx \Omega_e \cos\alpha$, where Ω_e is the electron gyrofrequency and α is the angle between the geomagnetic field and the scattering wave vector. They have been measured with the EISCAT VHF radar pointing northwards at 45° elevation, corresponding to an angle of 54.6° with the magnetic field at 200 km altitude. The lines were seen almost all the time when 30-min integration was used, for most of the time when 10-min integration was used, and often with only 1-2 min integration when the radar was operating at full power. The lines were observed at altitudes 100-270 km and were most intense at about 180 km. Typical intensities were 0.5-2.0% relative to the ion line. The upshifted and downshifted lines were almost symmetrical, but with a tendency for more power in the upshifted line. The observations indicate that the lines are generally stronger in the morning than in the evening as a result of photoelectron enhancement. Another indication of the photoelectron effect was the fact that there was a sudden drop in the power of the lines at the time of local sunset in the plasma volume. The data also show examples of enhanced gyro lines in the absence of photoelectrons, which are believed to be caused by secondary electrons from particle precipitation, see Fig. 36 (Malnes, Bjørnå, Hansen).

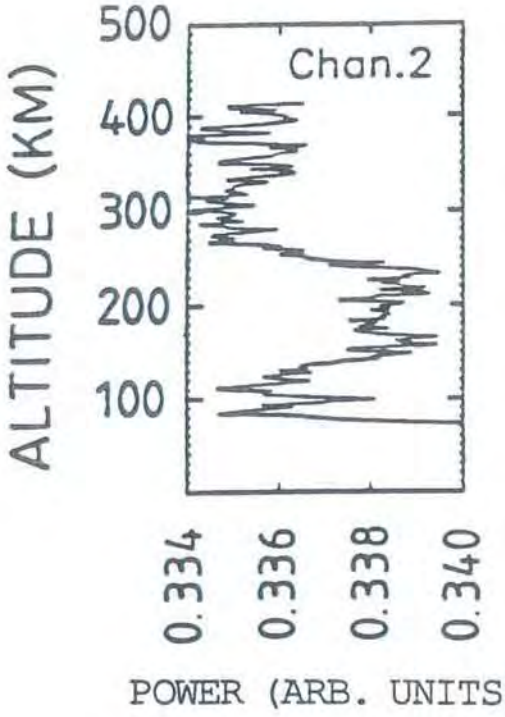

Fig. 36. Example of observations on 6 October 1992, 1900-1925 UT, when gyro line returns were seen from the whole height interval 110-250 km. The offset was -750 kHz, and the transmitted power 1.48 MW on one klystron and 1.40 MW on the other.

NATURAL PLASMA LINES

According to the generally accepted theory of incoherent scatter plasma lines, it is possible to determine the field aligned current from the difference in frequency between the upshifted and the down-shifted plasma lines. However, measurements which have been interpreted with theory assuming a Maxwellian electron distribution have indicated unreasonably large currents. The recent theory by Kofman et al. (1993) takes into account the heat flow induced by a temperature gradient, which has a significant influence on the result. Measurements of plasma lines during daytime conditions, for both high (1991) and low (1993) solar activity, as well as for both the backscatter (Tromsø) and remote site (Kiruna) case, have been compared to the standard Maxwellian theory as well as with the heat flow theory. The Kiruna measurements were found to give the same results as the Tromsø data (within the measurement accuracy), showing that the discrepancy between theory and measurements is not an artefact of the technique of measuring the plasma line cutoff at the peak of the F-region. An example of the measured difference between the upshifted and downshifted plasma line measured from Tromso and Kiruna on 27 July 1993, is shown in Fig. 37. Also shown is the theoretical prediction using standard (Maxwellian) theory, and with the addition of the heat flow term. The additional heat flow term accounts for most of the discrepancy between the theoretical prediction and the measurements, and may be slightly over-estimated during high solar activity, when the surrounding neutral atmosphere was much denser, which might reduce the heat flow. For the measurements made during low solar activity there is still a remaining discrepancy between theory and measurements after the addition of the heat flow term. This may be explained by an enhanced heat flow caused by runaway electrons, or by a thermal flow balancing a net photoelectron escape flux.

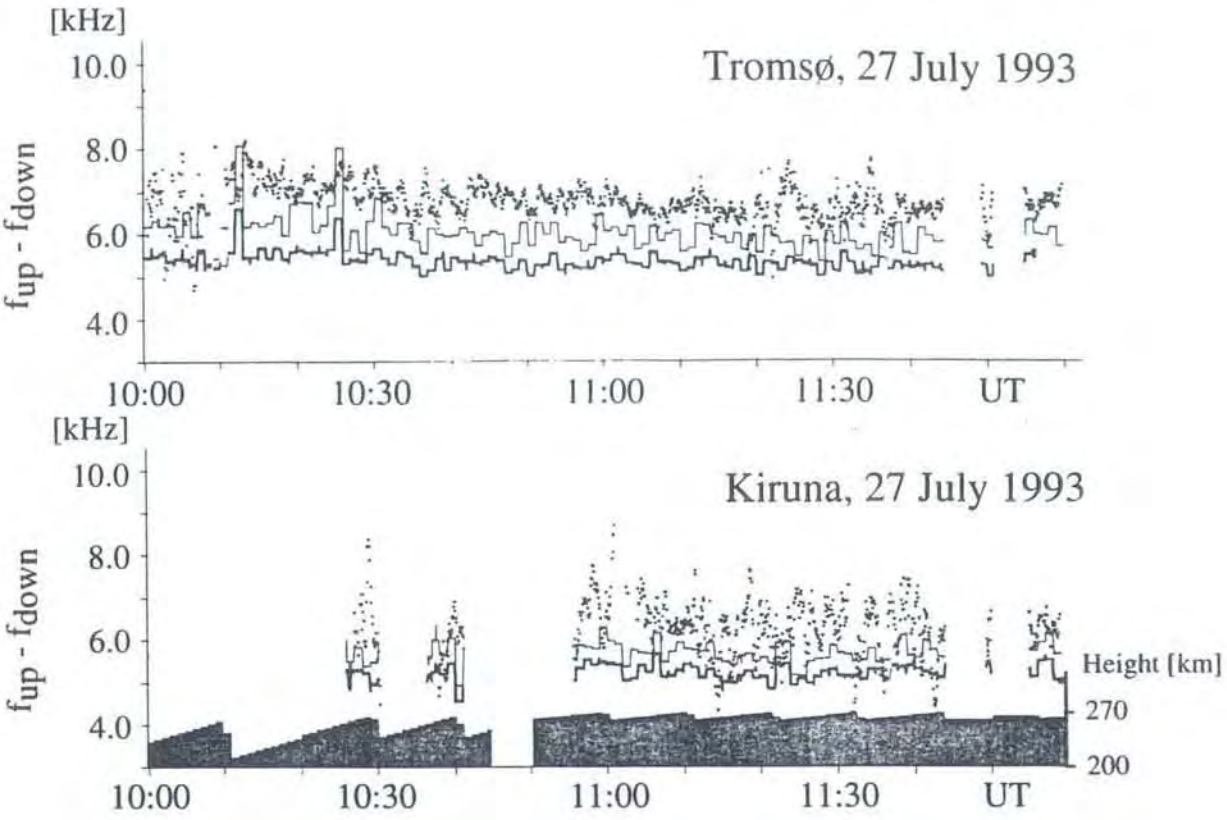

Fig. 37. Difference in frequency offset for the upshifted and downshifted plasma line for the Tromso (backscatter) and Kiruna measurements of 27 July 1993, indicated by the points. Also shown as solid lines are the theoretical prediction taking account of heat flow (grey line) and the standard theory prediction (black line). The heights of the observations are shown by the bars on the lower axis.

Further progress was made on the observation and interpretation of nighttime natural plasma lines during auroral precipitation. Initial observations were performed in February 1992 using power profiles and wideband spectral channels on the EISCAT UHF radar. These data have been analysed and reveal enhanced plasma line spectra in the F-region at a height of over 400 km (Fig. 38). The enhanced signals may have been produced by secondary electrons, either generated locally or transported from the E-region (Valladares, La Hoz and Isham).

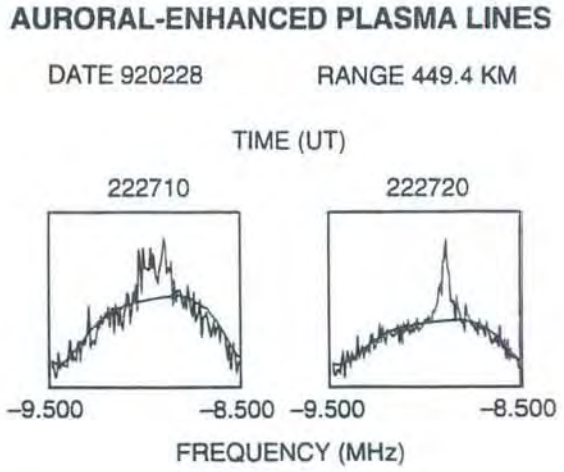

Fig. 38. Wideband spectra taken of the downshifted plasma line during an auroral precipitation event in February 1992. The pulse length was 128 ms. For technical reasons, no background noise samples were taken; the filter shape is thus seen in the broad curve of the noise level.

IONOSPHERIC MODIFICATION WITH HEATING EXPERIMENTS

In ionospheric modification experiments a powerful high-frequency electromagnetic pump wave is transmitted into the ionosphere from a ground-based facility. The powerful pump wave excites numerous different processes in the ionospheric plasma which have a wide range of interacting temporal and spatial scales. This occurs mainly in the ionospheric reflection region, where the pump wave velocity decreases, thereby causing the wave electric field amplitude to increase significantly.

A week-long campaign was performed in November 1992, which was organized as part of the transfer of the heating facility to EISCAT. This campaign included one of the first experiments in which heater-excited ionospheric plasma turbulence was studied with a tristatic radar configuration. The daytime background ionospheric F-region electron temperature was unusually low, implying that the so-often-detrimental electron Landau damping of Langmuir waves at the wavelength probed by the UHF radar system was negligible. Nevertheless, although the Langmuir waves were only weakly damped, the measured excited plasma turbulence varied considerably, which is one of the most important findings of the tristatic experiment. This variation in the plasma excitation is correlated with a varying intensity of natural small-scale plasma density irregularities in the ionospheric interaction region. Further, the tristatic measurements have shown that the properties of the excited plasma turbulence depend significantly on the angle to the geomagnetic field.

On some occasions extremely well-developed enhanced plasma lines were observed during conditions of a low ambient electron temperature. Enhanced plasma line spectra with as many as seven successive cascade lines shifted from the purely growing line by odd multiples of the ion-acoustic frequency (approximately 10 kHz for the scattering wavelength of the UHF radar) were detected. The total spectral width of approximately 150 kHz corresponds to a situation in which the cascading Langmuir waves have reached the so-called Langmuir condensate at which no further decay can occur. Such a wide plasma line spectrum has not previously been reported. For reasons that are not yet fully understood, the number of cascade lines is usually limited to three or less in EISCAT UHF measurements. These results thus show that fully developed cascade type spectra can be excited at high-latitudes (Westman, Leyser, Wannberg, Rietveld).

The November 1992 campaign also involved the first use of the new EISCAT digital chirp generator during a heating experiment. One of the main features of the chirp technique is that it allows the simultaneous observation of the natural and heater-enhanced plasma lines. Such measurements have been carried out in the past at Arecibo, where a consistently-observed frequency gap between the two lines indicates that the source region for the heater-enhanced line lies several kilometres above the expected location on the natural Langmuir frequency profile. In contrast, it has been inferred from past non-chirp EISCAT results that the source region at EISCAT is located on the natural Langmuir profile. The EISCAT chirp measurements now provide a "bridge" between these differing results by showing that the height of the heater-enhanced line continuously varies in an interval between the natural Langmuir profile and a point up to 8 km above. Especially significant is the conclusion that this variation is probably due to natural changes in the ambient background plasma (Isham, La Hoz, Leyser, Rietveld).

In March 1993 a second chirp experiment was carried out. During this campaign a new feature in the heater-enhanced plasma line spectrum was detected, offset by 100 to 200 kHz away from the heating frequency. This result confirms 1986 EISCAT observations of offset lines. Since the lines appear offset away from the heating frequency for both the up and downshifted plasma lines, this feature has been termed the outshifted line, Fig. 39 (Isham, La Hoz, Kohl, Hagfors, Rietveld).

Further results from the March 1993 campaign are displayed in Fig. 40, which shows twelve VHF-spectra of plasma line (top) and ion line (bottom) with 225 m gate separation. A significant change of the spectra is seen with increasing altitude (from left to right in the figure). While lower altitude spectra exhibit clear lines, broad and unstructured spectra are observed about 1 km higher. This is true for both plasma and ion lines and may be considered a clear indication that there is a transition from parametric decay to strong turbulence. It has to be emphasized, however, that Fig. 40 is an interesting example rather than the usual case.

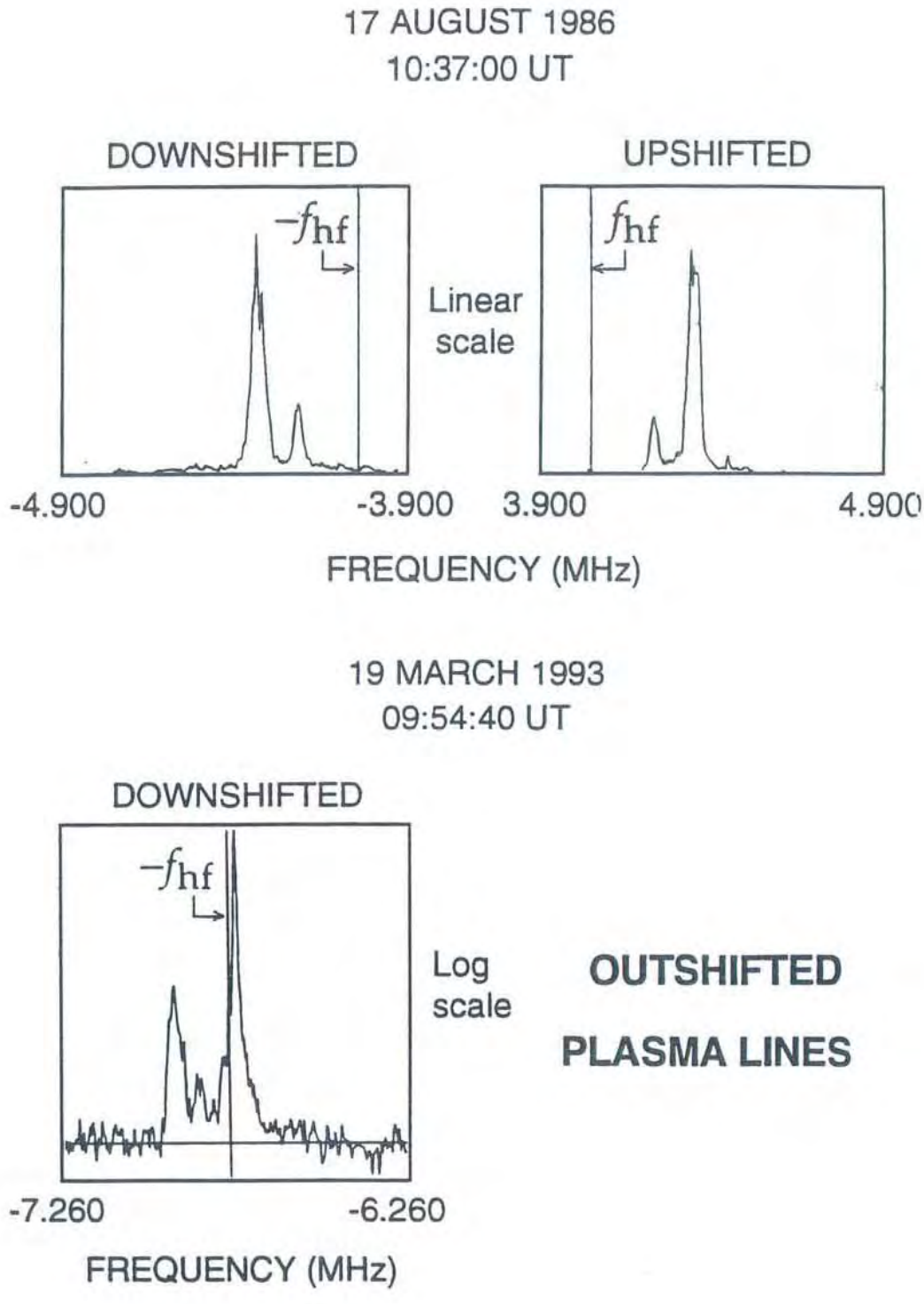

Fig. 39. Unchirped heater-on plasma line data from 17 August 1986 and 19 March 1993. In 1986 the heater was on for 20 s beginning on every even minute, the heating frequency was 4.04 MHz, and the heating power was 250 MW ERP. In 1993 the heater was on for 1 s at the beginning of every even 10 s period, the heating frequency was 6.77 MHz, and the heating power was 1 GW ERP. The plots show data averaged for 10 s and 2 s, respectively, starting at a heater turn-on. The vertical axes indicate the location of the HF pump frequency and the position of the usual heater-enhanced plasma line. The structure to the left (right) of the heating frequency in the downshifted (upshifted) plasma line channel is the outshifted line. Both data sets were taken using a 128 μs pulse sampled in quadrature at 1 μs.

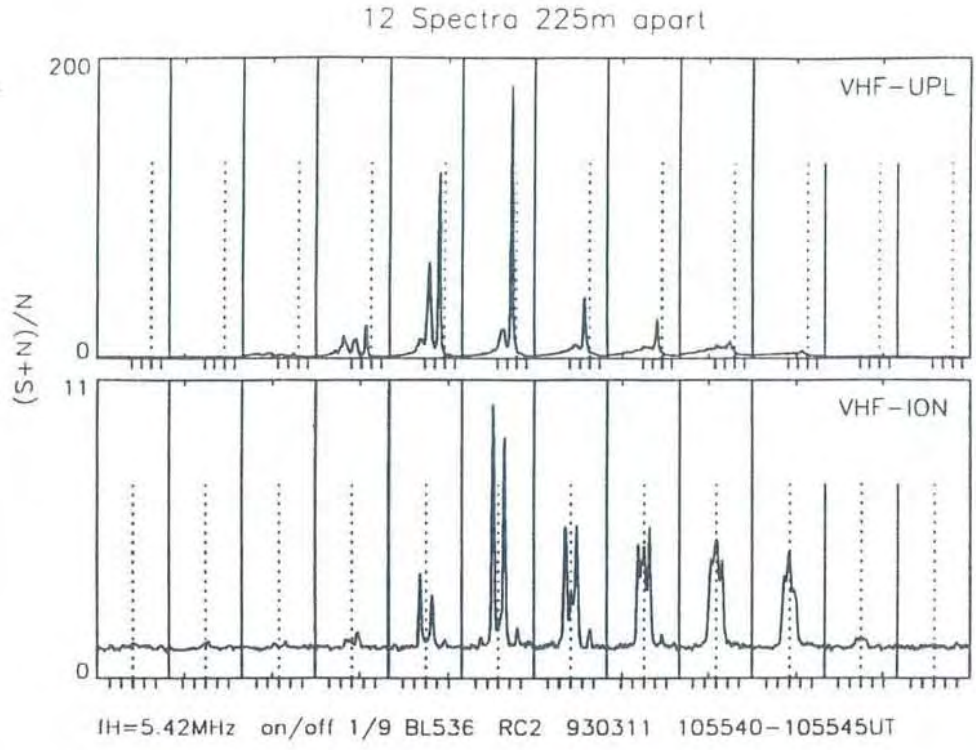

Fig. 40. Spectra of plasma line (top) and ion line (bottom) with 225 m gate separation, illustrating a variation of spectral shape with increasing altitude.

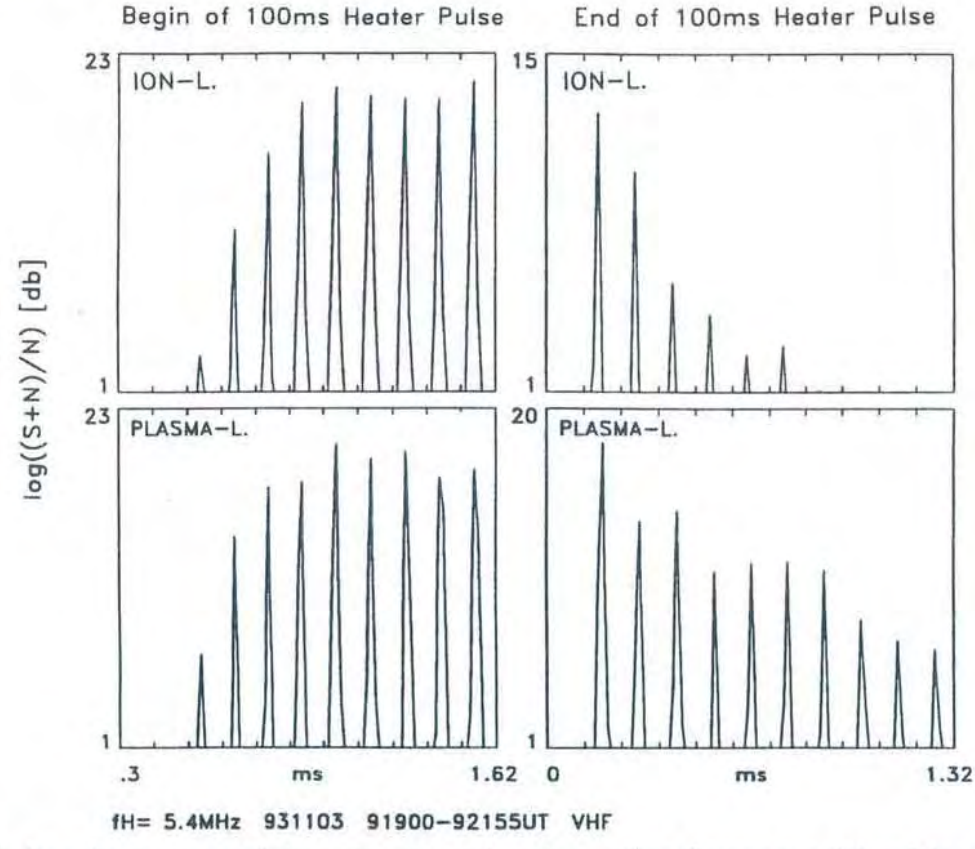

Fig. 41. Received power of the radar signal for plasma line (lower panels) and ion line (upper panels) during the 1 ms after heater turn-on (left panels) and after heater turn-off (right panels). The measurement scheme used a sequence of 15 μs pulses with 120 μs spacing.

In some of the ion spectra in the lower part of Fig. 40, weak lines are seen beside the two strong ones in the middle. Their frequency corresponds precisely to the third harmonic of the strong ion acoustic peaks. This was the first time that these lines have been observed. They are possibly a result of a coupling between the pump wave whose wavenumber and frequency is $(0,\omega_h)$ and the first cascade line $(2k_{radar},\omega_h-\omega_i)$, where ω_i is the ion acoustic frequency.

In another experiment the time development of the excitation for the first millisecond after heater on and heater off, respectively, was investigated. For that purpose a sequence of 15 μs pulses with spacing 120 μs was transmitted. Fig. 41 shows that the intensity of the radar signal increases with a time scale of about 100 μs until it finally saturates. This increase is surprisingly fast; previous measurements resulted in time scales about an order of magnitude longer. It was estimated that for the observed short time scales a heater E-field of 1.5 Vm^{-1} at the altitude of excitation would be necessary. This value is within possible limits, although it implies that D-region absorption was very low at the time of observation.

The decay of the scattered signal after heater off is faster for the ion line than for the plasma line. This indicates that the ion wave is subject to strong Landau damping, which is expected from theory. The damping rates corresponding to the present measurements are roughly 1000 s^{-1} for the plasma line and 4000 s^{-1} for the ion line, which is approximately in agreement with theoretical estimates (Kohl, Rietveld, Stalder).

One of the most important recent discoveries in auroral dynamics has been the observation of and explanation of anomalously high electron heating in the auroral electrojet due to the Farley-Buneman (FB) instability. It has recently been pointed out that artificial E-region heating by high-power radio waves should be affected by natural heating processes. According to a new unified theory of anomalous heating, RF heating of the E-region plasma is strongly dependent on the electron drift speed and becomes less effective in raising the electron temperature when FB wave heating effects are included (Robinson).

A technique previously used in the Soviet Union to investigate the ionosphere was applied to the auroral region for the first time at Tromsø using the Heating facility and dynasonde. The Artificial Periodic Irregularity (API) technique uses the standing wave of the heater reflected from the F-region to produce, by various physical mechanisms in different height regimes, weak electron density variations which cause Bragg scattering of other high power HF waves with the same wavelength probing the region. In one type of experiment the heater is switched on for several seconds to create the irregularities in the D and E regions. Immediately after heater-off the dynasonde starts sounding at the same frequency as the heater in a partial-reflection mode to detect the decay of these irregularities as a function of height and time, using some of the Heating transmitters as a powerful pulsed transmitter. Fig. 42 shows a contour plot of how these irregularities from the D-and E-regions decay in amplitude immediately after the heating transmitter is switched off. From the simultaneously measured phase variation as a function of time during this decay, a vertical velocity can be derived which may be interpreted as the vertical neutral wind velocity. The time constant also provides valuable input to models of D-region ion chemistry. The interpretation of data from the API technique at EISCAT is further aided by the use of simultaneous VHF radar data (Goncharov, Rietveld, Röttger, Turunen).

THEORY OF MEASUREMENTS

A new method of modulating pulse codes by alternating codes has been suggested. In this way, range resolutions similar to those given by Barker-coded pulse codes or alternating codes can be achieved, but, unlike in Barker codes, no side bands are present in the ambiguity functions. Experiments constructed using this rationale are approximately as fast as the corresponding Barker-coded pulse codes, but clearly slower than Barker-coded alternating codes. The principle of the method is demonstrated in Fig. 43, which shows the two-dimensional ambiguity functions of a two-pulse code modulated by a four-bit alternating code. Each pyramid at lags 5, 6, 7, 9, 10 and 11 is a separate ambiguity function associated with two data samples. Lags 1, 2 and 3 have two pyramids at different ranges. This is a range ambiguity corresponding to the ambiguity of the zero lag of an unmodulated two-pulse code. Lag 8 produces an ambiguity function which is a sum of four pyramids elongated in the range direction (Nygrén, Huuskonen, Pollari).

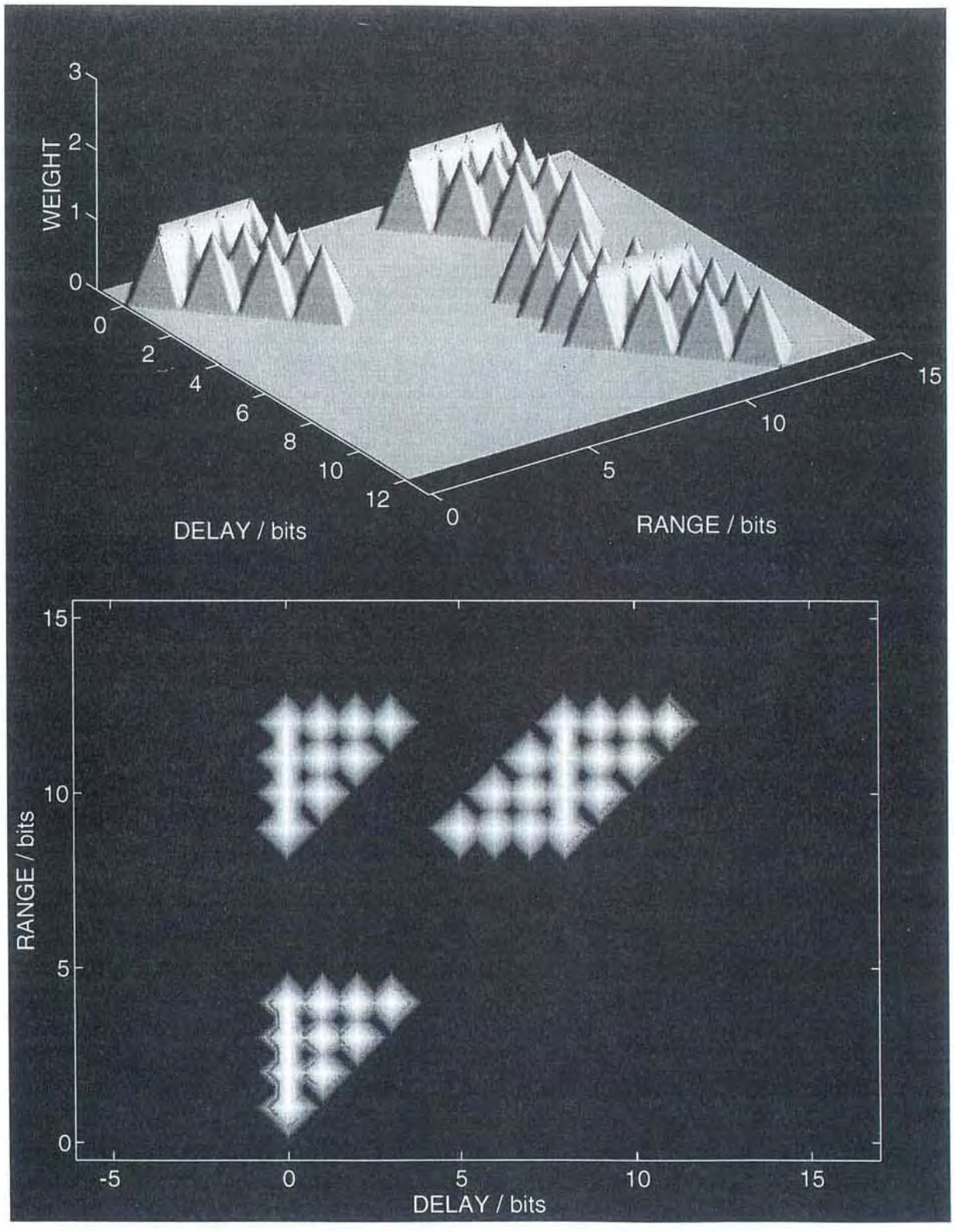

Fig. 43. The two-dimensional ambiguity functions of a two-pulse code modulated by a four-bit alternating code.

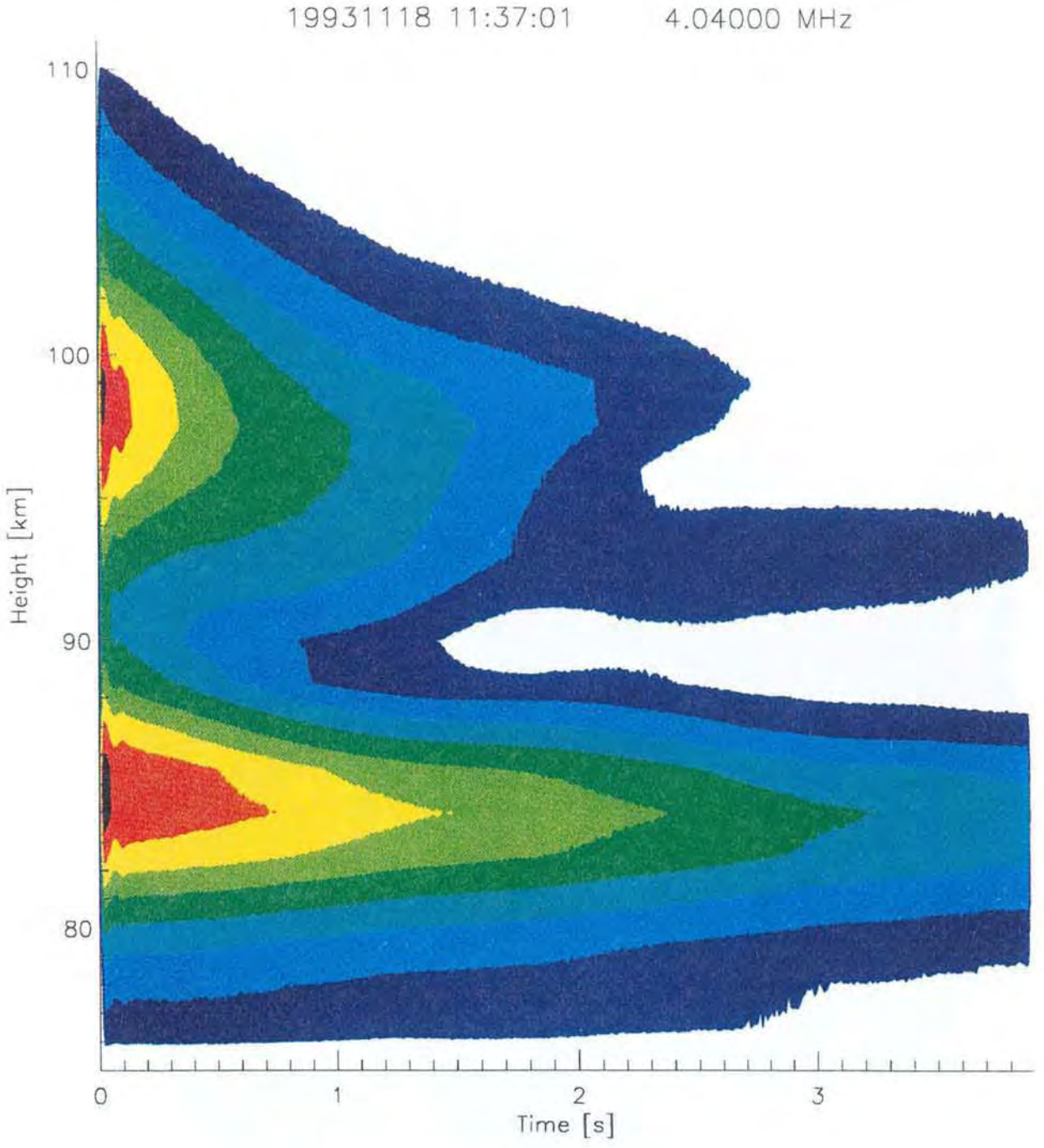

Fig. 42. A contour plot of the intensity of 4 MHz HF waves Bragg backscattered off artificial periodic irregularities in refractive index as a function of height and time after Heater turn off. The colours show in a linear scale from red to blue, how the intensity decreases as the irregularities decay. The data were taken with the dynasonde receiving system using simple long dipole antennas to detect the 30 μs pulses transmitted by the 12 heating transmitters of 90 kW each. In the 4 seconds prior to this plot the heater was on continuously, also at 4 MHz in the X-mode, thereby creating a standing wave pattern by reflection off the F-region. The refractive index fluctuations are caused by variations in electron density induced by the enhanced electron temperature in the standing wave pattern. The physical mechanism is thought to be thermal diffusion and recombination, in the height range depicted here.

INTERPLANETARY SCINTILLATIONS

EISCAT has been used to study the characteristics of the solar wind using the interplanetary scintillation technique. Three types of measurement have been made, providing estimates of scintillation strength, of the velocity of the solar wind and whether one or more velocity streams dominate the flow pattern, and of the scale of the irregularities in the plasma of the solar wind.

Modelling of the velocity characteristics of the solar wind allows an upper limit to be placed on the amplitude of Alfven waves in the plasma and so can be used to test theoretical models of the solar wind. Fig. 44 shows the results of a model fit to the correlation function associated with EISCAT observations of a radio source made from Kiruna and Sodankylä: the function shows evidence of a fast stream and a slow stream in the solar wind (Breen, Coles, Grall, Løvhaug, Markkanen, Misawa, Williams).

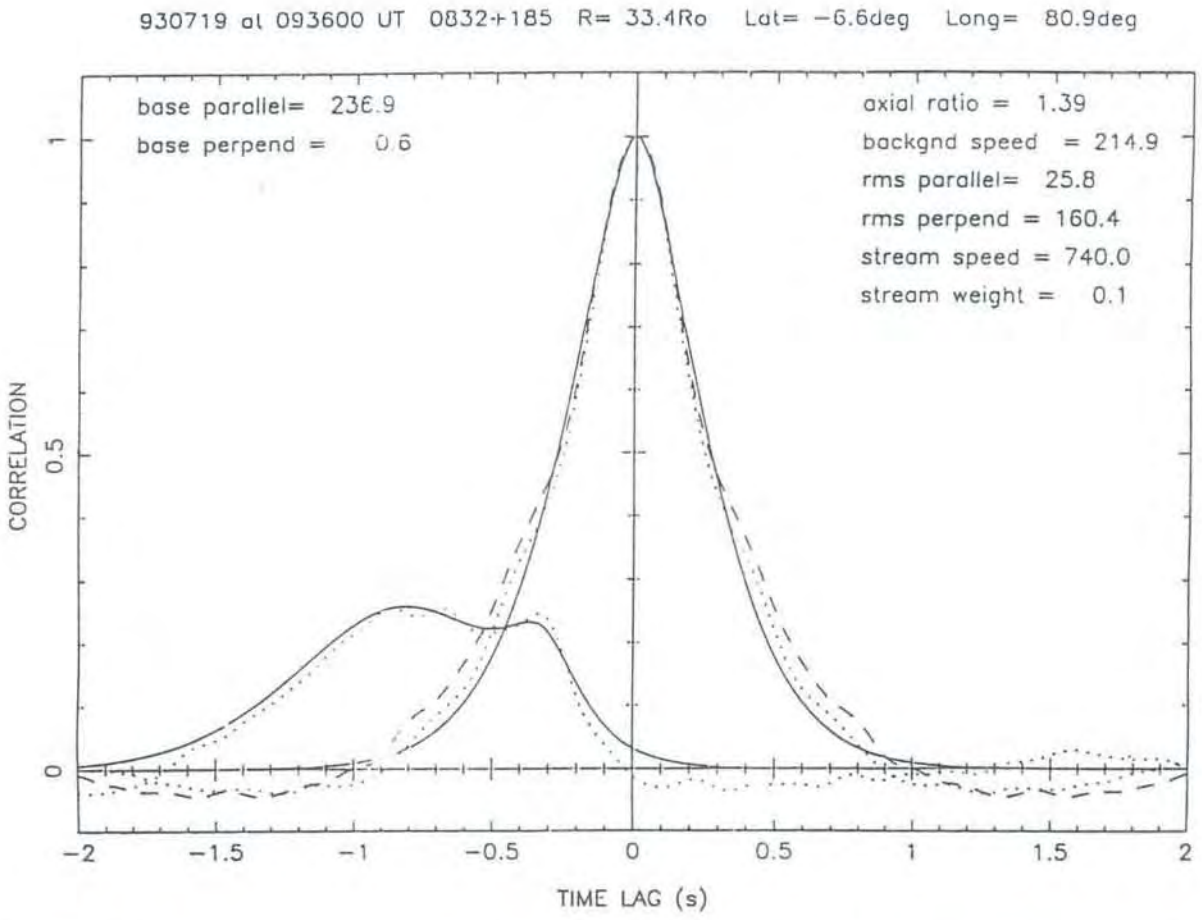

Fig. 44. The correlation function associated with observations of the source 0832+185 made at Tromsø and Sodankylä with a projected baseline of 236.9km. The function shows evidence of a fast stream and a slow stream.

PUBLICATIONS

Journals and books, 1993

Aikio, A.T., H.J. Opgenoorth, M.A.L. Persson and K.U. Kaila, Ground-based measurements of an arc-associated electric field, J. atmos. terr. Phys. 55, 797-808, 1993.

Alpers, M., T. Blix, S. Kirkwood, D. Krankowski, F-J. Lubken, S. Lutz, U. von Zahn, First simultaneous measurements of neutral and ionized iron densities in the upper mesosphere, J. geophys. Res. 98, 275-284, 1993

Barr, R. and P. Stubbe, ELF harmonic radiation from the Tromsø heating facility, Geophys. Res. Lett. 20, 2243-2246, 1993.

Blelly, P.L. and R.W. Schunk, A comparative study between standard, 8-, 13- and 16-moment approximations, Ann. Geophys. 11, 443-469, 1993.

Breen, A.R. and P.J.S. Williams, Real and spurious anti-correlations between short-period variations of field-parallel and field-perpendicular plasma velocities in EISCAT data, J. atmos. terr. Phys. 55, 675-682, 1993.

Brekke, A. and J. Moen, Observations of high latitude ionospheric conductances - a review, J. atmos. terr. Phys. 55, 1493-1512, 1993.

Chernyakov, S.M., E.D. Tereshchenko, B.E. Brunelli and T. Nygrén, Comparison of ionospheric total electron content measured using the difference Doppler and incoherent scatter methods, Ann. Geophys. 11, 10-16, 1993.

Forme, F., A new interpretation on the origin of enhanced ion acoustic fluctuations in the upper ionosphere, Geophys. Res. Lett. 20, 2347-2350, 1993.

Forme, F., J.-E. Wahlund, H.J. Opgenoorth, M.A.L. Persson and E.V. Mishin, Effects of current driven instabilities on the ion and electron temperatures in the topside ionosphere, J. atmos. terr. Phys. 55, 647-666, 1993.

Freeman, M.P., C.J. Farrugia, L.F. Burlaga, M.R. Haiston, M.E. Greenspan, J.M. Rouhoniemi and R.P. Lepping, The interaction of a magnetic cloud with the Earth: convection in the northern and southern hemispheres for a wide range of quasi-steady IMF conditions, J. geophys. Res. 98, 7633-7655, 1993.

Hanssen, A., E. Mjølhus, D.F. DuBois and H.A. Rose, Numerical test of the weak turbulence approximation to ionospheric Langmuir turbulence, J. geophys. Res. 97, 12073-12091, 1993.

Hargreaves, J.K., A.V. Shirochkov and A.D. Farmer, The polar cap absorption event of 19-21 March 1990: recombination coefficients, the twilight transition and the midday recovery, J. atmos. terr. Phys. 55, 857-862, 1993.

Honary, F., A.J. Stocker, T.R. Robinson, T.B. Jones, N.M. Wade, P. Stubbe and H. Kopka, EISCAT observations of electron temperature oscillations due to the action of high power HF radio waves, J. atmos. terr. Phys. 55, 1433-1448, 1993.

Hubert, D., N. Bonnard, C. Lathuillere and W. Kofman, A new scenario for the measurement of the auroral plasma parameters in the non-Maxwellian state, Geophys. Res. Lett. 20, 2691-2694, 1993.

Kaila, K.U., R. Rasinkangas and J. Kangas, Photometric calibration of auroral TV pictures during a pulsating patch event, Ann. Geophys. 11, 790-796, 1993.

Kamide, Y. and A. Brekke, Altitude variations of ionospheric currents at auroral latitudes, Geophys. Res. Lett. 20, 309-312, 1993.

Kersley, L., J.A. Heaton, S.E. Pryse and T.D. Raymund, Experimental ionospheric tomography with ionosonde input and EISCAT verification, Ann. Geophys. 11, 1064-1074, 1993.

Kirkwood, S. and U. von Zahn, Formation mechanisms for low-altitude Es and metal layers - results from the METAL campaign, J. geophys. Res. 98, 21549-21562, 1993.

Knipp, D.J., B.A. Emery, A.D. Richmond, N.U. Crooker, M.R. Hairston, J.A. Cumnock, W.F. Denig, F.J. Rich, O. de la Beaujardiere, J.M. Ruohoniemi, A.S. Rodger, G. Crowley, B.-H. Ahn, D.S. Evans, T.J. Fuller-Rowell, E. Friis-Christensen, M. Lockwood, H.W. Kroehl, C.G. Maclennan, A. McEwin, R.J. Pellinen, R.J. Morris, G.B. Burns, V. Papitashvili, A. Zaitzev, O. Troshichev, N. Sato, P. Sutcliffe and L. Tomlinson, Ionospheric convection response to slow, strong variations in a northward interplanetary magnetic field: A case study for January 14, 1988, J. geophys. Res 98, 19273-19292, 1993.

Knudsen, D.J., G. Haerendel, S. Buchert, M.C. Kelley, Å. Steen and U. Brändström, Incoherent scatter radar spectrum distortions from intense auroral turbulence, J. geophys. Res. 98, 9459-9471, 1993.

Kofman, W., J-P. St-Maurice and A.P. van Eyken, Heat flow effect on the plasma line frequency, J. geophys. Res. 98, 6079-6085, 1993.

Kohl, H., H. Kopka, P. Stubbe, M.T. Rietveld, Introduction to ionospheric heating experiments at Tromsø—II. Scientific problems, J. atmos. terr. Phys. 55, 601-613, 1993.

Kustov, A.V., M.V. Uspensky, G.O.L. Jones, P.J.S. Williams, G.F. Sofko, and J.A. Koehler, Electric field and electron density thresholds for coherent auroral echo onset, J. geophys. Res. 98, 7729-7736, 1993.

Lanchester, B.S., T. Nygren, M.J. Jarvis and R. Edwards, Gravity wave parameters measured with EISCAT and Dynasonde, Ann. Geophys. 11, 925-936, 1993.

Lester, M., Measurement and empirical model comparisons in the high latitude ionosphere during the equinoctial and solstitial SUNDIAL campaigns of 1988, Geomag. Aeron. (English edition) 33, 7-12, 1993.

Lester, M, A.J. Coates, R.A. Harrison, D. Rees, J.G. Roederer, M.J. Rycroft and M.A. Saunders, International solar terrestrial energy programme and the UK participation, Surveys Geophys. 14, 555-583, 1993.

Lester, M., O. de la Beaujardiere, J.C. Foster, M.P. Freeman, H. Lühr, J.M. Ruohoniemi and W. Swider, The response of the large-scale ionospheric convection pattern to changes in the IMF and substorms: results from the SUNDIAL 1987 campaign, Ann. Geophys. 11, 556-571, 1993.

Lewis, R.V., P.J.S. Williams, T.K. Yeoman, M. Lester and E. Nielsen, Measurements of bursts in plasma velocity during substorm activity, Adv. Space Res. 13, (4)139-(4)142, 1993.

Lockwood, M., Modelling the high-latitude ionosphere for time-varying plasma convection, IEE Proceedings (H) 140, 91-100, 1993.

Lockwood, M., H.C. Carlson and P.E. Sandholt, The implications of the altitude of transient 630 nm dayside aurora emissions, J. geophys. Res. 98, 15571-15587, 1993.

Lockwood, M., W.F. Denig, A.D. Farmer, V.N. Davda, S.W.H. Cowley and H. Lühr, Ionospheric signatures of pulsed reconnection at the Earth's magnetopause, Nature 361 (6411), 424-427, 1993.

Lockwood, M., I.W. McCrea, G.H. Millward, R.J. Moffett and H. Rishbeth, EISCAT observations of ion composition and temperature anisotropy in the high-latitude F-region, J. atmos. terr. Phys. 55, 895-906, 1993.

Lockwood, M., J. Moen, S.W.H. Cowley, A.D. Farmer, U.P. Løvhaug, H. Lühr and V.N. Davda, Variability of dayside convection and motions of the cusp/cleft aurora, Geophys. Res. Lett. 20, 1011-1014, 1993.

Ma, S.Y. and K. Schlegel, Non-linear wave-wave interactions related to gravity wave reflection in the auroral upper F-region observed with the EISCAT radar, J. atmos. terr. Phys. 55, 719-738, 1993.

Malnes, E. and N. Bjørnå, Enhancement of incoherent scatter gyro lines by suprathermal electrons, J. atmos. terr. Phys. 55, 667-674, 1993.

Malnes, E., N. Bjørnå and T.L. Hansen, European incoherent scatter VHF measurements of gyrolines, J. geophys. Res. 98, 21563-21569, 1993.

McCrea, I.W., M. Lester, T.R. Robinson, J-P. St-Maurice, N.M. Wade and T.B. Jones, Derivation of the ion temperature partition coefficient $\beta_{\|}$ from the study of ion frictional heating events, J. geophys. Res. 98, 15701-15715, 1993.

Mjølhus, E., On the small scale striation effect in ionospheric radio modification experiments near harmonics of the electron gyrofrequency, J. atmos. terr. Phys. 55, 907-918, 1993.

Moen, J. and A. Brekke, The solar flux influence on quiet time conductances in the auroral ionosphere, Geophys. Res. Lett. 20, 971-974, 1993.

Morelli, J.P., R.J. Bunting, S.W.H. Cowley, C.J. Farrugia, M.P. Freeman, E. Friis-Christensen, G.O.L. Jones, M. Lester, R.V. Lewis, H. Lühr, D. Orr, M. Pinnock, G.D. Reeves, P.J.S. Williams and T.K. Yeoman, Plasma flow bursts in the nightside auroral zone ionosphere and their relation to geomagnetic activity, Adv. Space Res. 13, (4)135-(4)138, 1993.

Peymirat, C. and A.D. Richmond, Modeling of the ion loss effect on the generation of region-2 field-aligned currents via equivalent magnetospheric conductances, J. geophys. Res. 98, 15467-15476, 1993.

del Pozo, C.F., C.J. Burns and J.K. Hargreaves, Dual-beam EISCAT radar observations of the dynamics of the disturbed D and E regions in the early morning sector, J. atmos. terr. Phys. 55, 1393-1415, 1993.

Ranta, H., A. Ranta, S. Yousef, J. Burns and P. Stauning, D-region observations of polar cap absorption events during the EISCAT operation in 1981-1989, J. atmos. terr. Phys. 55, 751-766, 1993.

Raymund, T.D., S.E. Pryse, L. Kersley and J.A.T. Heaton, Tomographic reconstruction of the ionospheric electron density with EISCAT radar verification, Radio Sci. 28, 811-818, 1993.

Rietveld, M.T. and P.N. Collis, Mesospheric observations with the EISCAT UHF radar during polar cap absorption events: 2. Spectral measurements, Ann. Geophys. 11, 797-808, 1993.

Rietveld, M.T., H. Kohl, H. Kopka and P. Stubbe, Introduction to ionospheric heating at Tromsø—I. Experimental overview, J. atmos. terr. Phys. 55, 577-599, 1993

Rishbeth, H. and A.P. van Eyken, EISCAT: early history and the first ten years of operation, J. atmos. terr. Phys. 55, 525-542, 1993.

Robinson, T.R. and F. Honary, Adiabatic and isothermal ion-acoustic speeds of stabilised Farley-Buneman waves in the auroral E-region, J. atmos. terr. Phys. 55, 65-77, 1993.

Röttger, J., Middle atmosphere studies with the EISCAT radars: Polar mesosphere summer echoes, in Coupling Processes in the lower and Middle Atmosphere, ed. Thrane et al., Kluwer Acad. Publ., Netherlands, 369-387, 1993.

Stocker, A.J., F. Honary, T.R. Robinson, T.B. Jones, and P. Stubbe, Anomalous absorption during artificial modification at harmonics of the electron gyrofrequency, J. Geophys. Res. 98, 13627-13634, 1993.

Turunen, E., EISCAT incoherent scatter radar observations and model studies of day to twilight variations in the D-region during the PCA event of August, 1989, J. atmos. terr. Phys. 55, 767-781, 1993.

Turunen, T., T. Nygrén and A. Huuskonen, Nocturnal high-latitude E-region in winter during extremely quiet conditions, J. atmos. terr. Phys. 55, 783-795, 1993.

Uspensky, M.V., A.V. Kustov and P.J.S. Williams, The amplitude of auroral backscatter: III Effect of tilted ionospheric layer, J. atmos. terr. Phys. 55, 1383-1392, 1993.

Virdi, T.S. and P.J.S. Williams, Altitude variations in the amplitude and phase of tidal oscillations at high latitude, J. atmos. terr. Phys. 55, 697-717, 1993.

Wahlund, J.-E., H.J. Opgenoorth, F.R.E. Forme, M.A.L. Persson, I. Häggström and J. Lilensten, Electron energization in the topside auroral ionosphere: on the importance of ion-acoustic turbulence, J. atmos. terr. Phys. 55, 623-645, 1993.

Williams, P.J.S., T.S. Virdi, R.V. Lewis, M. Lester, A.S. Rodger, I.W. McCrea and K.S.C. Freeman, Worldwide atmospheric gravity-wave study in the European sector, J. atmos. terr. Phys. 55, 683-696, 1993.

Wu, J. and C. Taieb, Observations of the structure of the thermospheric relative composition n(H)/n(O) with the EISCAT-VHF radar, Ann. Geophys. 11, 485-493, 1993.

Wu, J. and C. Taieb, Heat flux solutions of the 13-moment approximation transport equations in a multispecies gas, J. geophys. Res. 98, 15613-15619, 1993.

Other Publications; Theses, Proceedings, Reports

Davies, C.J., The interaction between the thermosphere and ionosphere at high latitudes, Ph.D. thesis, University of Southampton, UK, 1993.

Freeman, K.S.C., Measurements of Joule heating in the auroral ionosphere, Ph.D. thesis, University of Wales, UK, 1993.

Heaton, J.A.T., L. Kersley, S.E. Pryse, T.D. Raymund, D.L. Rice, P. Sheen, I.K. Walker and C. Willson, Tomographic imaging of electron density in the auroral ionosphere, IEE, CP370, 677-680, 1993.

Millward, G.H.G., A global model of the Earth's thermosphere, ionosphere and plasmasphere: theoretical studies of the response to enhanced high-latitude convection, Ph.D. thesis, University of Sheffield, UK, 1993.

Opgenoorth, H.J., The magnetospheric substorm as seen in ground-based data: some open questions, Proceedings of the Global Environmental Modelling (GEM) workshop on the physics of the Geotail and Substorms, Snowmass, Col., June/July, 1992, Boston University, 1993a.

Opgenoorth, H. J., Coordination of ground-based observations with Cluster, in the Cluster Mission and supporting activities, ESA SP-313, 1993b.

Raymund, T.D., J.A.T. Heaton, S.E. Pryse and L. Kersley, Tomographic investigation of the high-latitude ionospheric electron density with independent verification using EISCAT, Orif, Ionospheric Effects Symposium, Alexandria, VA, USA Paper 2B3 pp8.

Röttger, J., Coupling between the lower, middle and upper atmosphere in polar regions investigated by MST radar: possibilities for the EISCAT Svalbard Radar, 1991 NSSR (Nordic Society for Space Physics) Conference Proceedings, 157-163 (published as DMI Scientific Report 93-1, ed. P. Hoeg, Danish Meteorological Institute, Copenhagen, Denmark, 1993.

Turunen, E., High latitude D-region studies by incoherent scatter measurements, Ph.D. thesis, University of Oulu, Finland, 1993.

SUPPLEMENT 1992

Manson, A.H., C.E. Meek, A. Brekke and J. Moen, Mesosphere and lower thermosphere (80-120 km) winds and tides from near Tromsø (70^{o}N, 20^{o}E): comparison between radars (MF, EISCAT, VHF) and rockets, J. atmos. terr. Phys., 54, 927-950, 1992.

Hanssen, A., Electromagnetically driven Langmuir turbulence in the ionosphere, Dr. Scient. thesis, University of Tromsø, Norway, 1992.

EISCAT REPORTS AND MEETINGS

Reports 1993:
EISCAT Annual Report 1992

Brochure:
The EISCAT Svalbard Radar - An Evolutionary Step into EISCAT's Future

Meetings 1993:

COUNCIL	40th meeting, 20/21 May	Oslo, Norway
	41st meeting, 16/17 Nov	Hamburg, Germany
SAC	44th meeting, 1/2 April	Longyearbyen, Svalbard
	45th meeting, 2 Oct	Andenes, Norway
AFC	40th meeting, 20/21 April	Paris, France
	41st meeting, 21/22 Oct	Copenhagen, Denmark
Long-Term Planning Group	2 March	Copenhagen, Denmark

BALANCE SHEET AT 31 DECEMBER 1993

MSEK

Assets	At 31 Dec 1992	Additions Pool	Additions Cap Op	Additions Other	Depre-ciations	At 31 Dec 1993
FIXED ASSETS						
Buildings	9.4		0.1		0.3	9.2
Transmitters	23.0				1.8	21.2
UHF antennas	8.1				1.3	6.8
VHF antenna	11.4				1.6	9.8
Computers, etc	3.4		1.7		1.2	3.8
Other	4.6		2.3	-3.2	0.7	3.0
UHF Spare Klystron	0.7					0.7
ESR Transmitter	2.0		6.1			8.1
ESR Antenna			6.2			6.2
ESR Building			15.5			15.5
ESR Test hall			0.2			0.2
Total	62.6		32.1	-3.2	6.9	84.5
CURRENT ASSETS						
Debtors	4.9					0.2
Prepayments and accrued income						0.3
Cash and Ordinary Bank Accounts	12.1					21.0
Special Accounts						1.5
Total	17.0					23.0
GRAND TOTAL	79.6					107.5

MSEK

Liabilities	At 31 Dec 1992	At 31 Dec 1993
CAPITAL		
Contributions		
Pool	94.3	94.3
UHF Spare Klystron	0.7	0.7
Capital operating	23.6	24.4
In kind	25.1	25.1
Other	0.4	0.4
Heating Building	2.3	2.3
ESR Transmitter	2.0	8.1
ESR Antenna		6.2
ESR Building		15.5
ESR Test hall		0.2
	148.4	177.2
Depreciations	85.8	92.7
Total Capital	62.6	84.5
RESERVES		
Pool	1.2	2.0
Capital Operating	4.9	4.6
Other	2.8	6.4
Total Reserves	8.9	13.0
LIABILITIES		
Provisions	0.2	0.7
Other Liabilities	7.9	9.3
Total Liabilities	8.1	10.0
GRAND TOTAL	79.6	107.5

Total budget outcome in 1993 (MSEK): Recurrent chapter:

Personnel:	12.2
Administration:	5.2
Operations:	4.3
EISCAT Svalbard Radar:	3.4
Total:	25.1

(Totals may not match because of rounding; MSEK = Million Swedish Crowns)

EISCAT SCIENTIFIC ASSOCIATION

31 December 1993

	Finland	France	Germany	Norway	Sweden	United Kingdom
COUNCIL	J. Kangas A. Siivola	M. Aubry (1) G. Caudal W. Kofman	G. Haerendel T. Hagfors M. Meinecke	A. Brekke* B. Benterud	B. Hultqvist J. Gustavsson	S.W.H. Cowley T.B. Jones R.L.T. Street
SAC	M. Lehtinen	D. Fontaine D. Alcaydé*	W. Baumjohann K. Rinnert	C. La Hoz	H.Opgenoorth (2)	M. Lockwood P.J.S. Williams
AFC	E. Ikonen	D. Alloin*	C. Löw (3)	A. Andersen	F. Karlsson	P. Fletcher

SAC = Scientific Advisory Committee; AFC = Administrative and Finance Committee; * = Chairperson

EISCAT Senior Staff

Director: J. Röttger (on secondment from MPG)
Deputy Director Technical: U.G. Wannberg
Deputy Director Science: A.P. van Eyken
Head of Computer Operations: S. Buchert

Site Leaders:
Kiruna: I. Wolf
Sodankylä: M. Postila
Tromsø Radar: R. Jacobsen
Tromsø Heating: M. Rietveld

Non-Associate members of SAC were R. Fujii (Japan), J. Holt (USA) and P. Hoeg (Denmark).
(1) A. Berroir until 40th Council meeting. (2) SAC Chairman until 44th SAC meeting. (3) G. Hoch until 40th AFC meeting.

THE EISCAT ASSOCIATES

CNRS
Centre National de la Recherche Scientifique
France

SA
Suomen Akatemia
Finland

MPG
Max-Planck-Gesellschaft
Germany

Norges forskningsråd
Norway

NFR
Naturvetenskapliga forskningsrådet
Sweden

SERC
Science and Engineering Research Council
United Kingdom
(from April 1994: PPARC - Particle Physics and Astronomy Research Council)

December 1993

EISCAT Scientific Association

HEADQUARTERS

EISCAT Scientific Association
Box 812
S-981 28 KIRUNA, Sweden
Phone +46-980-79153
Fax +46-980-79161

SITES

Tromsø station

EISCAT
Ramfjordmoen
N-9027 RAMFJORDBOTN, Norway
Phone +47-776-92166
Fax +47-776-92380

Kiruna station

EISCAT
Swedish Institute of Space Physics
Box 812
S-981 28 KIRUNA, Sweden
Phone +46-980-79136
Telex 8754 IRF S
Fax +46-980-79161

Sodankylä station

EISCAT
Geophysical Observatory
FIN-99600 SODANKYLÄ, Finland
Phone +358-693-619880
Telex 37254 GEFSO SF
Fax +358-693-610375